Studies of solution-processed organic light-emitting diodes and their materials

by

Emily S. Hellerich

A dissertation submitted to the graduate faculty

in partial fulfillment of the requirements for the degree of

DOCTOR OF PHILOSOPHY

Major: Condensed Matter Physics

Program of Study Committee:

Joseph Shinar, Major Professor

Ruth Shinar

Adam Kaminski

Bruce Harmon

Craig Ogilvie

Jaeyoun Kim

Iowa State University

Ames, Iowa

2013

DEDICATION

I would like to dedicate this dissertation to my husband Dan, whose support and reassurance sustained me throughout my graduate studies. I would also like to thank my family for their loving support.

TABLE OF CONTENTS

Dissertation Organization

Chapter 1 consists of a general introduction to organic light-emitting diodes (OLEDs) and organic semiconducting materials. An explanation is given of many topics relevant to the studies presented herein. Hopefully the reader will find it interesting and educational.

Chapter 2 presents a hitherto unexplored approach in which a small molecule is used as a host to polymer guests in solution-processed OLEDs. We find that the small molecule host results in much more efficient devices than the often-used alternative polymer host when used for the guests presented. It is likely that nano- and microstructural differences between the hosts contribute to the improvements, which highlights some interesting characteristics that can help to better understand the nature of these mixtures. A number of the guests used in this study were newly synthesized benzobisoxazole-based copolymers discussed in chapter 3. Chapter 2 was published in Journal of Materials Chemistry C and has not been altered for this dissertation.

Chapter 3 presents new organic copolymers that are based on the chemical structure of benzobisoxazoles, which have been shown in the past to have good electron transporting properties. The novel concept in this publication pertains to a change in the direction of polymerization, also known as the conjugation pathway, which we show increases the emission efficiency. This work highlights a unique and useful property of organic semiconducting materials in that they can be synthesized to create the desired characteristics. The majority of the paper published in Macromolecules was written by J. J. Intemann with contributions from the author of this dissertation, M. Jeffries-EL, R. Shinar, and J. Shinar, with a majority of the conclusions drawn from discussions between the aforementioned. The device fabrication and testing were performed by the author of this dissertation. The material synthesis and photolu-

minescence spectra were performed by J. J. Intemann. The published paper has been edited so that only the information relevant to this dissertation, i.e. mainly device data, is presented and discussed herein. For more information on the synthesis of these new materials, please refer to the publication.

Chapter 4 is an earlier work that kick-started in our research group the use of small molecules in solution-processed OLEDs. Originally these devices were to be used in magnetoresistance studies, but the project took a different path when the devices were more efficient than expected. The efficient use of small molecules in solution-processed OLEDs is highlighted, which at the time was not often the case. Also, the important observation of the effect of solvent choice on the resultant film is emphasized, with discussion of the likely cause of these effects.

Chapter 5 introduces microcavity OLEDs in which the transparent anode ITO is replaced with semi-transparent thin silver, which creates an optical cavity within the devices. The goal was to expand a previous work that created an on-chip spectrometer covering wavelengths 493 to 639 nm. In this case, a spin-coated mixed emitting layer (EML) is used, consisting of a polymer and a small molecule that both emit in the near UV and blue. The resulting combined spectra gives a wide band that can be used to create narrow microcavity emission peaks of 373 to 469 nm, depending on the device thickness (i.e. the cavity's optical length). In the process of this effort, the mixed EML presented interesting complexities that we attempt to explain via simulation and morphology study. The simulation work and much discussion was contributed by R. Biswas and R. Heise. This work will be submitted for publication.

CHAPTER 1.

Introduction to OLEDs

1.1 History

The first electroluminescent (EL) organic devices were made in the 1950s by Bernanose et al., and were operated in AC-mode.[1] DC devices using single crystal anthracene were achieved in the early 1960s by Pope et al.[2] Following in 1977, relatively efficient devices also based on anthracene crystals were made, but still required high operating voltage.[3] Tang and VanSlyke demonstrated the potential of organic light-emitting diode (OLED) technology in 1987 by achieving external quantum efficiency (EQE) of $\sim$1% with the first multilayer tris(8-hydroxyquinolinato)aluminium (Alq_3)-based OLED.[4] Here, light emission was detected at a low bias of $\sim$ 2.5 V. Soon after, in 1990, Friend and coworkers reported the first polymer light-emitting diode (PLED) based on poly(p-phenylene vinylene) (PPV).[5] The PPV film was formed by annealing a film of a solution-processable precursor polymer. These discoveries kick-started the broader drive for research of organic devices.

Work by Forrest and coworkers in 1998 introduced phosphorescent OLEDs,[6] in which the phosphorescent emitting guest platinum octaethylporphyrin (PtOEP) increased efficiency compared to fluorescent guests by using both triplet and singlet excited states, also called excitons, for emission. Fluorescence is produced only by singlet excitons, which have a theoretical limit of 25% of the total exciton population. Using phosphorescent emitters increases the theoretical internal quantum efficiency to 100%.

In 1997, Tohoku Pioneer commercialized the first OLED display.[7] Now OLED displays

are commercially available in mobile phones, cameras, and TVs. Samsung and LG both have 55″ OLED TVs available in the consumer market.

Current research pushes for higher efficiency and longer lifetime of organic devices by using creative structures and novel materials. Currently the record EQE reaches 63%, with max power efficiency of 290 lm/W[8] using a green phosphorescent guest emitter. White OLEDs (WOLEDs) with power efficiency of $\sim$ 90 lm/W rival the efficiency of fluorescent tubes (60-70 lm/W).[9] For comparison, the record efficiency for fluorescent-based OLEDs is $\sim$ 6% EQE, specifically from a material exhibiting triplet-triplet fusion to singlets.[10] The record lifetime of a green OLED has reached one million hours[11], while record red and blue OLED lifetimes are around 62,000 and 38,000 hours, respectively. Here lifetime refers to the time until luminescence decays to half of the starting 1,000 cd/m^2 and is based on accelerated lifetime tests. OLED stability is largely dependent on the effectiveness of the encapsulation technique, as organic materials are highly susceptible to degradation from exposure to water, oxygen, and UV light.

OLEDs are particularly attractive because of a few basic properties that distinguish organic electronics from other technologies. In displays, organics yield brilliant colors, low power consumption, and wide viewing angles. There is no need for backlight, unlike LCD displays, which enables an OLED display to be very thin. The Samsung 55″ OLED TV panel on the market now is 4 mm thin. OLEDs can also be fabricated on flexible substrates, possibly producing rollable screens, and can be used for transparent displays. Current market trends show new curved OLED TVs that give more depth to the image.[12] The flexible and thin nature inherent in OLEDs make them particularly suited for on-chip applications, such as sensing and spectrometry, which is discussed in chapter 5.

OLEDs are diffuse, large area light sources, which are attractive characteristics for area lighting. OLEDs also present the opportunity for artistic lighting, having the ability to form curved or flexible shapes. Current lamps on the market use Lumiotec or Philips Lumiblade WOLED panels.[13]

1.2 Organic Semiconducting and Light-Emitting Materials

Organic materials are defined by being primarily composed of carbon. Small molecule organic materials are those with a low molecular weight (<1k), e.g. Alq_3, see Fig. 1.1. Polymers have large molecular weight that can vary greatly and are made up of a repeated base segment, the monomer. If a polymer is made up of one monomer, it is called a homopolymer, e.g. poly[2-methoxy-5-(2-ethylhexyloxy)-1,4-phenylenevinylene] (MEH-PPV), see Fig. 1.1. If there is more than one repeat unit, it is labeled a copolymer, e.g. polystyrene-block-poly(methyl methacrylate) (PS-b-PMMA). The organic materials are semi-conducting when the molecule consists of alternating double/single bonds. Such compounds are labeled conjugated hydrocarbons and are the basis of organic electronics.

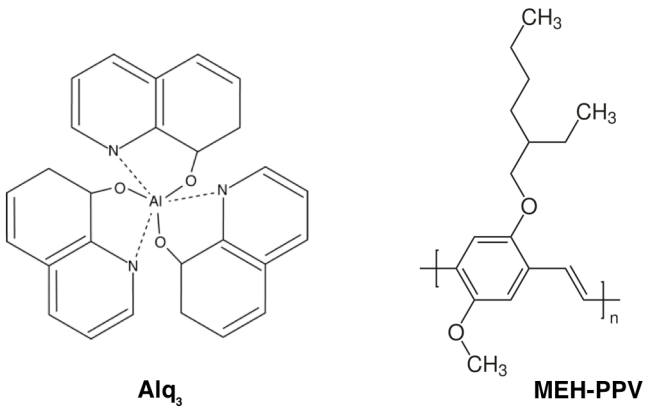

Figure 1.1 Chemical structures of Alq_3 and MEH-PPV

Organic semiconductors do not have free electrons as we understand in the conduction in metals but instead have electrons that are shared in a conjugated system. The charge transport is dominated by hopping between electron orbitals. When a carbon atom forms molecular bonds, having four valence electrons, its atomic orbitals form hybrid sp^2 or sp^3 orbitals, depending on the type of bond formation. In the case of a single bond, formed between, e.g., C-C or C-H, a sigma bond is formed from the merger of two atomic orbitals. The resulting molecular orbital (MO) is either bonding (lower energy) or anti-bonding (higher energy). A double bond can be

formed between two carbon atoms with sp^2 hybridized orbitals. The valence electrons will be in three in-plane hybrid orbitals and one non-hybrid p-orbital perpendicular to that plane. One sp^2 orbital from each atom will form a sigma bond (as described above), while the p-orbital electrons will form the second bond of the double bond, a π-bond, see Fig. 1.2.

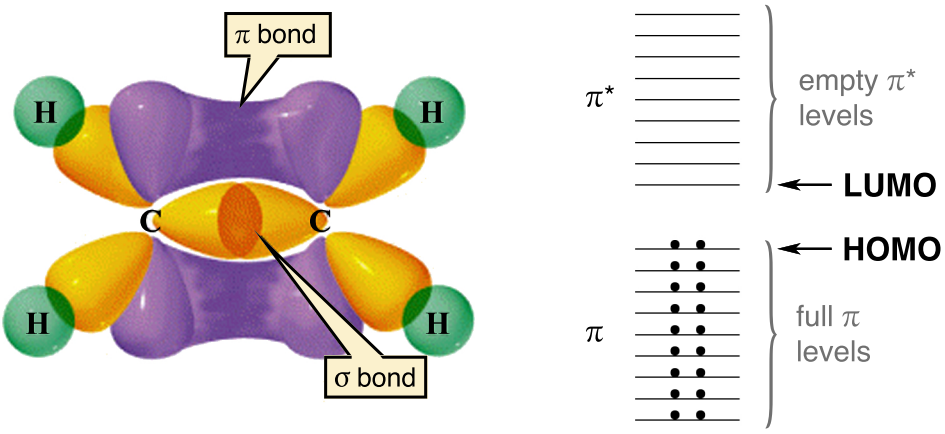

Figure 1.2 Diagrams of a double bond composed of π and sigma bonds; Diagram of filled and empty energy levels

Expanding this scenario into a ring or long chain of carbon atoms, the MOs become two semi-continuous bands of bonding and antibonding orbitals, forming the analog to an inorganic semiconductor's valance and conduction bands, respectively. According to the Pauli exclusion principle, each energy state can be occupied by two electrons (spin up and spin down). Therefore, in the ground state, only the bottom half of the energy levels are filled, as shown in Fig. 1.2. The filled energy levels are capped with the highest occupied molecular orbital (HOMO) and the empty levels begin at the lowest unoccupied molecular orbital (LUMO). The gap of unavailable energy states, called the energy gap or the band gap, has energy of E_g $\sim$ 1.5-3.5 eV in most organic materials,[14] covering the entire visible range, and defines the materials as semiconductors.

The well-known molecule benzene, a ring of six carbon atoms, is a good example of an alternating double-single bond system, see Fig. 1.3. Because of the overlapping MO wavefunc-

tions, the π-bond electrons become delocalized throughout, forming a π-conjugated system of semiconducting electrons. Such a system can be formed in rings, such as that of benzene, or in long chains, as seen in semi-conducting polymers such as polyacetylene.

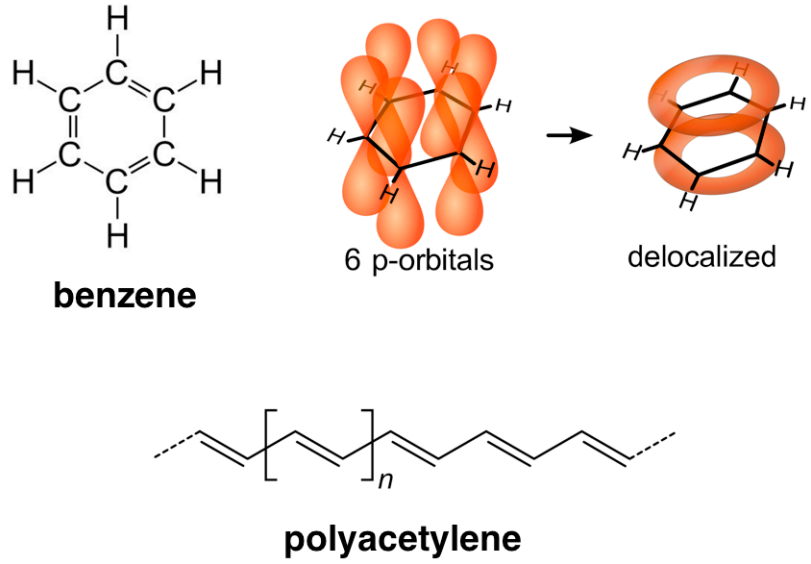

Figure 1.3 Chemical structures of benzene and polyacetylene, with a diagram of delocalized π-electrons in benzene

The structure and properties of π conjugated materials can be tuned via synthesis. Emission color (i.e. band gap), electronic properties such as charge mobility, and processing characteristics such as solubility can be modified by changing the molecular structure. Such capability has presented large opportunities for progress in chemical design, as is discussed in chapter 3.

1.3 Film and Device Fabrication

The thin films used in organic electronic devices are fabricated mainly by two processes: thermal evaporation and solution processing.

In thermal evaporation, the deposition is done in a vacuum chamber, at pressures P $\sim$ 4 x 10^{-7}mbar, located in an inert atmosphere glove box (nitrogen or argon). The organic material is placed in a quartz crucible that is heated by a tungsten wire basket. In the case of inorganic

or metal thin films, the material is placed directly on the wire basket. The basket is heated via high current flow, roughly 10–40 A. A substrate, typically glass or plastic, is placed at the top of the vacuum chamber. As the material evaporates, it coats the substrate surface evenly. The thickness of the deposited layer is monitored by a quartz crystal thickness monitor and controlled via the basket current. Various shutters are used to either control the exposed substrate area or to cover the material source.

Thermal evaporation yields even, high-density thin films and enables the fabrication of multi-layered devices, which have proven to be reliably highly efficient. Only small molecules can be thermally evaporated, as polymers will chemically degrade at high temperatures before they evaporate. Small molecules are generally more efficient and longer-lived when incorporated into devices.[15,16] However, thermal evaporation is not easily transferred to large-scale production. The requirement of vacuum environment increases production cost and the evenness of the coating will decrease with increasing substrate size because of limited chamber height.

Solution processing is much more viable for large-scale production, as various printing techniques can be used such as roll-to-roll printing, screen printing, and doctor blade.[17] Polymers are generally used as the primary material for solution-based methods, due to high solubility and good film formability.[18] However, some small molecules have proven quite well in solution-processed devices.[19] In fact, using small molecules to create efficient solution processed OLEDs is one of the main topics of the works presented herein. The solution processing technique referenced most in this dissertation is spin-coating. In this case, the material is dissolved in an appropriate solvent and dispensed onto a substrate, typically glass or plastic. The substrate is then spun at high speeds ($\sim$1000–4000 rpm) so that excess material is thrown off, leaving a thin, even film (t $\sim$ 30–60 nm), see Fig. 1.4.[20] Film thickness is determined mainly by the spin speed and the solution concentration. Increasing the spin speed will decrease the film thickness, while increasing the solution concentration will increase the thickness. The final thickness is reached after approximately 20 seconds, but the substrate is usually spun for

40–60 seconds to further dry the film before baking. The films are then baked to rid the film of residual solvent that could cause solvent-induced trapping and material degradation.[21] The baking temperature is typically below the glass transition temperature of the material, so that the film remains amorphous.

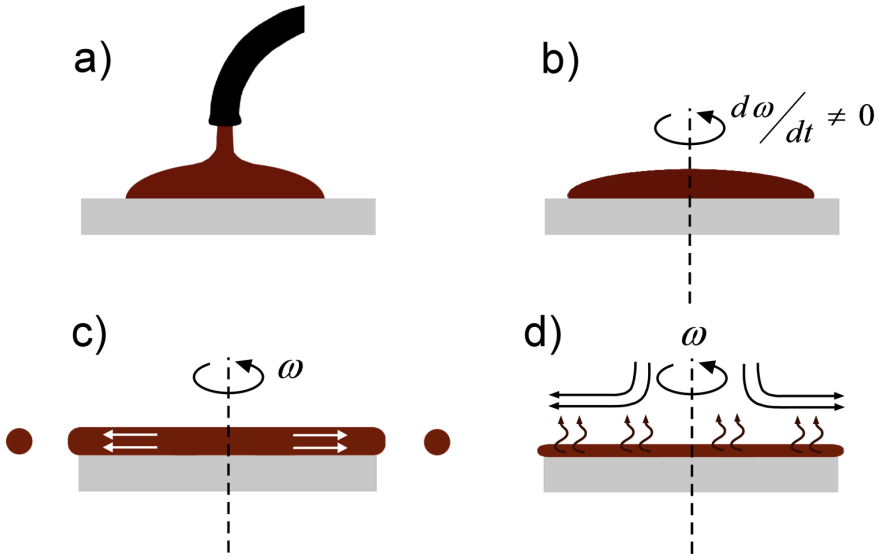

Figure 1.4 Spin-coating process: (a) dispensation, (b) acceleration, (c) flow dominated, (d) evaporation dominated[20]

Solution processing also presents opportunity for complex doping strategies. Thermal evaporation requires precise evaporation rates to obtain particular material ratios and becomes prohibitively difficult with more than two materials. In contrast, a simple weight ratio calculation can yield a precise multi-dopant solution and resultant film using solution processing.

1.4 OLED Device Structure

As mentioned earlier, the simplest OLED structure used in the first devices consisted merely of an organic thin film sandwiched between two metal electrodes. Vast improvements in efficiency were attained when a multi-layered structure was used, which improves charge injection, increases emission efficiency, and reduces various quenching processes. A typical structure is shown in Fig. 1.5. Between two conducting electrodes are the hole injection layer

(HIL), hole transport layer (HTL), emission layer (EML), electron transport / hole blocking layer (ETL, HBL), and electron injection layer (EIL).

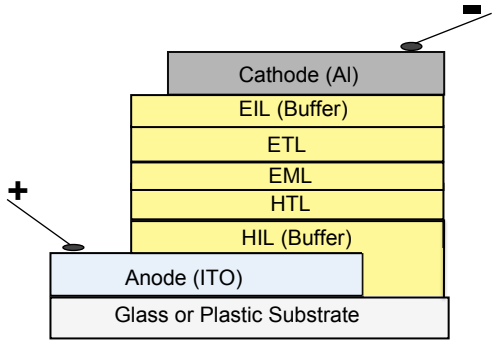

Figure 1.5 Typical OLED structure

Indium tin oxide (ITO) is often used as the transparent conducting electrode, though recent research has highlighted alternative transparent conductors, such as metal nanowires.[22] Semi-transparent metal layers, such as thin silver, are also used and further affect the device by creating an optical microcavity. ITO and silver are most often used as the anode, as their deep work functions facilitate hole injection.[23,24] The opposite electrode is most often thick ($\sim$100 nm) aluminum, which acts as an efficient cathode with a shallow work function[23] to enable electron injection. Aluminum also acts as a mirror, reflecting backward emission toward the transparent or semitransparent end.

Injection layers such as LiF and MoO_3 have a two-fold purpose at the cathode and anode, respectively. First, the EIL and HIL create a dipole layer at the interface, facilitating better charge injection by decreasing the injection energy barrier.[14,25] Injection layers also shield excitons from metal quenching caused by field exposure and gap states at the interface.[14,26] The HTL, such as N,N′-bis-(3-Naphthyl)-N,N′-biphenyl-(1,1′-biphenyl)-4,4′-diamine (NPB), and ETL, such as bathophenanthroline (BPhen), are chosen for their hole and electron mobility, respectively, and can improve efficiency by improving charge balance. The EML consists of a material in which efficient, emissive recombination of excitons (electron-hole pairs) can occur. In guest:host OLEDs, the EML is a mixed layer consisting mostly of a host material, usually

chosen for good mobility and a band gap wider than the emitting guest, and a small percentage (typically < 5 wt%) of a guest, chosen for efficient emission.

1.5 Charge Transport

As mentioned, charge transport in organics proceeds by hopping, as opposed to band transport seen in inorganic semiconductors. While charges are delocalized on the molecules, transfer between molecules (or between π-conjugation discontinuities) occurs by hopping between adjacent energy states, see Fig. 1.6. The transfer rate is dependent mainly on the energy difference of and the distance between the sites.[14] Energy levels vary not only among differing materials but also within a material depending on molecular interactions and disorder. Often in polymers the mobility of the material decreases if the chain is kinked or bent, causing disruption in the π-conjugation.

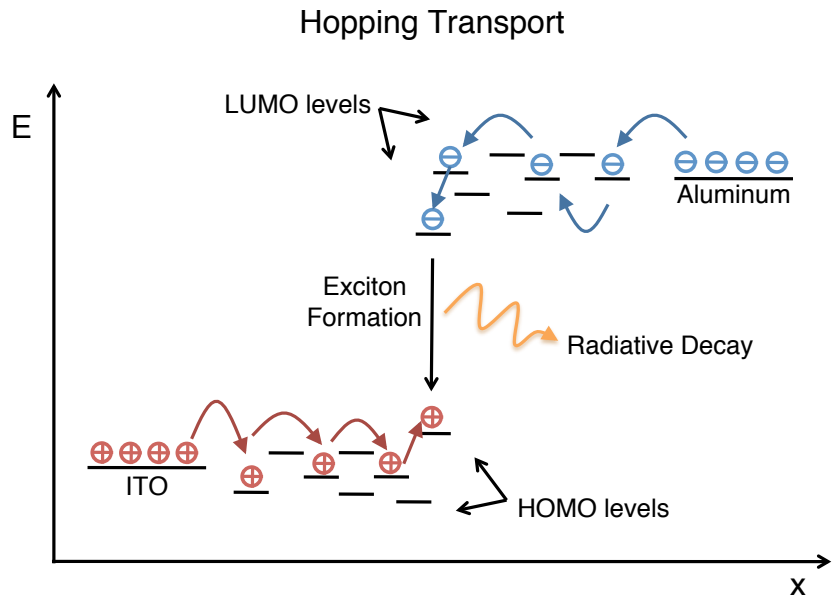

Figure 1.6 Diagram of hopping transport in an organic semiconducting device

Figure 1.7 shows the energy diagram of a device under forward bias. There is a roughly triangular barrier for both electron and hole injection.[14] As mentioned above, various materials are used to decrease this barrier and, consequently, decrease the drive voltage of the device.

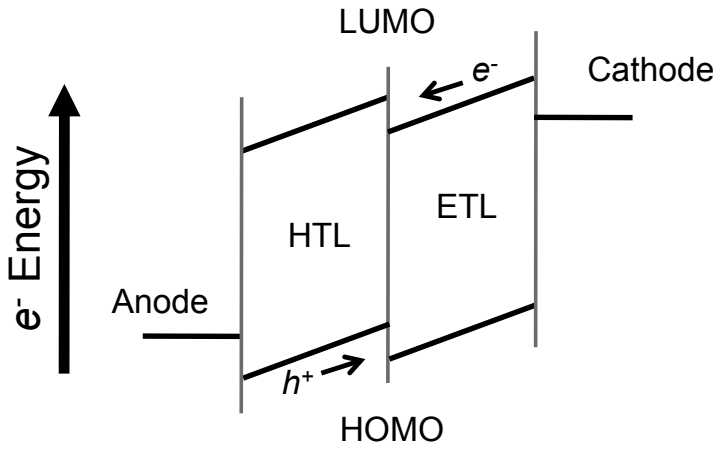

Figure 1.7 OLED under forward bias

Charge transport within the device is limited by injection in the low current regime, and therefore depends greatly on the characteristics of the metal–injection layer and injection layer–organic interfaces.[14] The charges can tunnel through the barrier or hop through via gap states at the interface. The current–voltage relationship can be approximated by the following:

$$J \propto V^2 exp\left(-\frac{b}{V}\right) \tag{1.1}$$

where b is a parameter dependent on the characteristics of the interface materials.

As drive voltage is increased, the injection becomes high and the current is limited by the lowest mobility material. Low mobility produces charge buildup, which partially screens the applied field, bringing the devices into the space-charge limited current (SCLC) regime.[14] The current–voltage relationship is superlinear:

$$J \propto V^{\alpha} \tag{1.2}$$

As deep traps in the organic materials are filled, the current increases rapidly and the device operates in the trapped-charge limited current (TCLC) regime.[27] Here, the current–voltage relationship is similar to eq.1.2, with $7 \leq \alpha \leq 9$.[14]

Mobility of a particular material can be determined by various methods, including time-of-flight, Hall effect, and delayed EL. The mobility is dependent on the field as shown in eq.1.3

$$\mu(E,T) = \mu(0,T)\ exp(\gamma\sqrt{E}) \tag{1.3}$$

where T is the temperature, $\mu(0,T)$ is the low field mobility, and γ is an empirically determined coefficient.[14] At low temperature, the mobility is dominated by effects of shallow traps. Therefore the mobility will increase with temperature, as hopping is thermally assisted. At higher temperature, the mobility goes like T^{-n}, decreasing with increasing temperature, as phonon scattering dominates.[27,29]

1.6 Exciton Formation and Recombination

Electrons and holes injected into the organic layer form more stable, lower energy polarons.[14] A polaron is a mobile charge that carries a lattice distortion, or phonons, with it as it travels. Unlike delocalized phonons in inorganic crystals, phonons in organic materials are localized vibrations on a molecule or conjugated segment. Two polarons that have the same charge can pair to form a bipolaron, which is likely stabilized by a counter charge of opposite sign.

A positively- and negatively-charged polaron (hole and electron, respectively) can combine to form an exciton. The most common type of exciton in organic semiconductors is a Frenkel exciton, where the electron and hole are both localized on the same molecule. The binding energy of such a pair is $E_b \sim 0.5$ eV with a radius of $r < 5$ Å.[27] The pair can also form a charge transfer exciton that is similar to the Wannier excitons found in inorganic semiconductors, in which the electron and hole are on neighboring molecules. In this case the charges are separated by $r \sim 10$ Å, but are still correlated.

As we know from quantum mechanics, the electron and hole have a spin of 1/2. In combining, the pair can form a singlet (spin-0) or a triplet (spin-1) exciton (SE or TE) with probability of 1/4 or 3/4, respectively, according to spin statistics. As the ground state is a singlet, only the SE is allowed by spin conservation to decay radiatively, see Fig.1.8. Light emitted by radiative recombination of SEs is called fluorescence. The lifetime of a fluorescent decay is of the order of 0.1–100 ns.

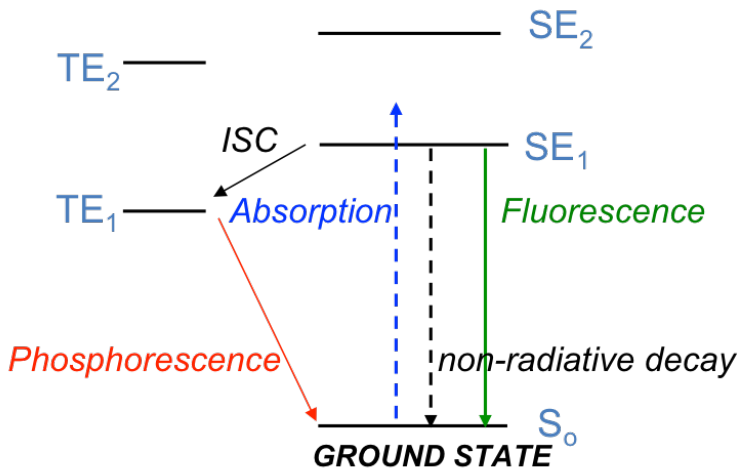

Figure 1.8 Jablonski diagram showing energy levels of SEs, TEs, and the ground state; ISC: inter-system crossing

Phosphorescent materials (or phosphors) enable radiative decay of both SEs and TEs. These materials generally employ a heavy atom that alters the probability of a triplet pair decaying to the ground state (lifetime $\sim$ μs–ms) and enables intersystem crossing (ISC) (SE $\rightarrow$TE) through spin-orbit coupling.[28,30,31] Phosphors such as tris(2-phenylpyridine) iridium(III) ($Ir(mppy)_3$) are often used as emitters in OLEDs, but are not the focus of this dissertation. Although phosphorescent materials are able to produce highly efficient luminescence, there still exists some difficulty with deep blue phosphors[32] and consequently fluorescent blue emitters are often used.

Excitons can also recombine nonradiatively, releasing phonons, or dissociate into polarons. SE quenching processes are often caused by interaction with free or trapped polarons or with

TEs, as shown in the equations below.[14] The SE energy can also be transferred to the quenching species, resulting in an excited TE* or polaron, $p^{+/-}*$.

$$p^{+/-} + SE \rightarrow p^{+/-*} + phonons \tag{1.4}$$

$$p^{+/-} + SE \rightarrow p^{+/-} + p^{+} + p^{-} + phonons \tag{1.5}$$

$$TE + SE \rightarrow TE^{*} + phonons \tag{1.6}$$

In guest:host OLEDs, emission from the guest can be initiated via two main paths. An exciton can be formed directly on the guest by charge trapping on the guest. The exciton can also form on the host and be transferred to the guest via energy transfer.

Cascade energy transfer, also known as "trivial" (for its simplicity), involves fluorescence emitted by the host that is then reabsorbed by the guest. The distance between the host and guest molecules can exceed 100 Å and the transfer probability decreases slowly with increasing distance, as compared to the following mechanism.[27,28]

The more common form of energy transfer is Förster resonance energy transfer (FRET). In the case of FRET, the host transfers the exciton energy to the guest by exchanging a "virtual" photon that is transferred via dipole-dipole interaction.[28] The transfer is called virtual because it occurs at a rate too fast for an actual photon to be emitted by the host and absorbed by the guest. A few characteristics dictate efficient FRET, including sufficient overlap of the host emission and guest absorption spectra, host-guest separation, and molecular dipole alignment. The rate of FRET from host to guest is defined by

$$K_{H\rightarrow G} = \left(\frac{1}{\tau_D}\right)\left(\frac{R_o}{R}\right)^6 \tag{1.7}$$

where R_o is the critical transfer distance at which the transfer rate is similar to the rate of radiative decay.[27] The alignment of transition dipole moments of the host and guest can be described by

$$f = \left(\frac{3}{2}\right)\left[\boldsymbol{\mu}_H \cdot \boldsymbol{\mu}_G - 3(\boldsymbol{\mu}_H \cdot \boldsymbol{r})(\boldsymbol{\mu}_G \cdot \boldsymbol{r})\right] \tag{1.8}$$

where $\boldsymbol{\mu}_H$, $\boldsymbol{\mu}_G$, and $\boldsymbol{r}$ are unit vectors parallel to the host dipole, guest dipole, and separation vector, respectively. R_o can then be is calculated via eq.1.9

$$R_o = \left[\frac{3f}{4\pi}\int\left(\frac{\lambda}{2\pi}\right)^4 F_H(\omega)\sigma_G(\omega)d\omega\right]^{1/6} \tag{1.9}$$

where λ is the wavelength of radiation and the integral determines the amount of spectral overlap of host emission (F_H) and guest absorption (σ_G). In chapter 3, the effect of molecular shape on FRET is discussed in terms of possible dipole changes.

Dexter transfer is a less common form of energy transfer in which an electron is also exchanged.[27]

1.7 Device Efficiency and Outcoupling

OLED brightness in the visible range is measured in terms of candela (cd), the SI unit of luminous intensity. The candela is weighted by the luminosity function (shown in Fig.1.9), which describes the wavelength dependence of the sensitivity of the human eye. Therefore, an OLED with emission in the green would have higher cd/m^2 brightness than a blue OLED, even if the emitted power in watts (W) is equal. Lumens is a measure of luminous flux: 1 lm = 1 cd·sr. The emission profile of an ITO-based device on glass will be approximately a

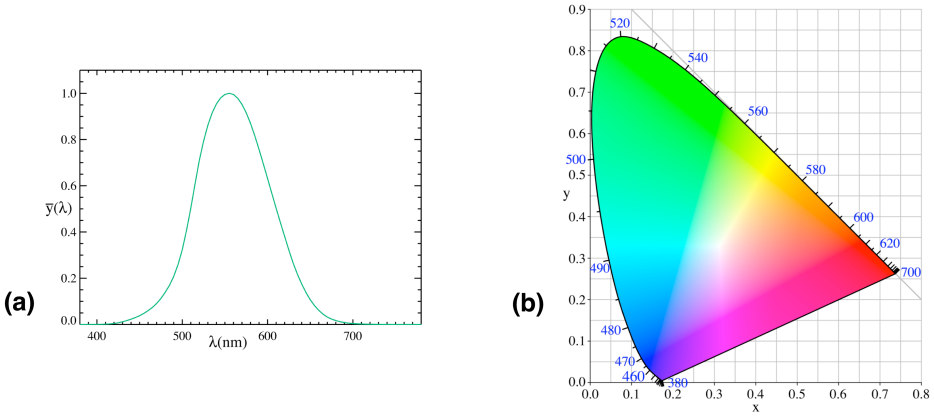

Figure 1.9 (a) Photopic luminosity function and (b) CIE 1931 color space diagram

Lambertian distribution, i.e. the intensity will go like $I_{max}cos(\theta)$. Therefore the total luminous flux in the forward direction would be πsr $\cdot I_{max}$. These units are helpful in defining brightness and efficiencies, such as luminous efficiency (cd/A) or power efficiency (lm/W), in terms of eye sensitivity. When comparing efficiencies of OLEDs with different spectra, it is necessary to calculate the external quantum efficiency (EQE, η_{ext}), which is equal to the ratio of photons emitted in the forward direction to electrons injected and can be written as

$$\eta_{ext} = \xi\gamma r_{ST}\eta_{PL} \tag{1.10}$$

where ξ is the outcoupling efficiency (fraction of photons emitted from front), γ is the ratio of excitons to injected electrons (fraction of electrons that pair with holes), r_{ST} is the ratio of SE to TE ($\sim$0.25 from simple spin statistics), and η_{PL} is the photoluminescence (PL) quantum yield (the efficiency of PL emission at a given excitation energy).[14] The outcoupling efficiency (ξ) can be estimated by the relationship

$$\xi \sim \frac{1}{2n^2} \tag{1.11}$$

where n is the refractive index of the organics, ~ 1.7. In a typical ITO-based device on glass, $\sim 20\%$ of the emission is extracted, the rest is waveguided either in the substrate ($\sim 30\%$) or the ITO/organic layers ($\sim 50\%$).[33,34] Outcoupling can be improved by lenses, index matching materials, and photonics structures.[35] The efficiency of exciton formation (γ) can be optimized by choosing materials to improve charge balance, as discussed in section 1.4. EQE can be calculated experimentally by eq.1.12

$$\eta_{ext} = \frac{\pi e}{683\ \hbar c}\,\eta_L\,\frac{\int g(\lambda)\lambda d\lambda}{\int g(\lambda)K(\lambda)d\lambda} \tag{1.12}$$

where η_L is luminous efficiency, $g(\lambda)$ is the OLED spectrum, and $K(\lambda)$ is the Commision International de l'Eclairage chromaticity (CIE) standard Photopic Luminous Efficiency Function.[36] CIE 1931 color space (shown in Fig.1.9b) defines each spectrum by giving it coordinates on a plane, enabling discussion of various shades of colors.

References

[1] A. Bernanose, M. Comte, P. Vouaux, *J. Chem. Phys.* **50**, 65 (1953).

[2] M. Pope, H.P. Kallmann, P. Magnante, *J. Chem. Phys.* **38**, 2042 (1963).

[3] J. Gu, M. Kawabe, K. Masuda, S. Namba, *J. Appl. Phys.* **48**, 2493 (1977).

[4] C. W. Tang, S. A. VanSlyke, *Appl. Phys. Lett.* **51**, 913 (1987).

[5] J. H. Burroughs, D. D. C. Bradley, A. R. Brown, R. N. Marks, K. Mackay, R. H. Friend, P. L. Burns, A. B. Holmes, *Nature* **347**, 539 (1990).

[6] M. A. Baldo, D. F. O'Brien, Y. You, A. Shoustikov, S. Sibley, M. E. Thompson, S. R. Forrest, *Nature* **395**, 151 (1998)

[7] http://pioneer.jp/topec/jigyo/oled/index-e.html

[8] Z. B. Wang, M. G. Helander, J. Qiu, D. P. Puzzo, M. T. Greiner, Z. M. Hudson, S. Wang, Z. W. Liu, Z. H. Lu, *Nature Photonics* **5**, 753 (2011).

[9] S. Reineke, F. Lindner, G. Schwartz, N. Seidler, K. Walzer, B. Lssem, K. Leo, *Nature* **459**, 234 (2009).

[10] C.-J. Chiang, A. Kimyonok, M. K. Etherington, G. C. Griffiths, V. Jankus, F. Turksoy, A. P. Monkman, *Adv. Funct. Mater.* **23**, 739 (2013)

[11] http://www2.dupont.com/Displays/en_US/news_events/article20090527.html

[12] http://www.oled-info.com/oled_devices/tv

[13] http://www.oled-info.com/oled_devices/oled_lighting_device

[14] J. Shinar, V. Savvateev, in *Organic Light-Emitting Devices: A Survey*, ed. J. Shinar, Springer, New York, 2004, ch. 1.

[15] C. Adachi, M. A. Baldo, S. R. Forrest, M. E. Thompson, *Appl. Phys. Lett.* **77**, 904 (2000).

[16] J. S. Huang, M. Pfeiffer, A. Werner, J. Blochwitz, K. Leo, and S. Y. Liu, *Appl. Phys. Lett.* **80**, 139 (2002).

[17] D.A. Pardo, G.E. Jabbour, and N. Peyghambarian, *Adv. Mater.* **12**, 1249 (2000).

[18] M. Granstrom and O. Inganas, *Appl. Phys. Lett.* **68**, 147 (1996).

[19] K.-H. Kim, S.-Y. Huh, S.-m. Seo, and H. H. Lee, *Appl. Phys. Lett.* **92**, 093307 (2008); L. Hou, L. Duan, J. Qiao, W. Li, D. Zhang, and Y. Qiu, *Appl. Phys. Lett.* **92**, 263301 (2008); D. Wang, Z. Wu, X. Zhang, D. Wang, and X. Hou, *J. Lumin.* **130**, 321 (2010); D. Wang, Z. Wu, X. Zhang, B. Jiao, S. Liang, D. Wang, R. He, and X. Hou, *Org. Electron.* **11**, 641 (2010); L. He, J. Liu, Z. Wu, D. Wang, S. Liang, X. Zhang, B. Jiao, D. Wang, and X. Hou, *Thin Solid Films* **518**, 3886 (2010); M. Cai, T. Xiao, E. Hellerich, Y. Chen, R. Shinar, and J. Shinar, *Adv. Mater.* **23**, 3590 (2011); E. S. Hellerich, J. J. Intemann, M. Cai, R. Liu, M. D. Ewan, B. C. Tlach, M. Jeffries-EL, R. Shinar and J. Shinar, *J. Mater. Chem. C* **1**, 5191 (2013).

[20] S. L. Hellstrom, *Basic Models of Spin Coating*, Stanford University, (2007), URL: http://large.stanford.edu/courses/2007/ph210/hellstrom1/.

[21] L. Duan, L. Hou, T.-W. Lee, J. Qiao, D. Zhang, G. Dong, L. Wang, Y. Qiu, *J. Mater. Chem.* **20**, 6392 (2010).

[22] M.-G. Kang, H. J. Park, S. H. Ahn, T. Xu, L. J. Guo, *IEEE J. Sel. Top. Quant.* **6**, 1807 (2010); L. Hu, H. Wu, Y. Cui, *MRS Bulletin* **36**, 760 (2011); D. P. Puzzo, M. G. Helander,

P. G. O'Brien, Z. Wang, N. Soheilnia, N. Kherani, Z. Lu, G. A. Ozin, *Nano Lett.* **11**, 1457 (2011).

[23] P. A. Tipler, R. A. Llewellyn, *Modern Physics, 3rd Ed.*, W.H. Freeman, 1999.

[24] Y. Park, V. Choong, Y. Gao, B. R. Hsieh, C. W. Tang, *Appl. Phys. Lett.* **68**, 2699 (1996); Kiyoshi Sugiyama, Hisao Ishii, Yukio Ouchi, Kazuhiko Seki, *J. Appl. Phys.* **87**, 295 (2000).

[25] H.Ishii, K.Sugiyama, E.Ito, K.Seki, *Adv. Mater.* **11**, 605 (1999).

[26] V.-E. Choong, Y. Park, Y. Gao, B. R. Hsieh, C. W. Tang, *Macromol Symp* **125**,83 (1998).

[27] M. Pope, C. E. Swenberg, *Electronic processes in organic crystals and polymers, 2nd Ed.*, Oxford University Press, 1999.

[28] M. Klessinger, J. Michl, *Excited States and Photochemistry of Organic Molecules*, VCH Publishers, New York, 1995.

[29] B. L. Anderson, R. L. Anderson, *Fundamentals of Semiconductor Devices*, McGraw-Hill, Boston, 2005.

[30] M. A. Baldo, M. E. Thompson, S. R. Forrest, *Nature* **403**, 750 (2000).

[31] M. A. Baldo, D. F. OBrien, Y. You, A. Shoustikov, S. Sibley, M. E. Thompson, S. R. Forrest, *Nature* **395**, 151 (1998).

[32] K. S. Yook, J. Y. Lee, *Adv. Mater.* **24**, 3169 (2012).

[33] M. Cai, Z. Ye, T. Xiao, R. Liu, Y. Chen, R. W. Mayer, R. Biswas, K.-M. Ho, R. Shinar, J. Shinar, *Adv. Mater.* **24**, 4337 (2012).

[34] D. S. Mehta, K. Saxena, *Proc. of ASID '06*, 198 (2006).

[35] J.-M. Park, Z. Gan, W. Y. Leung, R. Liu, Z. Ye, K. Constant, J. Shinar, R. Shinar, K.-M. Ho, *Opt. Express* **19** A786 (2011); Y. Sun, S. R. Forrest, *J. Appl. Phys.* **100**, 073106 (2006); J.Lim, S.S.Oh, D.Y.Kim, S.H.Cho, I.T.Kim, S.H.Han, H.Takezoe, E.H.Choi, G.S.Cho, Y.H.Seo, S. O. Kang, B. Park, *Opt. Express* **14**, 6564 (2006); H.Y.Lin, Y.H.Ho, J.H.Lee, K.Y.Chen, J.H.Fang, S.C.Hsu, M.K.Wei, H.Y.Lin, J.H.Tsai, T.C. Wu, *Opt. Express* **16**, 11044 (2008); S.-H. Eom, E. Wrzesniewski, J. Xue, *Org. Electron.* **12**, 472 (2011); W.-K. Huang, W.-S. Wang, H.-C. Kan, F.-C. Chen, *Jpn. J. Appl. Phys.* **45**, L1100 (2006); J. A. Zimberlin, P. Wadsworth, A. J. Crosby, *Cell Motil. Cytoskeleton* **65**, 762 (2008); S. Reineke, F. Lindner, G. Schwartz, N. Seidler, K. Walzer, B. Lssem, K. Leo, *Nature* **459**, 234 (2009); R. Liu, Z. Ye, J.-M. Park, M. Cai, Y. Chen, K.-M. Ho, R. Shinar, J. Shinar, *Opt. Express* **19**, A1272 (2011); A. Bay, N. Andre, M. Sarrazin, A. Belarouci, V. Aimez, L. A. Francis, J. P. Vigneron, *Opt. Express* **21**, A179 (2013).

[36] H. Lia, C. Zhanga, D. Lia, Y. Duan, *J. Lumin.* **122**, 626 (2007).

CHAPTER 2.

Fluorescent polymer guest:small molecule host solution-processed OLEDs

Emily S. Hellerich,[a] Jeremy J. Intemann,[b] Min Cai,[a] Rui Liu,[a] Monique D. Ewan,[b] Brian C. Tlach,[b] Malika Jeffries-EL,[b] Ruth Shinar,[c] and Joseph Shinar[a]

published in: *J. Mater. Chem. C* **1**, 5191 (2013).

[a]Ames Laboratory-USDOE and Department of Physics and Astronomy, Iowa State University, Ames, IA 50011, USA.

[b]Department of Chemistry, Iowa State University, Ames, IA 50011, USA

[c]Microelectronics Research Center and Department of Electrical and Computer Engineering, Iowa State University, Ames, IA 50011, USA.

2.1 Abstract

Solution-processed OLEDs with polymer hosts and polymer or small molecule guests have been studied extensively. More recently, efficient solution-processed OLEDs with small molecule hosts and small molecule guests were also reported. However, small molecule hosts of polymer guests in solution-processed fluorescent OLEDs have not been investigated. In this work guest:host systems consisting of the small molecule 4,4′-bis(9-carbazolyl)-biphenyl (CBP) as host to polymer guests such as novel benzobisoxazole (BBO)-containing copolymers and well-known poly(2-methoxy-5-(2′-ethyl-hexyloxy)-1,4-phenylene vinylene) (MEH-PPV) are compared to those with poly(*N*-vinyl carbazole) (PVK) host, which previously yielded

highly efficient phosphorescent OLEDs. In the case of MEH-PPV, guest:host OLEDs are also compared to those with a neat MEH-PPV emitting layer. It is found that replacing the polymer host PVK with the small molecule host CBP improves efficiencies by up to 100%. A blue emissive BBO-polymer:CBP device reaches a luminous efficiency ($\eta_{L,max}$) of 3.4 cd/A (external quantum efficiency η_{ext} = 2.4%), while the PVK-based device exhibits $\eta_{L,max}$ = 1.7 cd/A (η_{ext} = 1.2%). A green emissive BBO:CBP OLED exhibits $\eta_{L,max}$ = 5.7 cd/A (η_{ext} = 2.1%), while that in the PVK host is 3.1 cd/A (η_{ext} = 1.1%). For MEH-PPV:CBP these values are 3.7 cd/A (η_{ext} = 1.4%), compared to 2.9 cd/A (η_{ext} = 1.0%) for MEH-PPV:PVK and 0.7 cd/A (η_{ext} = 0.4%) for the neat MEH-PPV device. Possible origins of the improvement are discussed, including increased charge mobility, smoother film morphology, and the potential effect of multiple non-coiling host small molecules (in contrast to the likely coiled PVK) surrounding a polymer guest.

2.2 Introduction

The wide use of organic light emitting diodes (OLEDs) is materializing as devices exhibit enhanced performance. Still, there is a need for new emissive materials with higher efficiency, especially in the sky and deep blue wavelengths, and host materials that are compatible with emissive guests in band energy and processability. Much attention has been placed on finding quality solution-processable materials amenable to roll-to-roll fabrication methods. High solubility and good film formability intrinsic to polymers have led to their use in the majority of solution-processed devices.[1–4] As an example, the well-known polymer poly(*N*-vinyl carbazole) (PVK) has been successfully used as a host for highly efficient devices (up to 65 lm/W)[5] with small molecule phosphorescent guests.[2,6–10] Hence, it is often the choice host for new polymer emissive guests that cannot be used in a neat film form due to self-quenching.[11–13] However, the poor stability and low charge carrier mobility of PVK beg for exploration of new options.[14] To our knowledge, no investigation has been reported on the

use of small molecules as hosts to the vast catalog of emissive polymers.

Small molecule OLEDs that are advantageous due to their higher charge mobility, stability and efficiency are typically fabricated by thermal evaporation.[15–19] Previous studies have reported intrinsic problems with solution-processed small molecules, including low solubility, tendency to crystallize upon deposition, and a less dense film structure, which leads to poorer stability due to film porosity.[1,15,20,21] However, by adequately controlling the morphology through use of high boiling point solvents and optimized baking, studies have demonstrated efficient solution-processed small molecule devices.[8,9,15,20,22] Specifically, the small molecule 4,4′-bis(9-carbazolyl)-biphenyl (CBP) has been successfully employed in solution-processed OLEDs with small molecule phosphorescent and hole- and electron-transporting guests to yield highly efficient devices (70 lm/W without outcoupling enhancing structures).[1,9]

Investigations of polymer–small molecule mixtures, with the exception of phosphorescent-doped polymer devices, have largely focused on weight ratios larger than the typical dopant level, i.e. 10-50 wt% mixture.[21,23] In some cases, such a mixture tends to phase separate upon drying, a characteristic used for improving transistors and organic solar cells, but detrimental for OLEDs.[1,8,9,20,24,25] Yet, polymer–small molecule mixtures can yield homogeneous, smooth films, as seen in polymer–small molecule mixed-host OLEDs.[1,8]

Based on the above, it is interesting to explore small molecules that are successfully solution-processable, do not phase separate in mixtures with polymers, form smooth films, and can consequently be hosts for polymer guests in solution-processed devices, increasing the variety and options for hosts to polymer emitting materials.

To investigate the utility of small molecules as hosts for polymer guests in solution-processed OLEDs, we compare devices made with hosts of the small molecule CBP or polymer PVK. The polymer guests were novel benzobisoxazole (BBO)-containing copolymers, recently described by Intemann et al.,[11] and the well-known poly(2-methoxy-5-(2′-ethyl-hexyloxy)-1,4-phenylene vinylene) (MEH-PPV), usually used as a neat film.[3] The BBO-polymers include: poly[(9,9-dioctylfluorene-2,7-ethynylene) - *alt* - (2,6-dihexyl- benzo[1,2-*d*:4,5-*d*′] bisoxazole-

4,8-diyl)] (PBOF-O), a fluorene-based polymer; poly[(9,9-bis(3,7-dimethyloctyl)fluorene-2,7-ethynylene) - *alt* - (2,6-dihexyl-benzo[1,2-*d*:4,5-*d*′] bisoxazole-4,8-diyl)] (PBOF-DMO), a polymer similar to the previous but with branched side chains; and poly[(1,4-dodecyloxyphenylene-2,5-ethynylene) - *alt* - (2,6- dihexyl-benzo[1,2-*d*:4,5-*d*′] bisoxazole-4,8-diyl)] (PBOP-D), a phenylene-based polymer.[11] The structures are shown in Fig. 2.1.

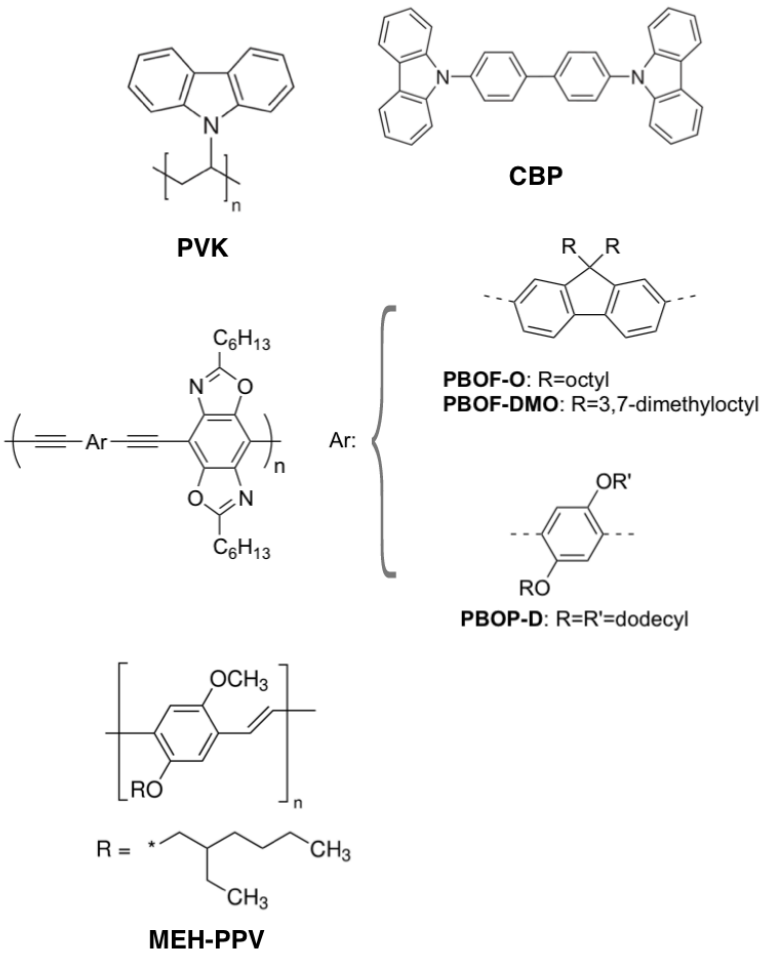

Figure 2.1 Structures of materials used in the EMLs

2.3 Results and discussion

2.3.1 AFM and STEM images

Atomic force microscopy (AFM) images confirmed the quality of the spin-coated polymer guest:small molecule host films. Fig. 2.2 and 2.3 show images of the emitting layers (EMLs) of selected devices. The root-mean-square roughness (R_{RMS}) values of the films are listed in Table 2.1.

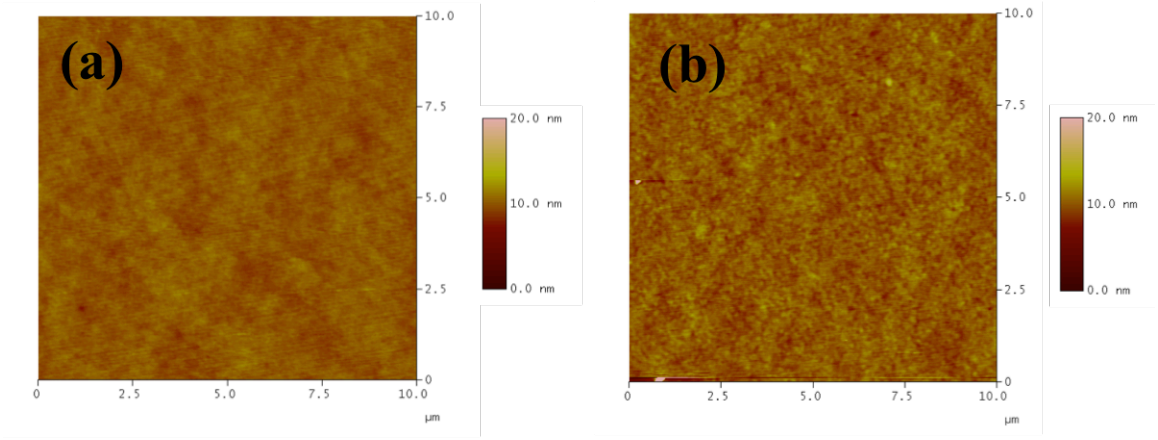

Figure 2.2 AFM images of (a) PBOF-O (1.0 wt%):CBP, $R_{RMS} \sim 0.59$ nm and (b) PBOF-O (1.0 wt%):PVK, $R_{RMS} \sim 0.80$ nm.

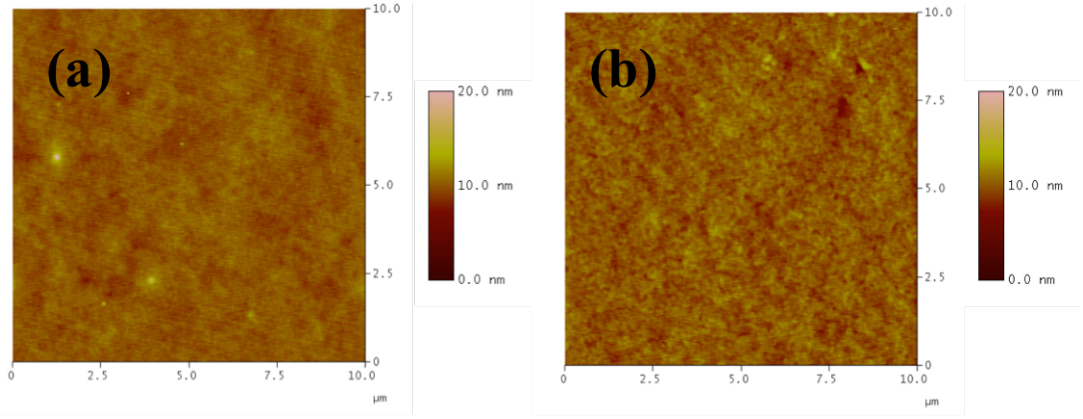

Figure 2.3 AFM images of (a) MEH-PPV (1.0 wt%):CBP, $R_{RMS} \sim 0.66$ nm and (b) MEH-PPV (1.0 wt%):PVK, $R_{RMS} \sim 0.80$ nm.

From the images it is apparent that both CBP- and PVK-based films are smooth and that R_{RMS} is relatively unaffected by the choice of guest. However, all CBP- based films are slightly smoother with an average $R_{RMS} \sim 0.61 \pm 0.07$ nm, compared to $R_{RMS} \sim 0.80 \pm 0.02$ nm for the PVK-based films. The neat MEH-PPV film strongly exceeds all in roughness, with $R_{RMS} \sim 5.6 \pm 0.5$ nm. The R_{RMS} values of the guest:host films highlight previous findings that replacing PVK with CBP improves the morphology and smoothens the film.[9] It was previously shown that AFM images may identify areas of phase separation and aggregation in mixed films.[2,9] The AFM results show smooth films suggesting no significant phase separation of the polymer guest and small molecule host.

Table 2.1 Values of R_{RMS} from AFM scans on various EML films.

Film[a]			
Polymer:Host	wt%[b]	R_{RMS} (nm)	Spread in R_{RMS} (nm)
PBOF-O:CBP	1.0	0.54	0.05
PBOF-O:PVK	1.0	0.78	0.16
PBOF-DMO:CBP	0.5	0.62	0.02
PBOF-DMO:PVK	0.5	0.79	0.04
PBOP-D:CBP	0.5	0.60	0.08
PBOP-D:PVK	0.5	0.82	0.01
MEH-PPV:CBP	1.0	0.66	0.04
MEH-PPV:PVK	1.0	0.80	0.01
MEH-PPV	neat	5.6	0.5

[a]Film structure: ITO/PEDOT:PSS/EML; [b]wt% of polymer in host

The AFM images are consistent with the scanning transmission electron microscopy (STEM) images (shown in Fig. 2.4). Fig. 2.4(a)-(d) show the smooth, featureless compositions of the films of 1.0, 10, & 20 wt% PBOF-O and 1.0 wt% MEH-PPV in the CBP host. The large dark features seen in the 200 nm scale images are uncoated regions. In contrast, Fig. 2.4(e) & (f) show that the PBOF-O(50 wt%):CBP film contains aggregates that are ∼10s of nm in diameter. These are seen as bright spots due to increased absorption in the thicker agglomerations and are consistent with phase separation of the polymer and small molecules at such high

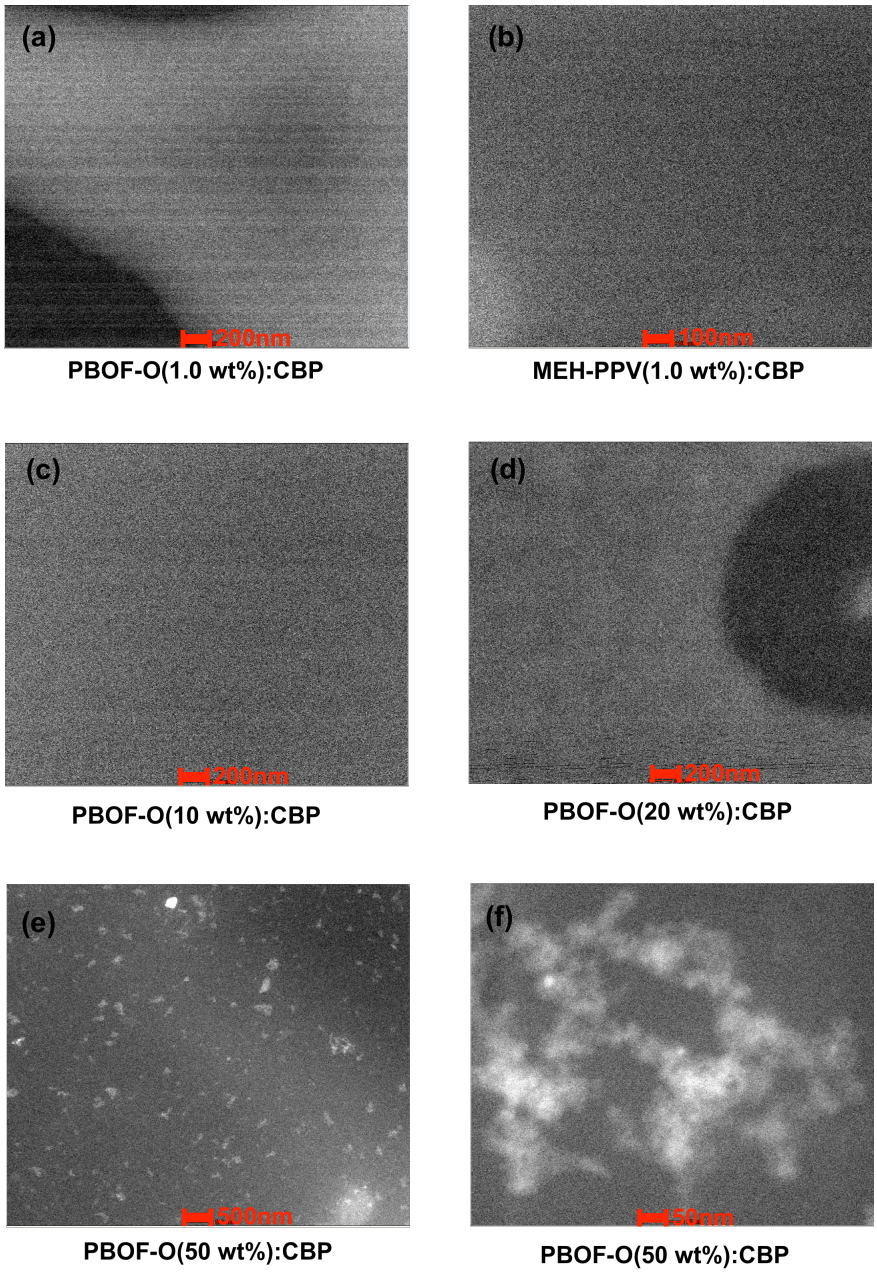

Figure 2.4 STEM images of (a) PBOF-O(1.0 wt%):CBP, (b) MEH-PPV(1.0 wt%):CBP, (c) PBOF-O(10 wt%):CBP, (d) PBOF-O(20 wt%):CBP, (e & f) PBOF-O(50 wt%):CBP.

guest concentrations. Hence, we conclude that the smooth STEM images of the PBOF-O (1.0 wt%):CBP and MEH-PPV (1.0 wt%):CBP suggest there is no phase separation on the ∼10s of nm scale and that the polymer–small molecule mixtures are homogeneous.

2.3.2 Emission spectra

The emission spectra of selected guest:host devices are shown in Fig. 2.5(a), 2.6(a), 2.7(a), 2.8(a). The spectral peak and CIE coordinates for all devices are listed in Table 2.2. Practically no host emission is present in the spectra of any of the guest:host pairs.

The efficient blue PBOF-O guest devices show no host emission. The emission is narrow, peaking at ∼ 460 nm with a shoulder near 500 nm in both hosts.

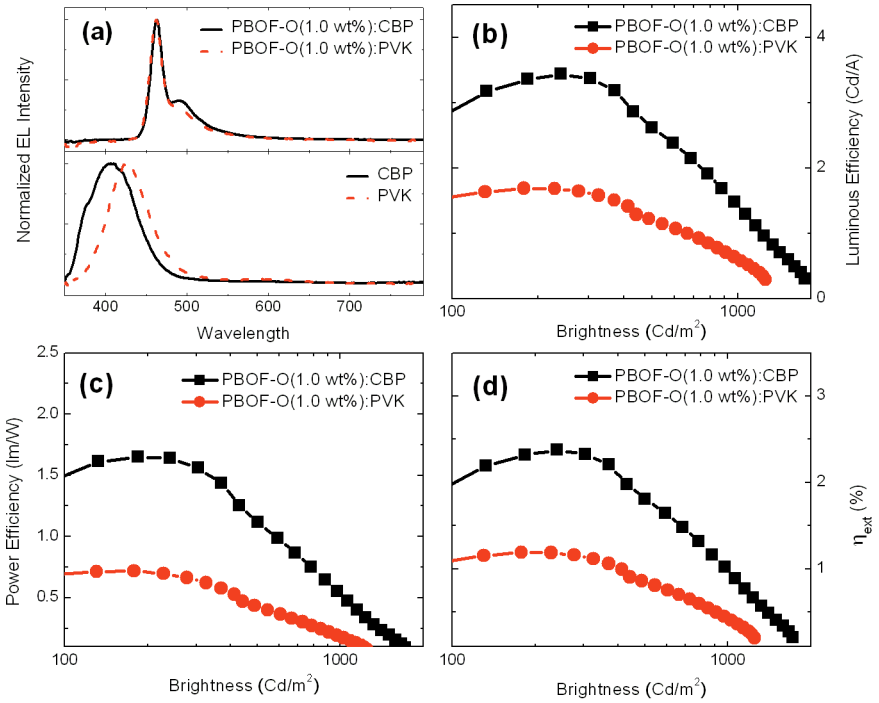

Figure 2.5 Comparison of devices containing PBOF-O in CBP (solid line, squares) or PVK (dashed line, circles): (a) EL spectra of guest:host devices and of neat CBP (solid) and PVK (dashed), (b) luminous efficiency, (c) power efficiency, and (d) η_{ext} vs. brightness.

PBOF-DMO devices have an emission peak at 458 nm and exhibit a wider band with a tail into the deeper blue that decreases with increasing guest concentration. The tail may indicate a small amount of host emission, but it is seen in both CBP and PVK-based devices.

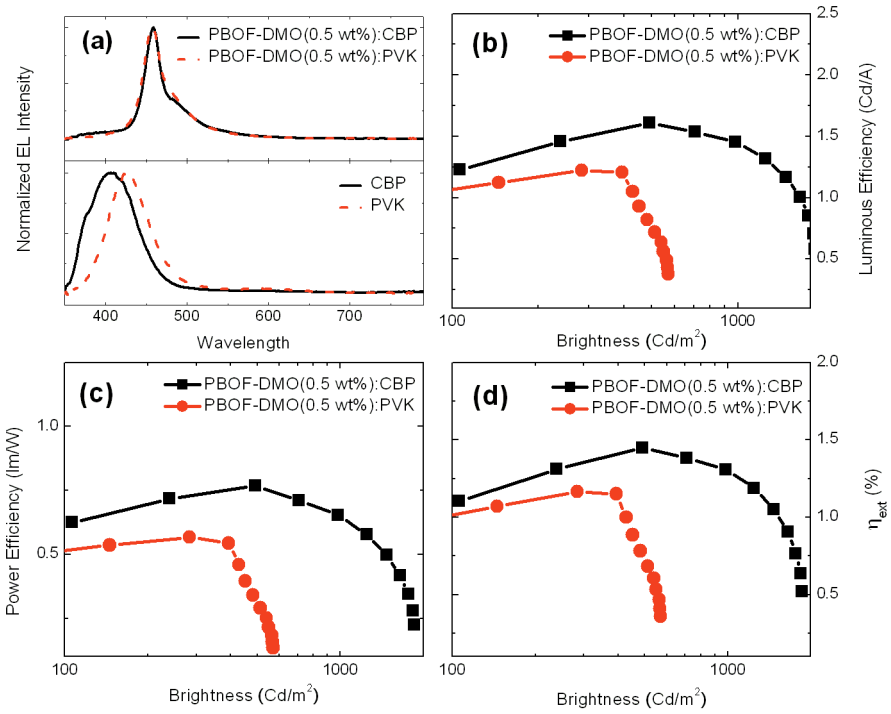

Figure 2.6 Comparison of devices containing PBOF-DMO in CBP (solid line, squares) or PVK (dashed line, circles): (a) EL spectra of guest:host devices and of neat CBP (solid) and PVK (dashed), (b) luminous efficiency, (c) power efficiency, and (d) η_{ext} vs. brightness.

The green emitting PBOP-D devices have a peak near 500 nm. In the PBOP-D:CBP devices this peak is slightly red shifted.

The devices with the MEH-PPV guest show emission peaks ranging from 570 to 585 nm depending on the guest concentration (compared to 592 nm for the neat device) (Table 2.2). The spectra of the 0.5 wt% devices are shown in Fig. 2.8(a), along with spectra of the neat PVK, CBP, and MEH-PPV for comparison. There is no host emission observed in either CBP- or PVK-based devices with guest concentrations of 1 wt% and higher (not shown). At a MEH-

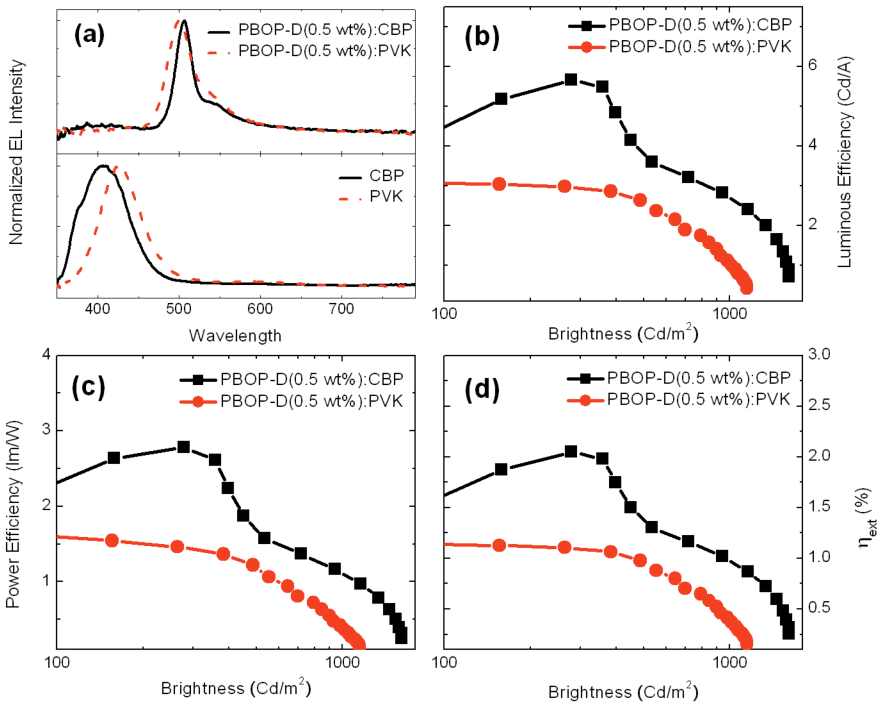

Figure 2.7 Comparison of devices containing PBOP-D in CBP (solid line, squares) or PVK (dashed line, circles): (a) EL spectra of guest:host devices and of neat CBP (solid) and PVK (dashed), (b) luminous efficiency, (c) power efficiency, and (d) η_{ext} vs. brightness.

PPV concentration of 0.5 wt% there is a slight host emission; the CIE coordinates change from (0.59, 0.41) in the neat film to (0.52, 0.44) in the 0.5 wt% CBP-based device. This blue shift is probably due to both the weak host emission and the elimination of the interchain interactions between neighboring MEH-PPV chains, which red-shift the emission.[26] The 0.1 wt% devices (not shown), with either CBP or PVK as host, showed significant host emission, shifting the emission color to the blue.

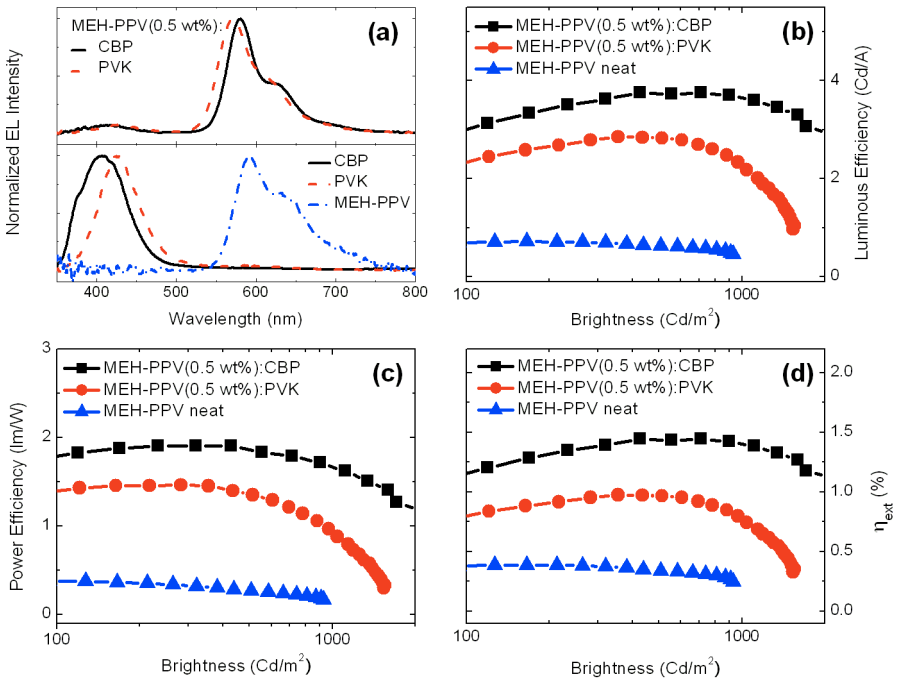

Figure 2.8 Comparison of devices with EML of MEH-PPV in CBP (solid line, squares) or PVK (dashed line, circles) and as a neat film (triangles): (a) EL spectra of guest:host devices and of neat CBP (solid), PVK (dashed), and MEH-PPV (dashed/dotted), (b) luminous efficiency, (c) power efficiency, and (d) η_{ext} vs. brightness.

For each guest, the shoulder at longer wavelengths strengthens with increasing concentration, and is observed in both hosts. In the case of MEH-PPV, the shoulder is the strongest in the emission of the neat film devices. It likely arises from aggregation of the emissive polymer or, in general, π-π overlap.[26,27]

As noted above, in the case of low concentrations of MEH-PPV and PBOP-D the emission spectra in the CBP host are slightly but consistently red-shifted relative to the emission in the PVK host. We speculate that this results from greater structural relaxation of the guest polymer chains in the small molecule host than in the polymer host. Such structural relaxation likely increases the average conjugation length, lowering the average HOMO-LUMO gap.[28] Such a red-shift is not seen in PBOF-O and PBOF-DMO because these guests are planarized by bridging bonds, are consequently more rigid, and therefore are not as structurally affected by the host.

2.3.3 Device efficiency

To compare CBP and PVK as hosts of polymer guests, devices with the structure: ITO/ PEDOT:PSS/ EML/ BPhen/ LiF/ Al were fabricated. The EML was a guest:host system of polymer guest and either PVK or CBP host, or a neat film of MEH-PPV. Neat film devices made from the other guests were very poor, likely due to concentration quenching, and are not shown here.[11] The dramatic improvement in efficiency of the devices with polymer guests in the CBP host is shown in Figs. 2.5, 2.6, 2.7, 2.8. The typical variation in efficiency values is $\pm$ 10 %. Characteristics of all devices are listed in Table 2.2.

The CBP-based devices doped with the blue PBOF-O (1.0 wt%) show a maximal luminous efficiency ($\eta_{L,max}$) (Fig. 2.5(b)) of 3.4 cd/A, an increase of 100% compared to the most efficient PVK-based device. Efficiencies in the mid-brightness range, most used in displays ($\sim$ 100-500 cd/m^2), are significantly improved for blue PBOF-O:CBP. The external quantum efficiency (η_{ext}) for these devices reaches 2.4% (Fig. 2.5(d)).

For devices with the PBOF-DMO guest, the blue emitter with branched side chains, $\eta_{L,max}$ increases from 1.2 cd/A with the PVK host to 1.6 cd/A with CBP (Fig.2.6(b)). The PBOF-DMO:CBP devices persist to higher brightness, increasing the operating range from a few hundred to over 2000 cd/m^2.

The value of $\eta_{L,max}$ for the green PBOP-D:CBP devices (Fig. 2.7(b)) exceeds 5.7 cd/A, an

improvement of over 80% compared to the PVK device (3.1 cd/A). The η_{ext} for PBOP-D:CBP reaches 2.1% (Fig. 2.7(d)).

The mixing of CBP with MEH-PPV to create a 1:1 wt. ratio mixed EML improves the efficiency to 1.3 cd/A ($\eta_{ext} \sim 0.6\%$) compared to 0.7 cd/A ($\eta_{ext} \sim 0.4\%$) of the device with the neat MEH-PPV film. The efficiencies of the MEH-PPV:CBP devices continue to increase with increasing CBP fraction. However, $\eta_{L,max}$ of PVK-based devices with MEH-PPV content higher than 5 wt% are below 0.5 cd/A, showing that mixing PVK and MEH-PPV at these ratios reduces the efficiency compared to the neat film. The CBP-based devices reach $\eta_{L,max}$ of 3.7 cd/A ($\eta_{ext} \sim 1.4\%$) at a MEH-PPV dopant level of 0.5 wt% (Fig. 2.8). The MEH-PPV(0.5 wt%):PVK devices trail slightly, with $\eta_{L,max}$ of only 2.9 cd/A ($\eta_{ext} \sim 1.0\%$).

Previously published results vary with regard to the effect of replacing the PVK host with a small molecule host in devices with an Ir-complex guest. One study found an improvement similar to that seen here in replacing PVK with CBP,[9] but in another study, devices with small molecule hosts (CBP or 1,3,5-tris[4-(diphenylamino)phenyl]benzene (TDAPB)) showed decreased efficiency compared to the polymer host or the mixed-host devices.[1,8]

Hole-transporting *N*,*N*′-diphenyl-*N*,*N*′-bis(3-methyl-phenyl)- [l,l′-biphenyl] -4,4′-diamine (TPD) and electron-transporting 2- (4-biphenylyl) -5- (4-*tert*-butylphenyl) -1,3,4-oxadiazole (PBD) were added to the EML to improve efficiency, as described previously.[9,10] However, the results were much poorer than the devices without TPD and PBD. It is suspected that the shallow highest occupied molecular orbital (HOMO) of TPD (5.5 eV) causes exciton dissociation by transfer of holes to the TPD molecule, thus quenching the emission (see Fig. 2.9).

2.3.4 Carrier & excitation dynamics

As mentioned, the AFM images of the polymer guest in the small molecule host matrix show smooth surfaces, suggesting no large-scale ($\sim$ 300 nm) phase separation or significant aggregation.[2,9] This assertion is supported by STEM images, which show aggregates at high (50 wt%) guest concentrations but smooth, homogeneous films at a nm scale with lower (20

wt% and below) guest concentrations. Hence, the AFM and STEM images confirm that the guest and host are likely homogeneously mixed, and therefore support a scenario where many CBP molecules surround a polymer guest chain.

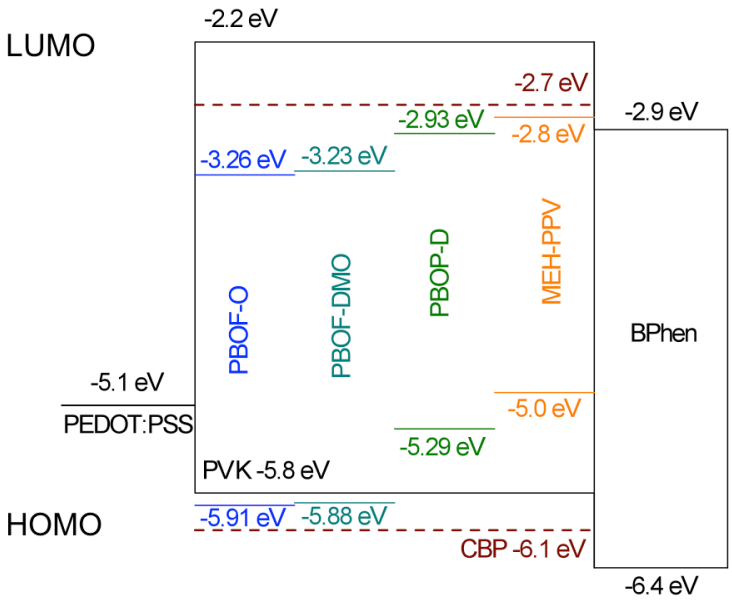

Figure 2.9 Diagram of the HOMO and LUMO energy levels of the various materials used in this study

To elucidate the carriers dynamics in the two host systems, transient electroluminescence (EL) measurements, previously shown to distinguish between energy and charge transfer from host to guest,[29,30] were performed. In such measurements, devices with emission dominated by charge transfer and consequent trapping on the guest show spikes in the transient EL. The results shown in Fig. 2.10 display such spikes in CBP-based devices but not in PVK-based devices. This behavior suggests that the charge transfer mechanism is more significant in the CBP-based devices, while energy transfer is key in the PVK-based devices. Because the energetics in both hosts would allow charge transfer to the guest (see Fig. 2.9), the observed difference in the transient EL may indicate the lack of sufficient close contact needed for charge

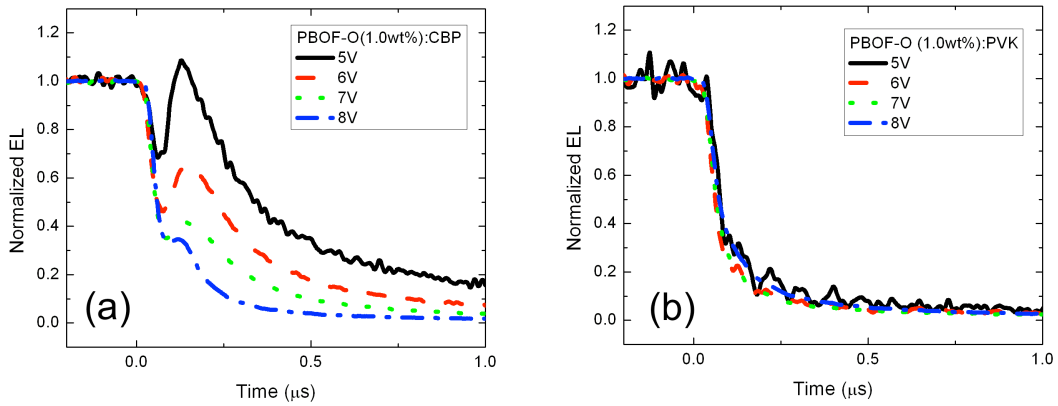

Figure 2.10 Transient EL of devices with EML of (a) PBOF-O (1.0 wt%):CBP and (b) PBOF-O (1.0 wt%):PVK.

transfer in the PVK system. Such contact is likely dependent on the conformation of the host molecules.

It is known that polystyrene, a non-conjugated polymer, coils upon itself in a high-density film.[31,32] We therefore suspect that PVK, with its non-conjugated backbone, also coils on itself; the degree of coiling is unknown, as it also depends on the spin-coating conditions. With a coiled polymer host, charge transfer to a guest may be hindered by trapping within the coiled chain, depending on the nature of the arrangement of the PVK chains.[33] Such charge trapping in PVK may help explain its low carrier mobility. It will also likely increase the prevalence of polaron-induced quenching of the radiative exciton decay,[34,35] leading to the observed lower efficiencies in these devices. This conformation can also increase the average distance between the PVK conjugated side groups and the polymer guest, thus inhibiting the closer contact needed for charge transfer.[34,35]

As a small molecule host cannot coil, it likely enables, in general, easier charge and energy transfer. Moreover, the small molecule CBP size would allow multiple CBP host molecules to contact a guest polymer, further increasing the probability of charge and energy transfer. Hence, the increased efficiency of CBP host devices is probably partially due to the difference

in the nanostructure of the CBP- and PVK-based films. That is, the tendency of PVK's backbone to coil likely limits host-guest interaction and increases the prevalence of nonradiative decay caused by trapped charges.

2.4 Experimental

OLEDs were fabricated on nominally 12 Ohm per sq, 140 nm thick ITO-coated glass substrates purchased from Colorado Concept Coatings. The substrates were cleaned using surfactant, acetone, and isopropanol and treated with UV-ozone to increase the work function of ITO. A hole injection layer of poly(3,4-ethylenedioxythiophene):poly(4-styrenesulfonate) (PEDOT:PSS), purchased from Heraeus Materials Technology, was fabricated by spin-coating the solution in air at a speed of 1000 rpm for 60 s, followed by baking at 120 °C for 1 h in air and 30 min in argon atmosphere. The EML solution, a guest:host mixture or a polymer neat layer with total concentration of 9 mg/mL in chlorobenzene, was spin-coated in an argon glovebox ($<$ 20 ppm O_2) atop the PEDOT:PSS, then baked at 60 °C for 30 min. Following the final annealing, the samples were transferred into a thermal evaporation system and pumped to a vacuum pressure of $\sim$4x10^{-7} mbar overnight to remove residual solvent. The films used for roughness analysis were removed and then measured by two or more AFM scans (model MM AFM-2 from Digital Instruments, working at contact mode) to obtain an average value of R_{RMS} and the related spread for that film. Those used to fabricate devices were kept under vacuum to thermally evaporate the subsequent layers, including 4,7-diphenyl-1,10-phenanthroline (BPhen) (an electron transport/ hole blocking layer), LiF cathode buffer, and Al, which was deposited through a mask. The structure was: ITO/ PEDOT:PSS 60 nm/ EML/ BPhen 40 nm/ LiF 1 nm/ Al 100 nm. The resulting devices were 1.5 mm diameter pixels.

Films used for STEM measurements were fabricated by spin-coating the above mentioned EML solutions at 1000 rpm on a 3 mm diameter carbon grid. The grids were then baked at 60 °C for 30 min and pumped at $\sim$4x10^{-7} mbar overnight. They were then imaged using a

Tecnai F20 TEM.

Devices were characterized by current-voltage-luminescence measurements, using a Kepco DPS 40-2M programmable power supply, a Keithly multimeter 2000, and a Minolta luminance meter LS-110, and by EL spectra obtained using an Ocean Optics CHEM2000 spectrometer.

2.5 Conclusions

We demonstrate the successful use of the small molecule CBP as a host to polymer guests in solution-processed OLEDs. Unlike OLEDs with small molecule or polymer guests in a polymer host, this field has not been explored. AFM images of the small molecule CBP host films indicate smooth surfaces and no phase separation at the $\sim$ 300 nm scale in the polymer guest:small molecule host systems studied. STEM images confirm homogeneity on the $\sim$ 10 nm scale in films with guest concentrations up to at least 20 wt% in CBP. Using CBP as the host for BBO-containing copolymer guests and for the well-known polymer MEH-PPV produces devices with efficiencies exceeding those of the analogous PVK-based devices and the devices with the neat emitting MEH-PPV layer as well. The luminous and power efficiencies of PBOF-O:CBP-based devices exceed those of the PBOF-O:PVK-based devices by 100%. Doping MEH-PPV at 0.5 wt% into CBP results in a significant improvement, increasing the luminous efficiency from 0.7 cd/A for the neat MEH-PPV devices to 3.7 cd/A, compared to 2.9 cd/A with the PVK host. The advantages of CBP over PVK likely stem from its higher charge mobility and the nanostructure of the guest:host film. The smooth AFM and STEM images are consistent with a polymer guest:small molecule host system in which the guest polymer chain is surrounded by multiple CBP molecules. Such an environment is preferable to the PVK-based system, where the differences in polymer size and conformation (probably coiling of the nonconjugated PVK backbone) limit the host–guest interaction, lower the carrier mobility, and likely produce trapped polarons that are exciton-quenching centers. Hence, apart from the higher mobility, improved charge balance, and moderately improved smoothness of the EML

due to the use of CBP instead of PVK, this nanostructure of the polymer guest:CBP host system likely increases the efficiency by increasing the probability of energy and/or charge transfer and decreasing the prevalence of trap-induced nonradiative decay. The results of this study demonstrate that small molecules can be very efficient hosts for polymer guests in solution-processed OLEDs, opening options for the synthesis of these materials and their use in such new device designs.

2.6 Acknowledgements

Ames Laboratory is operated by Iowa State University for the US Department of Energy (USDOE) under Contract no. DE-AC 02-07CH11358. The research was partially supported by Basic Energy Sciences, Division of Materials Science and Engineering, USDOE. JJI, MDE, BCT and MJE thank the National Science Foundation (DMR-0846607) for partial support of this work.

Table 2.2 Device characteristics

Device[a] **Polymer:Host**	**wt%**[b]	$\mathbf{V}_{on}$ (V)	$\boldsymbol{\eta_{L,max}}$ (cd/A)	$\boldsymbol{\eta_{P,max}}$ (lm/W)	$\boldsymbol{\eta_{ext,max}}$ (%)	$\boldsymbol{\lambda_{max}}$ ($\boldsymbol{\lambda_{2nd}}$) (nm)	**CIE 1931** (x, y)
PBOF-O:CBP	0.5	5.4	2.5	1.1	1.9	462	(0.14, 0.12)
	1	**4.4**	**3.4**	**1.7**	**2.4**	**463**	**(0.14, 0.13)**
	2	4.4	1.5	0.76	0.8	463	(0.15, 0.17)
	4	3.6	0.86	0.54	0.53	463	(0.15, 0.15)
PBOF-O:PVK	0.5	5	1.7	0.86	1.1	462	(0.14, 0.12)
	1	**5.4**	**1.7**	**0.72**	**1.2**	**462**	**(0.14, 0.13)**
	2	5.2	1.1	0.47	0.92	462	(0.15, 0.15)
	4	4.2	2.5	1.1	1.9	462	(0.14, 0.14)
PBOF-DMO:CBP	**0.5**	**4.9**	**1.6**	**0.77**	**1.5**	**458**	**(0.15, 0.12)**
	1	5.4	1.2	0.51	1.1	459	(0.15, 0.11)
	2	4.8	0.35	0.19	0.24	459	(0.17, 0.19)
	4	4.8	0.19	0.1	0.12	460	(0.16, 0.17)
PBOF-DMO:PVK	**0.5**	**5.6**	**1.2**	**0.57**	**1.2**	**458**	**(0.15, 0.11)**
	1	6	1.2	0.49	1.1	458	(0.15, 0.11)
	2	6.5	0.56	0.22	0.59	459	(0.15, 0.09)
	4	8	0.22	0.07	0.14	460	(0.16, 0.16)
PBOP-D:CBP	**0.5**	**5.2**	**5.7**	**2.8**	**2.1**	**506**	**(0.20, 0.55)**
	1	5.3	4.3	1.8	1.3	507	(0.22, 0.62)
	2	4.6	1.5	0.63	0.49	517	(0.26, 0.60)
	4	3.1	0.51	0.4	0.16	519	(0.35, 0.56)
PBOP-D:PVK	**0.5**	**4**	**3.1**	**1.6**	**1.1**	**501**	**(0.18, 0.50)**
	1	4.4	2.4	1.2	0.88	500	(0.21, 0.51)
	2	4.7	0.25	0.1	0.07	519	(0.35, 0.61)
	4	4.3	0.81	0.36	0.28	517	(0.25, 0.54)
MEH-PPV:CBP	0.1	4.5	1.7	0.82	3.1	410 (575)	(0.20, 0.09)
	0.5	**3.3**	**3.7**	**1.9**	**1.4**	**580 (416)**	**(0.52, 0.44)**
	1	2.6	2.6	1.8	1.1	585	(0.56, 0.44)
	5	2.4	2.2	2.1	0.94	579	(0.54, 0.46)
	20	2.2	1.7	1.7	0.76	579	(0.55, 0.45)
	50	2.3	1.3	1.2	0.61	583	(0.57, 0.44)
MEH-PPV:PVK	0.1	3.7	2.5	1.3	1.4	427 (570)	(0.30, 0.24)
	0.5	**3.4**	**2.9**	**1.5**	**1**	**571 (425)**	**(0.48, 0.47)**
	1	2.7	2.3	1.3	0.81	575	(0.52, 0.47)
	5	3.2	0.44	0.27	0.19	585	(0.55, 0.44)
	20	2.7	0.45	0.37	0.18	585	(0.55, 0.45)
MEH-PPV	neat	4	0.71	0.37	0.39	592	(0.59, 0.41)

[a]Device structure:ITO/PEDOT:PSS/EML/BPhen/LiF/Al; [b]wt% of polymer in host

References

[1] E. Y. Choi, J. H. Seo, Y. Y. Jin, H. M. Kim, J. T. Je, Y. K. Kim, *J. Nanosci. Nanotechnol.* **11**, 10737 (2011).

[2] Y.-Y. Noh, C.-L. Lee, J.-J. Kim, K. Yase, *J. Chem. Phys.* **118**, 2853 (2003).

[3] T.-F. Guo, F.-S. Yang, Z.-J. Tsai, T.-C. Wen, S.-N. Hsieh, Y. S. Fu, *Appl. Phys. Lett.* **87**, 013504 (2005).

[4] J. H. Burroughes, D. D. C. Bradley, A. R. Brown, R. N. Marks, K. Mackay, R. H. Friend, P. L. Burns and A. B. Holmes, *Nature***347**, 539 (1990).

[5] X. Yang, D. C. Mu?ller, D. Neher and K. Meerholz, *Adv. Mater.***18**, 948 (2006).

[6] X. Yang, D. Neher, D. Hertel and T. D?aubler, *Adv. Mater.***16**, 161 (2004).

[7] Y. Kawamura, S. Yanagida and S. R. Forrest, *J. Appl. Phys.* **92**, 87 (2002).

[8] Y. Hino, H. Kajii and Y. Ohmori, *Jpn. J. Appl. Phys.* **44**, 2790 (2005).

[9] M. Cai, T. Xiao, E. Hellerich, Y. Chen, R. Shinar and J. Shinar, *Adv. Mater.* **23**, 3590 (2011).

[10] S. A. Choulis, V.-E. Choong, M. K. Mathai and F. So, *Appl. Phys. Lett.* **87**, 113503 (2005).

[11] J. J. Intemann, E. S. Hellerich, B. C. Tlach, M. D. Ewan, C. A. Barnes, A. Bhuwalka, M. Cai, J. Shinar, R. Shinar and M. Jeffries-EL, *Macromolecules* **45**, 6888 (2012).

[12] J. J. Intemann, J. F. Mike, M. Cai, S. Bose, T. Xiao, T. C. Mouldin, R. A. Roggers, J. Shinar, R. Shinar and M. Jeffries-EL, *Macromolecules* **44**, 248 (2011).

[13] J. F. Mike, J. J. Intemann, M. Cai, T. Xiao, R. Shinar, J. Shinar and M. Jeffries-EL, *Polym. Chem.* **2**, 2299 (2011).

[14] P. W. M. Blom, M. J. M. de Jong and M. G. van Munster, *Phys. Rev. B: Condens. Matter Mater. Phys.* **55**, R656 (1997).

[15] L. Duan, L. Hou, T.-W. Lee, J. Qiao, D. Zhang, G. Dong, L. Wang and Y. Qui, *J. Mater. Chem.* **20**, 6392 (2010)

[16] C. W. Tang and S. A. VanSlyke, *Appl. Phys. Lett.* **51**, 913 (1987).

[17] C. Adachi, M. A. Baldo, S. R. Forrest and M. E. Thompson, *Appl. Phys. Lett.* **77**, 904 (2000).

[18] B. W. D'Andrade, M. E. Thompson and S. R. Forrest, *Adv. Mater.* **14**, 147 (2002).

[19] J. Shinar and R. Shinar, *J. Phys. D: Appl. Phys.* **41**, 133001 (2008).

[20] M.-B. Madec, P. J. Smith, A. Malandraki, N. Wang, J. G. Korvink and S. G. Yeates, *J. Mater. Chem.* **20**, 9155 (2010).

[21] H. Rudmann and M. F. Rubner, *J. Appl. Phys.* **90**, 4338 (2001).

[22] L. He, J. Liu, Z. Wu, D. Wang, S. Liang, X. Zhang, B. Jiao, D. Wang and X. Hou, *Thin Solid Films* **518**, 3886 (2010).

[23] M. C. Suh, B. D. Chin, M.-H. Kim, T. M. Kang and S. T. Lee, *Adv. Mater.* **15**, 1254 (2003).

[24] J. H. Park, H. Lim, H. Cheong, K. M. Lee, H. C. Sohn, G. Lee and S. Im, *Org. Electron.* **13**, 1250 (2012).

[25] J. Smith, R. Hamilton, I. McCulloch, N. Stingelin-Stutzmann, M. Heeney, D. D. C. Bradley and T. D. Anthopoulos, *J. Mater. Chem.* **20**, 2562 (2010).

[26] T.-Q. Nguyen, V. Doan and B. J. Schwarz, *J. Chem. Phys.* **110**, 4068 (1999).

[27] Y. Shi, J. Liu and Y. Yang, *J. Appl. Phys.* **87**, 4254 (2000).

[28] J. Roncali, *Chem. Rev.* **97**, 173 (1997).

[29] R. Liu, Z. Gan, R. Shinar and J. Shinar, *Phys. Rev. B: Condens. Matter Mater. Phys.* **83**, 245302 (2011).

[30] Z. Gan, R. Liu, R. Shinar and J. Shinar, *Appl. Phys. Lett.* **97**, 113301 (2010).

[31] R. Qian, L. Wu, D. Shen, D. H. Napper, R. A. Mann and D. F. Sangster, *Macromolecules* **26**, 2950 (1993).

[32] G. Xue, Y. Lu, G. Shi and Q. Dai, *Polymer* **35**, 892 (1994).

[33] Y. Yang, Y. Shi, J. Liu and T.-F. Guo, in *Electronic and Optical Properties of Conjugated Molecular Systems in Condensed Phases*, ed. S. Hotta, Research Signpost, Kerala, India, 2003, ch. 13.

[34] (a) M.-K. Lee, M. Segal, Z. G. Soos, J. Shinar and M. A. Baldo, *Phys. Rev. Lett.* **94**, 137403, (2005); (b) M. Segal, M. A. Baldo, M. K. Lee, J. Shinar and Z. G. Soos, *Phys. Rev. B: Condens. Matter Mater. Phys.* **71**, 245201 (2005).

[35] J. Shinar, *Laser Photonics Rev.* **6**, 767 (2012).

CHAPTER 3.

Fluorescent OLEDs based on new benzobisoxazole-based emitters with altered conjugation pathways

modified from: J. J. Intemann,[a] E. S. Hellerich,[b] B. C. Tlach,[a] M. D. Ewan,[a] C. A. Barnes,[a] A. Bhuwalka,[a] M. Cai,[b] J. Shinar,[b] R. Shinar,[c] M. Jeffries-EL,[a] *Macromolecules* **45**, 6888 (2012).

[a]Department of Chemistry, Iowa State University, Ames, IA 50011, USA

[b]Ames Laboratory-USDOE and Department of Physics and Astronomy, Iowa State University, Ames, IA 50011, USA.

[c]Microelectronics Research Center and Department of Electrical and Computer Engineering, Iowa State University, Ames, IA 50011, USA.

3.1 Abstract

Benzobisoxazoles (BBOs) are known to increase the electron affinities and improve the electron transporting properties of materials containing them. However, BBO copolymers generally do not perform well as emissive guests in guest-host PLEDs due to inefficient Förster resonance energy transfer (FRET) between host and guest. The incomplete FRET results in a large amount of host emission and limits the potential efficiencies of the devices. In all previously reported BBO copolymers, the conjugation pathway was through the oxazole rings. Herein we report six new BBO copolymers with backbone connectivity directly on the central benzene ring, resulting in a conjugation pathway for the polymers that is perpendicular to the previously reported pathway. Guest-host PLEDs made using these polymers show that the new conjugation pathway improves FRET between the poly(N-vinylcarbazole) host and

the BBO-containing polymer guest. Because of highly efficient FRET, no host emission is observed even at lower guest concentrations. The improved energy transfer results in devices with luminous efficiencies up to 3.1 Cd/A, a 3-fold improvement over previously reported BBO-based PLEDs. These results indicate that the conjugation pathway plays a critical role in designing emissive materials for guest-host PLEDs.

3.2 Introduction

Organic light-emitting diodes (OLEDs) are an advancing technology for use in flat panel display and solid-state lighting applications.[1–3] Polymer LEDs (PLEDs) have advantages over other OLED-based display technologies such as their low cost processing via solution-based inkjet printing.[4,5] In the two decades since PLEDs were first reported,[6] research has been aimed at developing polymers with efficient and stable red, green, and blue emission necessary for full color displays.[7] Unfortunately, most emissive conjugated polymers have low electron affinities (EAs) that diminish electron mobilities in thin films. These materials also have higher hole mobilities, which collectively result in an imbalance in charge injection and transport within the device, reducing efficiencies and overall performance.[8,9] Various strategies have been developed to overcome these limitations including the fabrication of multilayer devices containing an electron transport layer, the use of low-work function electrodes, such as calcium,[10] and alkali fluoride buffer layers to improve electron injection.[11] Alternatively, electron-deficient moieties can be incorporated into the backbone of the emissive polymer resulting in increased EAs, potentially improving electron injection and transport.[12–17] For these reasons, benzobisoxazoles (BBOs) are promising building blocks in semiconducting polymers as they increase the EAs,[16] electron transport,[10,18–20] photoluminescence (PL),[21,22] and oxidative and thermal stability[23,24] of materials containing them. Additionally, the starting materials are readily synthesized from low-cost reagents, making large-scale synthesis economical.[25]

The synthesis and characterization of a series of vinylene-linked copolymers based on BBOs and 9,9-dialkylfluorene was recently reported.[26] These polymers exhibited reversible reduction processes and stable blue electroluminescence (EL) peaking at 470 nm with luminous efficiencies up to 0.93 cd/A when used as guest emitters in a poly(*N*-vinylcarbazole) (PVK) host. It is believed that the performance of these materials in PLEDs was limited largely due to fluorescence quenching caused by aggregation of the polymer in the PVK host. This aggregation may be the result of the large extended π-system of the BBO moiety and the limited number of side chains per repeat unit to disrupt π-stacking. The devices were also plagued by incomplete Förster resonance energy transfer (FRET) between the PVK host and the BBO copolymer guest, giving rise to substantial host contributions to the EL spectrum. In general, the efficiency of FRET is largely dependent on the spectral overlap between the host emission and guest absorption and the extent of excited-state dipole-dipole coupling between the host and guest.[27] While the previously reported BBO copolymers had good spectral overlap with the host emission, they still did not exhibit complete energy transfer, suggesting that weak coupling between the excited state dipoles of the host and guest was the problem. The latter could be caused by poor alignment of the host and guest dipoles, which is necessary for energy transfer, or the result of a very weak excited state dipole in the guest.

In order to overcome these limitations, we developed six new BBO copolymers with a conjugation pathway directly through the central benzene ring and an alkynyl group between the comonomers, see Figure 3.1. These materials differ from all previously reported BBO copolymers that have a conjugation pathway through the oxazole rings (Figure 3.2) and feature single or double bonds between the arenes. This modification results in materials that incorporate the beneficial properties of the BBO moiety, while allowing for alkyl substitution at the 2- and 6- positions to improve solubility and disrupt π-stacking between polymer chains. These new BBO copolymers exhibit external quantum efficiencies as high as 1.2% in guest:host PLEDs, nearly a 2-fold improvement over our previously reported materials, demonstrating that conjugation pathway plays an important role in designing emissive polymers for PLEDs.

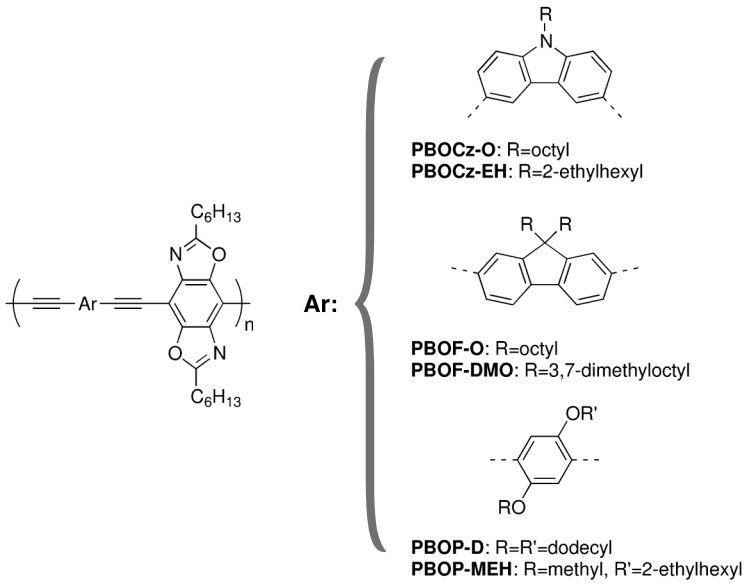

Figure 3.1 Molecular structures of new BBO-based copolymers.

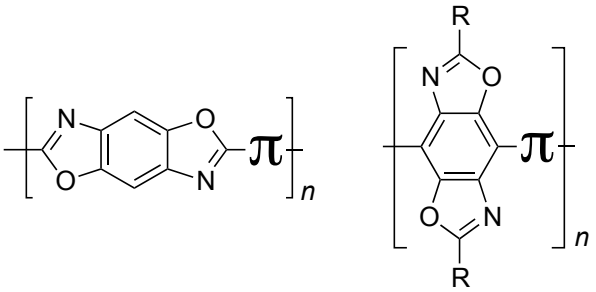

Figure 3.2 Drawing of a traditional BBO copolymer (left) that has a conjugation pathway through the oxazole rings and the new BBO copolymer (right) that has a conjugation pathway through the central benzene ring.

3.3 Results and Discussion

3.3.1 Optical Properties

The PL characteristics of the polymers, both in dilute solutions and thin films, were examined using fluorescence spectroscopy. The normalized PL spectra of the polymers are shown in Figure 3.3 and the data are summarized in Table 3.1. In both solution and film the carbazole copolymers have the widest optical bandgap among the six polymers.[28] This is a result of the unfavorable steric interactions caused by the 3,6-substitution on the carbazole moiety, which distorts the polymer backbone, reducing the effective conjugation length.[29]

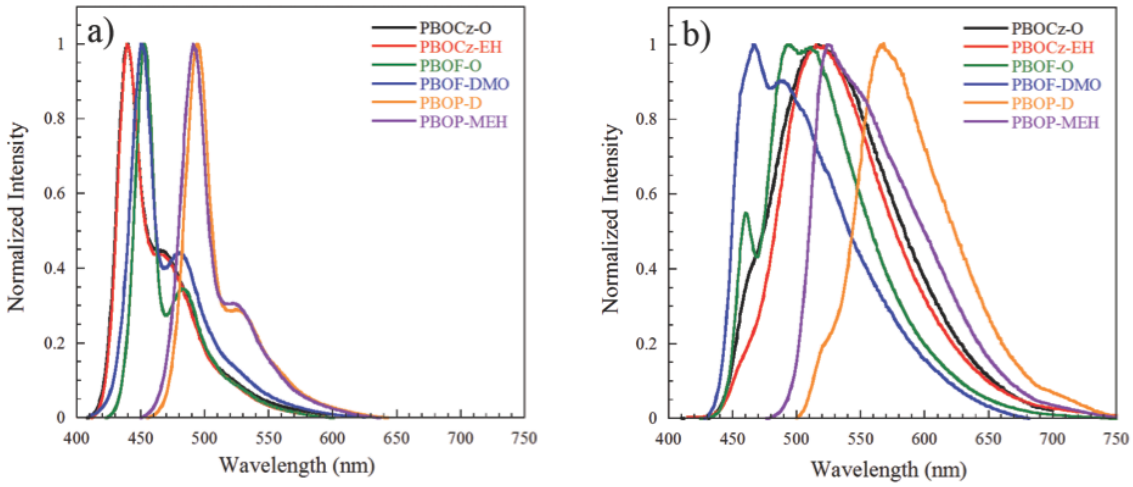

Figure 3.3 Photoluminescence spectra of benzobisoxazole polymers (a) in chloroform solutions and (b) as thin films.

In solution, the carbazole copolymers have the deepest blue emission (∼440 nm) with the fluorene copolymers also exhibiting blue emission (∼452 nm), whereas the phenylene copolymer emits in the blue-green region (∼492 nm). In all cases, PL emission was independent of side chain substitution.

As thin films, the PL of the polymers shows significant broadening of the emission peaks accompanied by red-shifts of varying degrees. The carbazole-containing polymers both exhibit a red-shift of ∼76 nm relative to the solution spectra, indicating that alkyl substitution

Table 3.1 Optical Properties of Benzobisoxazole Polymers

	solution		thin film	
Polymer	λ_{max}^{PL} (nm)	Φ^a	λ_{max}^{PL} (nm)	E_g^{opt} (eV)^b
PBOCz-O	440	0.33	517	2.72
PBOCz-EH	439	0.43	515	2.69
PBOF-O	453	0.68	495	2.72
PBOF-DMO	451	0.35	466	2.76
PBOP-D	494	0.57	566	2.36
PBOP-MEH	491	0.47	525	2.44

[a]Quantum yields measured in dilute chloroform solutions relative to Coumarin 152.
[b]Optical band gap measured from the onset of absorption in films.[28]

has little impact on the conformation and the degree of aggregation of both polymers even in thin films. In contrast, the emission wavelength of the fluorene and phenylene-containing polymers exhibit a strong dependence on the alkyl chain substitution as the polymers with branched side chains are blue-shifted relative to polymers with linear side chains. The fluorene polymers exhibit similar emission bands although the relative intensity of those bands is different, resulting in a deeper blue emission from PBOF-DMO. Conversely, the emission bands of the phenylene polymers are different as PBOP-MEH gives yellow-green emission at 525 nm, whereas PBOP-D exhibits orange emission at 566 nm. The red-shifted emission of PBOP-D relative to PBOP-MEH is a combination of the increased planarity and π-stacking of the PBOP-D.

The PL quantum yields of the polymers in dilute solutions of chloroform were taken relative to Coumarin 152, the results of which are listed in Table 3.1. PBOF-O and PBOP-D possess the highest quantum yields at 0.68 and 0.57, respectively. As expected, the branched alkyl derivatives PBOF-DMO and PBOP-MEH had lower quantum yields (0.35 and 0.47, respectively) than their linear chain counterparts.[30] Overall, PBOCz-O and PBOCz-EH have lower quantum yields than the fluorene- and phenylene-containing polymers. This can be attributed to the twisted backbone of the carbazole-containing polymers, resulting in a less rigid polymer that can vibrationally relax more effectively.

3.3.2 Electroluminescent Devices

The polymers were first evaluated as neat emissive layers in PLEDs; however, these devices either did not emit light or failed to provide a useful brightness (<100 cd/m^2) due to strong concentration quenching in the neat film. We then fabricated guest:host PLEDs using the polymers as guests in PVK. A device architecture of ITO/ PEDOT:PSS/ polymer:PVK/ BPhen/ LiF/ Al was adopted where PEDOT:PSS (poly(3,4-ethylenedioxy thiophene):poly(4-styrenesulfonate)) was used as a hole transporting layer and BPhen (4,7-diphenyl-1, 10- phenanthroline) was used as a hole blocking/electron transporting layer, which also prevented exciton quenching at the metal cathode. The energy level diagram in Figure 3.4 illustrates the various energy levels of the different device materials.[31–33] The highest occupied molecular orbital

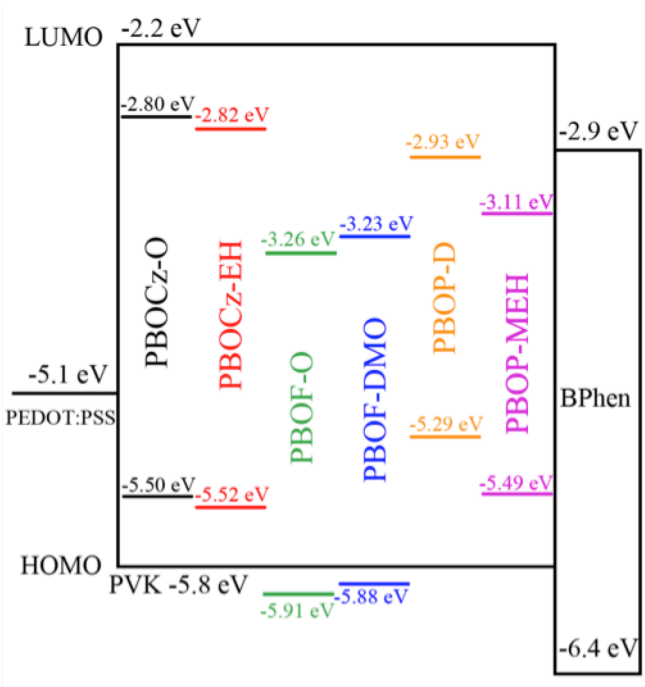

Figure 3.4 Energy level diagram for the guest:host PLEDs.

(HOMO) of the BBO copolymers was measured via ultraviolet photoelectron spectroscopy (UPS) and the optical band gap was determined from the onset of absorption in films.[28] All of the devices were optimized by using 0.5, 1.0, 2.0, and 4.0 wt% of polymer guest in PVK. The

device characteristics are summarized in Table 3.2; typical variation in efficiencies is $\pm$ 10 %. The EL spectra of the devices are shown in Figure 3.5.

The carbazole-containing polymers provide the deepest blue PLEDs but possess the lowest external quantum efficiencies (EQE). Of the PBOCz-O-based devices, 1 wt% PBOCz-O in PVK gives the best performance but with a maximum brightness of only 210 cd/m^2 and a maximum EQE of 0.68% with a luminous efficiency of 0.72 cd/A. The PBOCz-EH-based devices are slightly brighter but have worse efficiencies, with the best results obtained from 0.5 wt% PBOCz-EH in PVK, giving a maximum brightness of 330 cd/m^2, a maximum EQE of 0.58%, and a luminous efficiency of 0.59 cd/A. The poor efficiencies of the PBOCz-O- and PBOCz-EH-based devices are a consequence of the low PL quantum yields of the polymers that results in energy loss due to nonradiative decay pathways. Figure 3.6 shows the device efficiencies for the 1 wt% PBOCz-O- and PBOCz-EH-based devices as a function of brightness. The maximum efficiencies for the PBOCz-O- and PBOCz-EH-based devices all occur at very low brightness and decrease quickly with increased brightness. The branched alkyl chain-containing PBOCz-EH-based device is not as good in this respect with a brightness of only $\sim$20 cd/m^2 at its peak luminous and power efficiency. Interestingly, even though the linear alkyl chain-containing PBOCz-O-based device has a larger maximum luminous and power efficiency than the branched alkyl chain-containing PBOCz-EH-based device, the PBOCz-EH-based device has a higher efficiency at higher luminous intensities. The efficiencies of the PBOCz-EH-based device surpass those of the PBOCz-O- based device at a brightness of $\sim$180 cd/m^2, giving it better efficiencies at luminous intensities commonly used for displays. Collectively, this indicates that in this instance the alkyl chains have an important impact on the device properties.

As seen from the EL spectra, devices based on the carbazole-containing polymers display a broad emission between $\sim$400–500 nm with EL maxima in the range of 452–462 nm. The PBOCz-O- and PBOCz-EH-based devices show little variation in their emission profile as their concentration is increased, but the latters EL spectrum narrows and a shoulder at $\sim$480

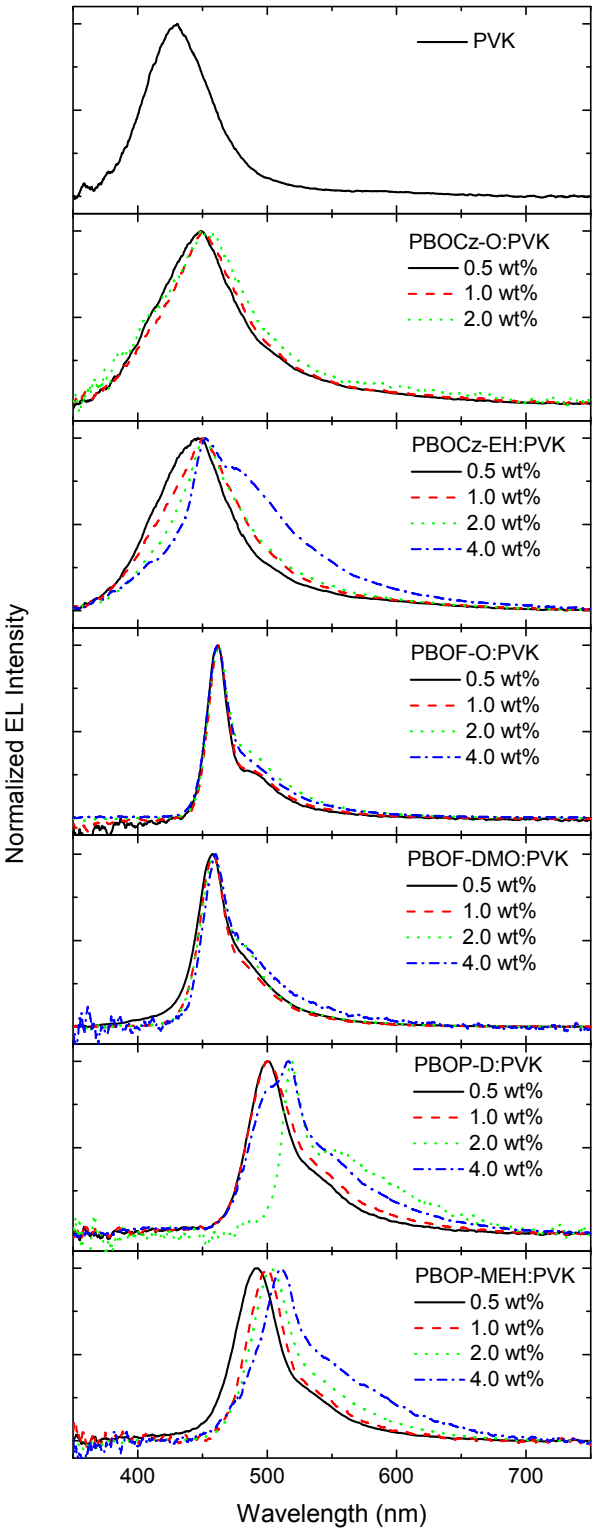

Figure 3.5 Normalized electroluminescent spectra of devices with different wt% concentrations of the BBO copolymers in PVK.

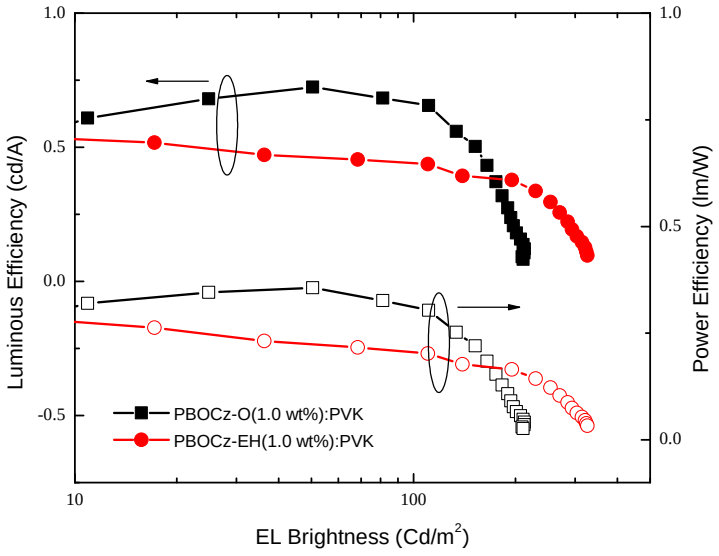

Figure 3.6 Luminous and power efficiency as a function of PLED brightness for devices using 1 wt% of PBOCz-O or PBOCz-EH as a guest in a PVK host.

nm appears for 4 wt% of the guest. While a reduction of the PBOCz-EH EL emission in the ∼400–430 nm range may be due to a decrease in the host emission (PVK emits at ∼400–420 nm) as the guest concentration increases, the change in the emission is small and is not seen in the PBOCz-O-based devices.

Devices based on the fluorene-containing polymers also gave stable blue emission with the highest PBOF-O-based device EQE resulting from 1.0 wt% in PVK. This device gave a maximum brightness of 1250 cd/m^2, a maximum EQE of 1.2%, and a luminous efficiency of 1.7 cd/A at a peak emission wavelength of 463 nm. These efficiency and brightness values represent a large improvement over identical devices made from BBO and fluorene copolymers that featured the traditional conjugation pathway through the oxazole rings, which had previously only achieved EQEs up to 0.69%.[34,35]

The PBOF-DMO-based devices display similar EQEs to the PBOF-O devices, though they have a more rapid decline in efficiency with increasing concentration in PVK. The best PBOF-DMO-based device is made using 0.5 wt% polymer in PVK, which gives a maximum bright-

ness of 660 cd/m^2, a maximum EQE of 1.2%, and a maximum luminous efficiency of 1.2 cd/A. The decrease in luminous efficiency in the PBOF-DMO-based PLEDs relative to the PBOF-O is a consequence of the weighted photopic luminosity function which peaks in the green region of the visible spectrum and decreases quickly with shorter wavelength light.[36] The result is the deeper blue emitting PBOF-DMO-based devices having lower luminous efficiencies than the PBOF-O-based devices. Figure 3.7 shows that the peak efficiencies for the PBOF-O-based device occur at a brightness of only ∼120 cd/m^2, though it maintains a high efficiency over a broad range of luminous intensities. The peak efficiency for the PBOF-DMO-based device

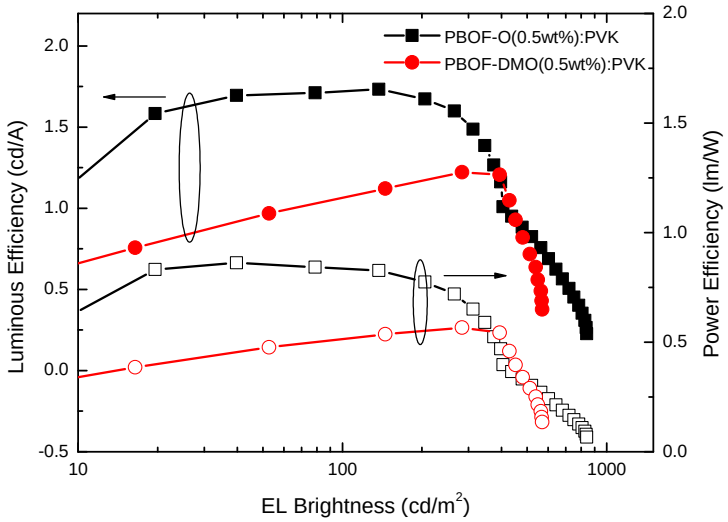

Figure 3.7 Luminous and power efficiency as a function of PLED brightness for devices using 0.5 wt% of PBOF-O or PBOF-DMO in a PVK host.

occurs at a brightness of ∼300 cd/m^2 and decreases faster than the PBOF-O-based device with decreasing brightness. The efficiency for the PBOF-O-based device also drops off quickly above 300 cd/m^2, while the efficiency in the PBOF-DMO-based device does not decrease rapidly until it exceeds a brightness of 400 cd/m^2. Unlike the carbazole-containing polymer-based devices, the PBOF-DMO-based device does not surpass the PBOF-O-based device in efficiency at higher luminous intensities. Instead, the efficiencies converge around 400 cd/m^2.

The EL spectra for the PBOF-O- and PBOF-DMO-based devices show only guest emission with no contribution from the host. Both PBOF-O- and PBOF-DMO-based devices display emission bands peaking at 462 and 458 nm, respectively. These bands are extremely narrow with full widths at half-maxima of ∼22 nm. An additional weak peak at ∼490 nm is seen in the PBOF-O-based devices and appears as a shoulder in the PBOF-DMO-based PLEDs. The EL spectra are virtually identical to the solution PL spectra of the polymers, suggesting that the fluorene-containing polymers are not aggregating within the host matrix, even at higher concentrations.

Devices made from the phenylene-containing polymers give blue-green emission with slightly lower EQEs than the PBOF-O devices. The PBOP-D-based device with the highest EQE was made from 0.5 wt% in PVK, which displays a maximum brightness of 1150 cd/m^2 and a maximum EQE of 1.1%. Because of the higher photopic response in the PBOP-D-based PLED, the device has a higher maximum luminous efficiency of 3.1 cd/A compared to the PBOF-O devices. This represents the highest efficiency to date for any guest:host PLED using a BBO copolymer guest, irrespective of the BBO isomer or emission color. Devices made from PBOP-MEH display similar EQEs as the PBOP-D-based PLEDs, though the devices possess lower luminous efficiencies due to the decreased photopic response of their blue-shifted EL spectra. The device with the highest EQE made from PBOP-MEH is obtained with 0.5 wt% in PVK and exhibits a maximum brightness of 1380 cd/m^2, a maximum EQE of 1.1%, and a maximum luminous efficiency of 2.3 cd/A. Figure 3.8 shows that, similar to the other devices, the peak efficiency is higher for the linear side chain-containing PBOP-D-based device than for the branched side-chain-containing PBOP-MEH-based device, with efficiency remaining fairly consistent over a broad range of luminous intensities. The efficiency of the PBOP-D-based device displays a steep drop-off above a brightness of 500 cd/m^2. The PBOP-MEH-based device, on the other hand, does not show a sharp decline in efficiencies until reaching a brightness slightly above 700 cd/m^2. The efficiencies of the PBOP-D- and PBOP-MEH-based devices converge at a brightness of ∼600 cd/m^2, with the PBOP-MEH-based device becoming

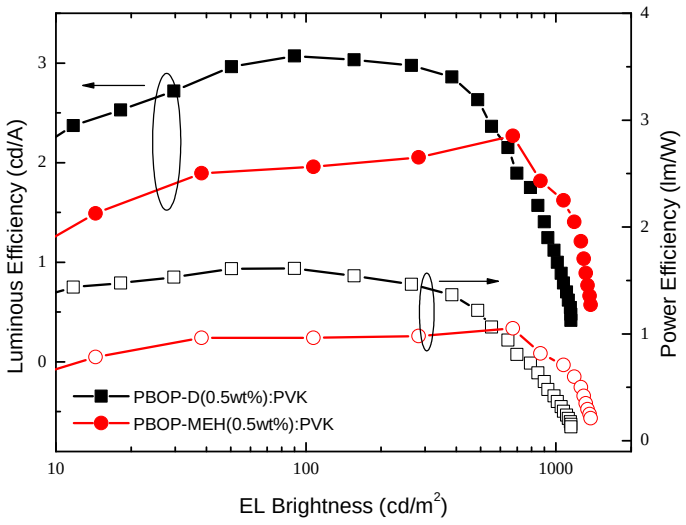

Figure 3.8 Luminous and power efficiency as a function of PLED brightness for devices using 0.5 wt% of PBOP-D or PBOP-MEH in a PVK host.

more efficient above this brightness, despite its disadvantage in the photopic response of its emission compared to the PBOP-D device.

The EL spectra of the PBOP-D- and PBOP-MEH-based PLEDs are much broader than the spectra of the PBOF-O- and PBOF-DMO-based devices, though all exhibit emission exclusively from the guest, with no host emission observed. The EL emission maxima of PBOP-D and PBOP-MEH are heavily dependent on guest concentration, with an increasing red-shift seen as the guest concentration is increased. This EL dependence on guest concentration is likely caused by π-stacking. As the EL spectrum of the PBOP-D-based devices red-shifts with increasing guest concentration, a shoulder at $\sim$560 nm grows in intensity, suggesting lower energy excimer emission due to increased aggregation of the guest in the host material. Such behavior is not seen to the same extent in the PBOP-MEH- based devices, which have a much weaker shoulder that does not grow significantly in intensity as the guest concentration is increased. It is likely that the branched side chains of the PBOP-MEH polymer disrupt aggregate

formation slightly better than the linear side chains in PBOP-D, resulting in less excimer emission compared to the latter.

The most surprising aspect of these devices is the efficient FRET from host to guest, which results in no observable host emission in the fluorene- and phenylene-containing PLEDs and only an inconclusive presence of host emission in the carbazole-containing PLEDs. Our previous reports of BBO copolymers used as guests in PVK-based PLEDs showed very poor guest emission with host emission dominating the EL spectrum. In a device made with 1 wt% PFVBBO-O, emission from the PVK was 4 times more intense than the emission from the guest.[34] The previously reported PFTBBO showed an intensity ratio of host to guest emission of 4:3 for 1 wt% guest in the PVK host with an identical device architecture.[35] The rate of energy transfer is generally dependent on the overlap of the host emission spectrum and the guest absorption spectrum.[37] The carbazole- and fluorene-containing polymers do have slightly better spectral overlap with PVK than the previously reported materials, which would lead to the conclusion that the wider bandgap of these materials leads to the improved energy transfer. However, the phenylene-containing polymers have worse spectral overlap than either PFVBBO or PFTBBO, yet they do not show any evidence of incomplete FRET between host and guest, i.e. no host emission, and in fact have significantly improved efficiencies in PVK-based PLEDs. Therefore, the improved FRET is not solely from increased spectral overlap but is the result of other factors. We speculate that by altering the orientation of the BBO moiety within the conjugated structure of the polymer, so that the electron-withdrawing oxazole rings become perpendicular to the backbone, the excited state dipole of the polymer is changed. The change in the excited state dipole may be in its direction, which causes the polymer dipole to align more favorably with the excited state dipole of the host, or an increased excited state dipole magnitude. Either of these factors would result in increased excited state dipole-dipole coupling, increasing the probability of energy transfer.[27] Further studies are currently underway to better understand this phenomenon.

3.4 Conclusions

In conclusion, six new BBO copolymers possessing a novel conjugation pathway directly through the central benzene ring were synthesized. These BBO copolymers contain either N-alkylcarbazole, 9,9-dialkylfluorene, or 2,5-dialkoxybenzene bearing either linear or branched alkyl side chains and have a conjugation pathway through the central benzene ring. Guest:host PLEDs made with these materials as guest emitters in PVK exhibited substantially higher brightness and efficiencies than any PLEDs previously reported based on BBO copolymers. These higher efficiencies are a result of the improved FRET between the host and guest. Alkyl chain substitution did not have a significant impact on the EQE of the PLEDs, though the branched side chain-bearing polymers produced devices with lower luminous efficiencies due to their blue-shifted EL relative to the linear side chain-bearing polymers. The devices containing the branched alkyl chain polymer generally exhibited better efficiencies at higher brightness levels. These discoveries will greatly benefit the future development of BBO copolymers as electron transporting emissive materials for high efficiency guest:host PLEDs, and work is currently underway to better understand the nature of the improved host–guest energy transfer.

Table 3.2 Device Characteristics of PLEDs Based on Benzobisoxazole Polymers

Device[a]							
Polymer	**wt%**[b]	$\mathbf{V}_{on}$[c] (V)	$\eta_{L,max}$ (cd/A)	$\eta_{ext,max}$ (lm/W)	$\eta_{P,max}$ (%)	λ_{max} (nm)	**CIE 1931** (x, y)
PBOCz-O	0.5	5.2	0.50	0.48	0.27	449	(0.17, 0.11)
	1	5.2	0.72	0.68	0.36	451	(0.17, 0.12)
	2	6.6	0.50	0.57	0.20	449	(0.18, 0.14)
	4	5.8	0.18	——	0.08	—-	——
PBOCz-EH	0.5	6	0.53	0.58	0.25	446	(0.17, 0.10)
	1	5.2	0.59	0.51	0.28	451	(0.17, 0.12)
	2	5	0.53	0.46	0.28	452	(0.17, 0.12)
	4	6	0.63	0.40	0.27	452	(0.18, 0.21)
PBOF-O	0.5	5	1.7	1.1	0.86	462	(0.14, 0.12)
	1	5.4	1.7	1.2	0.72	462	(0.14, 0.13)
	2	5.2	1.1	0.92	0.47	462	(0.15, 0.17)
	4	6	0.07	0.05	0.03	462	(0.15, 0.15)
PBOF-DMO	0.5	5.6	1.2	1.2	0.57	458	(0.15, 0.11)
	1	6	1.2	1.1	0.49	458	(0.15, 0.11)
	2	6.5	0.56	0.59	0.22	459	(0.15, 0.09)
	4	8	0.22	0.14	0.07	460	(0.16, 0.16)
PBOP-D	0.5	4	3.1	1.1	1.6	501	(0.18, 0.50)
	1	4.4	2.4	0.88	1.2	500	(0.21, 0.51)
	2	4.7	0.25	0.07	0.10	519	(0.35, 0.61)
	4	4.3	0.81	0.28	0.36	517	(0.25, 0.54)
PBOP-MEH	0.5	5.4	2.3	1.1	1.1	491	(0.16, 0.36)
	1	5.5	1.9	0.73	0.86	500	(0.17, 0.49)
	2	6	0.40	0.14	0.15	502	(0.21, 0.53)
	4	6	0.28	0.09	0.13	511	(0.27, 0.54)

[a] Device architecture: ITO/PEDOT:PSS/Polymer:PVK/BPhen/LiF/Al.
[b] wt% is the weight percent of the polymer in the host.
[c] Turn-on voltage is the voltage applied to produce 1 cd/m^2.

3.5 Experimental

Photoluminescence spectra were obtained using an excitation wavelength equal to the wavelength of maximum absorption for the UV spectra. Quantum yield measurements were taken of the polymers in dilute solutions of chloroform relative to Coumarin-152 in acetonitrile.[38]

PLEDs were fabricated on nominally 20 ohm/sq, 140 nm thick ITO-coated glass substrates (Colorado Concept Coatings). The substrates were first cleaned with a detergent and organic solvents and then treated in a UV/ozone oven to increase the work function of the ITO and hence facilitate hole injection, as described elsewhere.[39] A 60 nm PEDOT:PSS layer was spin-coated onto the ITO and then baked in air at 120 °C for 1 h and then in an argon-filled glovebox at 120 °C for another 30 min. Blends of PVK and BBO copolymers in chlorobenzene solutions were spin-coated on top of the PEDOT:PSS layer in the argon-filled glovebox. The combined concentration of the PVK and guest material was kept constant at 9 mg/mL. The solution was spin-coated at 4000 rpm for 60 s. The fabricated structure was then annealed at 60 °C for 30 min. Following this annealing step, the samples were transferred to a thermal evaporator within the glovebox, and the Bphen, LiF, and Al layers were deposited sequentially by thermal evaporation at a base pressure of $\sim$ 1 x 10^{-6} Torr. The PLEDs were characterized by monitoring their EL spectra, brightness as a function of the applied voltage, and luminous and power efficiencies.

3.6 Acknowledgements

We thank the 3M Foundation and the National Science Foundation (DMR-0846607) for partial financial support of this work. Partial support for this work was also provided by the Director of Energy Research, Office of Basic Energy Sciences, USDOE. Ames Laboratory is operated by Iowa State University for the US Department of Energy (USDOE) under Contract DE-AC 02-07CH11358.

3.7 Supporting Information

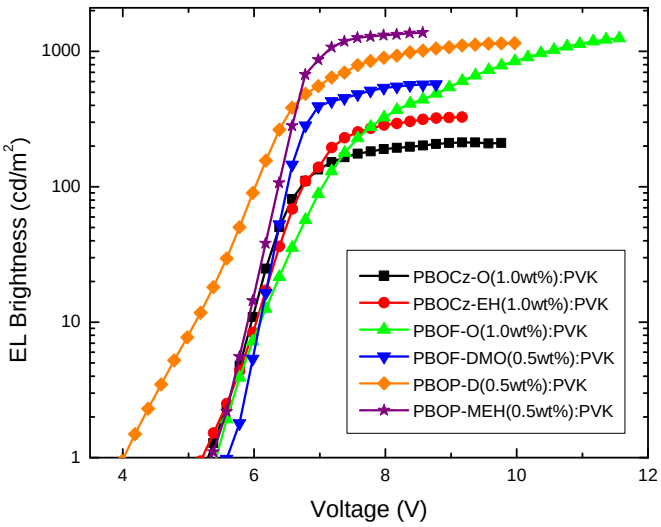

Figure 3.9 Brightness as a function of applied voltage for the best wt% performing devices for each polymer.

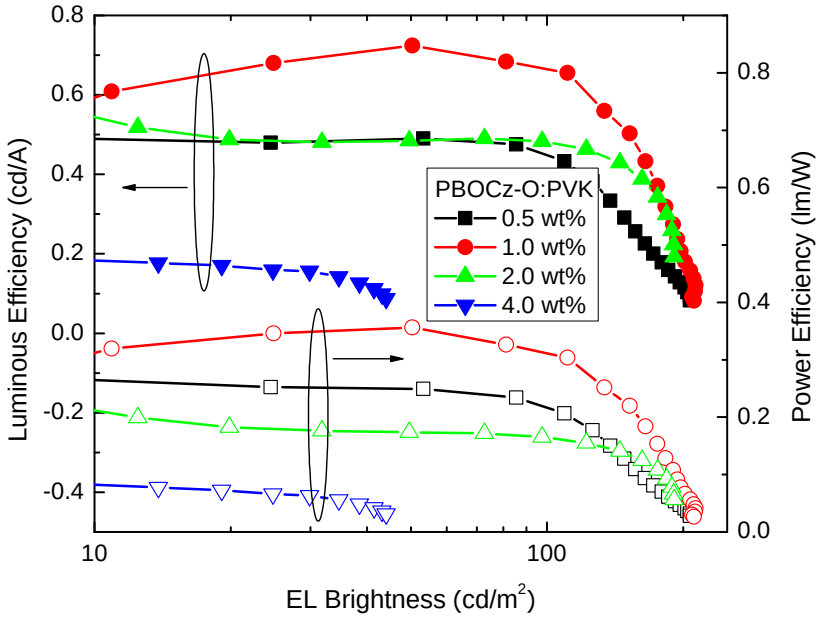

Figure 3.10 Efficiency as a function of brightness for all PBOCz-O-based PLEDs.

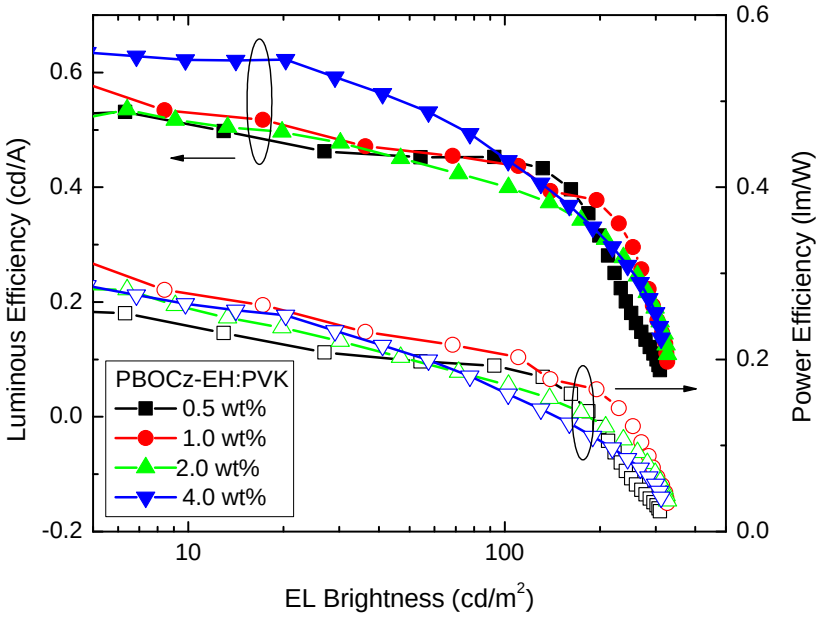

Figure 3.11 Efficiency as a function of brightness for all PBOCz-EH-based PLEDs.

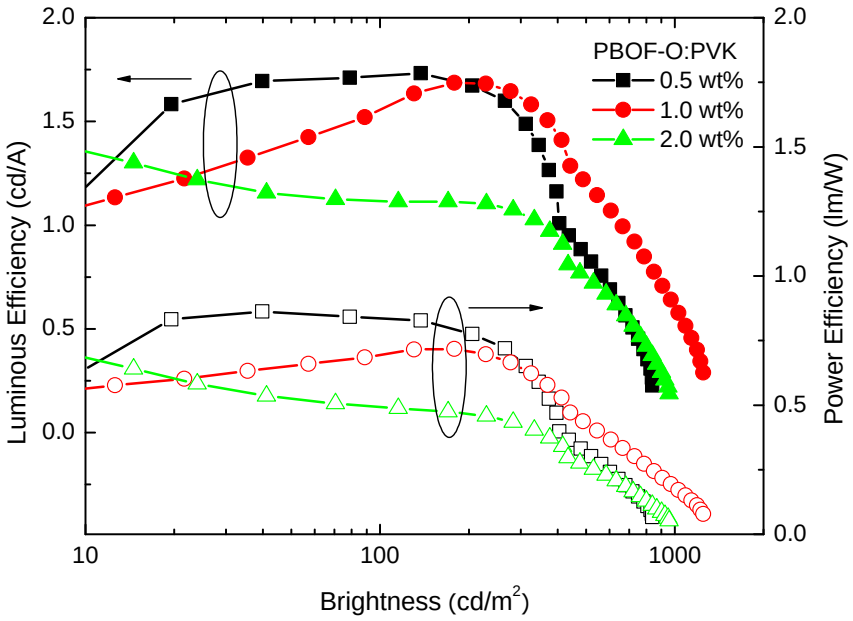

Figure 3.12 Efficiency as a function of brightness for all PBOF-O-based PLEDs.

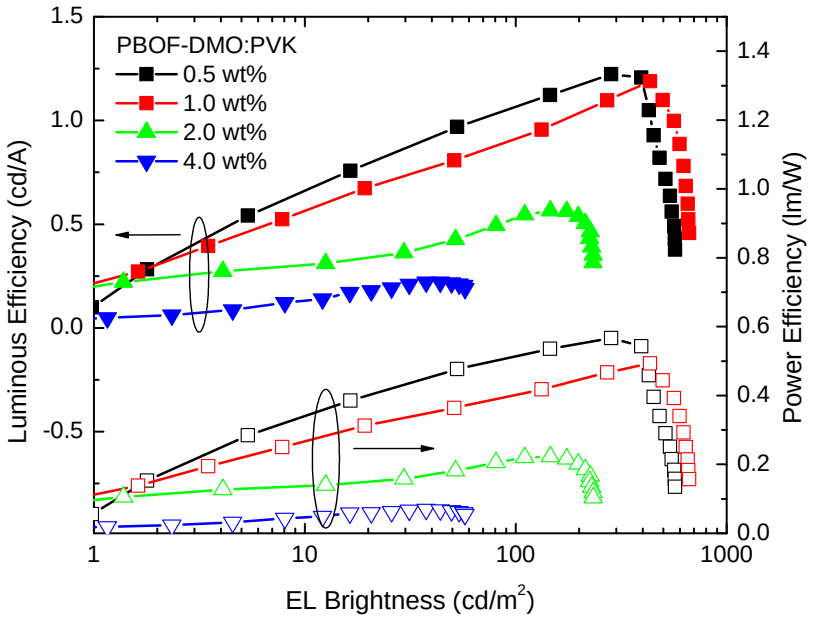

Figure 3.13 Efficiency as a function of brightness for all PBOF-DMO-based PLEDs.

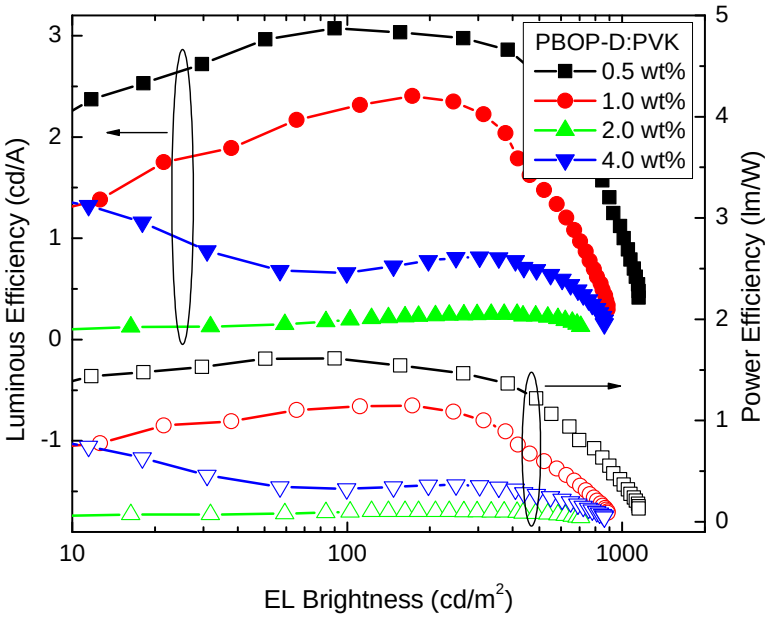

Figure 3.14 Efficiency as a function of brightness for all PBOP-D-based PLEDs.

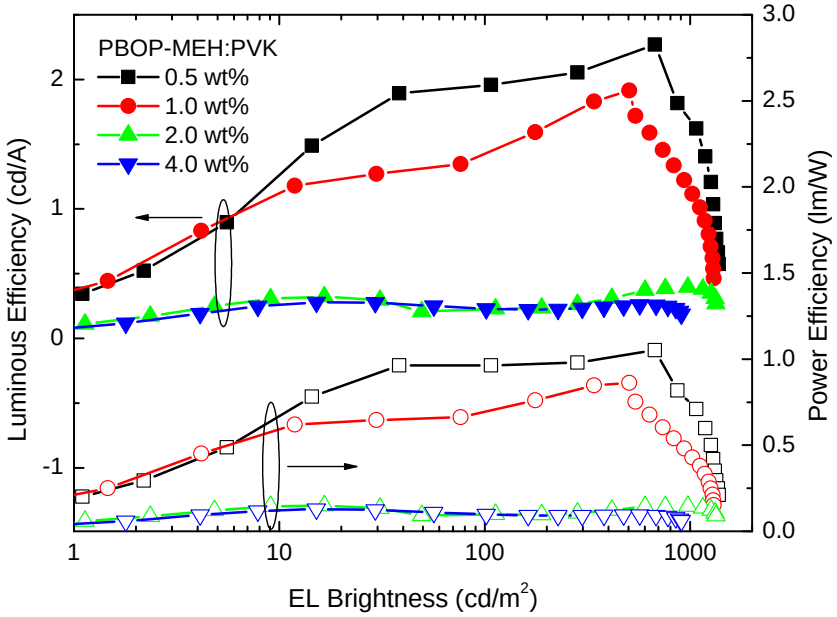

Figure 3.15 Efficiency as a function of brightness for all PBOP-MEH-based PLEDs.

References

[1] C. W. Tang, S. A. Vanslyke, *Appl. Phys. Lett.* **51**, 913 (1987).

[2] R. H. Friend, R. W. Gymer, A. B. Holmes, J. H. Burroughes, R. N. Marks, C. Taliani, D. D. C. Bradley, D. A. D. Santos, J. L. Bredas, M. Logdlund, W. R. Salaneck, *Nature* **397**, 121 (1999).

[3] S. Reineke, F. Lindner, G. Schwartz, N. Seidler, K. Walzer, B. Lussem, K. Leo, *Nature* **459**, 234 (2009).

[4] M. T. Bernius, M. Inbasekaran, J. OBrien, W. Wu, *Adv. Mater.* **12**, 1737 (2000).

[5] M.I.S, *Synth. Met.* **111**, 119 (2000).

[6] J. H. Burroughes, D. D. C. Bradley, A. R. Brown, R. N. Marks, K. Mackay, R. H. Friend, P. L. Burns, A. B. Holmes, *Nature* **347**, 539 (1990).

[7] A. C. Grimsdale, K. L. Chan, R. E. Martin, P. G. Jokisz, A. B. Holmes, *Chem. Rev.* **109**, 897 (2009).

[8] A. Kraft, A. C. Grimsdale, A. B. Holmes, *Angew. Chem., Int. Ed.* **37**, 402 (1998).

[9] S. R. Tseng, Y. S. Chen, H. F. Meng, H. C. Lai, C. H.Yeh, S. F. Horng, H. H. Liao, C. S. Hsu, *Synth. Met.* **159**, 137 (2009).

[10] S. A. Jenekhe, L. R. de Paor, X. L. Chen, R. M. Tarkka, *Chem. Mater.* **8**, 2401 (1996).

[11] G. E. Jabbour, Y. Kawabe, S. E. Shaheen, J. F. Wang, M. M. Morrell, B. Kippelen, N. Peyghambarian, *Appl. Phys. Lett.* **71**, 1762 (1997).

[12] C. J. Tonzola, A. P. Kulkarni, A. P. Gifford, W. Kaminsky, S. A. Jenekhe, *Adv. Funct. Mater.* **17**, 863 (2007).

[13] C. Haiying, C. Junwu, Q. Chengfeng, B. Z. Tang, W. Man, K. Hoi-Sing, *IEEE J. Sel. Top. Quantum Electron.* **10**, 10 (2004).

[14] L. Zhang, S. Hu, J. Chen, Z. Chen, H. Wu, J. Peng, Y. Cao, *Adv. Funct. Mater.* **21**, 3760 (2011).

[15] C.-F. Shu, R. Dodda, F.-I. Wu, M. S. Liu, A. K. Y. Jen, *Macromolecules* **36**, 6698 (2003).

[16] E. Ahmed, F. S. Kim, H. Xin, S. A. Jenekhe, *Macromolecules* **42**, 8615 (2009).

[17] J. A. Mikroyannidis, K. M. Gibbons, A. P. Kulkarni, S. A. Jenekhe, *Macromolecules* **41**, 663 (2007).

[18] M. M. Alam, S. A. Jenekhe, *Chem. Mater.* **14**, 4775 (2002).

[19] A. Babel, S. A. Jenekhe, *Adv. Mater.* **14**, 371 (2002).

[20] A. Babel, S. A. Jenekhe, *J. Phys. Chem. B* **106**, 6129 (2002).

[21] Y. Chen, S. Wang, Q. Zhuang, X. Li, P. Wu, Z. Han, *Macromolecules* **38**, 9873 (2005).

[22] D. Feng, S. Wang, Q. Zhuang, P. Wu, Z. Han, *Polymer* **45**, 8871.

[23] J. F. Wolfe, F. E. Arnold, *Macromolecules* **14**, 909 (1981).

[24] J. F. Wolfe, B. H. Loo, F. E. Arnold, *Macromolecules* **14**, 915 (1981).

[25] M. Inbasekaran, R. Strom, *OPPI Briefs* **23**, 447 (1994).

[26] J. J. Intemann, J. F. Mike, M. Cai, S. Bose, T. Xiao, T. C. Mauldin, R. A. Roggers, J. Shinar, R. Shinar, M. Jeffries-EL, *Macromolecules* **44**, 248 (2011).

[27] K. O. Cheon, J. Shinar, *Appl. Phys. Lett.* **84**, 1201 (2004).

[28] J. J. Intemann, E. S. Hellerich, B. C. Tlach, M. D. Ewan, C. A. Barnes, A. Bhuwalka, M. Cai, J. Shinar, R. Shinar, M. Jeffries-EL, *Macromolecules* **45**, 6888 (2012).

[29] J.-F. Morin, M. Leclerc, D. Ades, A. Siove, *Macromol. Rapid Commun.* **26**, 761 (2005).

[30] G. Barbarella, L. Favaretto, G. Sotgiu, M. Zambianchi, V. Fattori, M. Cocchi, F. Cacialli, G. Gigli, R. Cingolani, *Adv. Mater.* **11**, 1375 (1999).

[31] S. A. Choulis, V.-E. Choong, M. K. Mathai, F. So, *Appl. Phys. Lett.* **87**, 113503 (2005).

[32] M. Y. Chan, C. S. Lee, S. L. Lai, M. K. Fung, F. L. Wong, H. Y. Sun, K. M. Lau, S. T. Lee, *J. Appl. Phys.* **100**, 094506 (2006).

[33] M. A. Baldo, M. E. Thompson, S. R. Forrest, *Pure Appl. Chem.* **71**, 2095 (1999).

[34] J. J. Intemann, J. F. Mike, M. Cai, S. Bose, T. Xiao, T. C. Mauldin, R. A. Roggers, J. Shinar, R. Shinar, M. Jeffries-EL, *Macromolecules* **44**, 248 (2010).

[35] J. F. Mike, J. J. Intemann, M. Cai, T. Xiao, R. Shinar, J. Shinar, M. Jeffries-EL, *Polym. Chem.* **2**, 2299 (2011).

[36] H. Li, C. Zhang, D. Li, Y. Duan, *J. Lumin.* **122**, 626 (2007).

[37] M. Pope, C. E. Swenberg, *Electronic Processes in Organic Crystals*; Oxford University Press: Oxford, 1982.

[38] S. Nad, M. Kumbhakar, H. J. Pal, *Phys. Chem. A* **107**, 4808 (2003).

[39] Z. Zhou, R. Shinar, A. J. Allison, J. Shinar, *Adv. Funct. Mater.* **17**, 3530 (2007).

CHAPTER 4.

Efficient chlorobenzene/chloroform-processed fluorescent small molecule OLEDs

Emily S. Hellerich,[a] *Min Cai,*[a] *Ying Chen,*[a] *Rui Liu,*[a] *Teng Xiao,*[a]

Ruth Shinar,[b] *and Joseph Shinar* [a]

[a]Ames Laboratory-USDOE and Department of Physics and Astronomy,
Iowa State University, Ames, IA 50011, USA.

[b]Microelectronics Research Center and Department of Electrical and Computer Engineering,
Iowa State University, Ames, IA 50011, USA.

4.1 Abstract

Efficient spin-coated small molecule fluorescent OLEDs with N,N′-bis-(3-Naphthyl)-N,N′-biphenyl-(1,1′-biphenyl)-4,4′-diamine (NPB):tris-(8-hydroxyquinoline)-Al (Alq_3) emitting layers (EMLs) are demonstrated. Thermally-evaporated and spin-coated EMLs using various chlorobenzene:chloroform mixtures are compared. The root mean square roughness R_{rms} of EMLs prepared from chloroform is 4.7 nm; it decreases to 1.1 nm using 3:1 chlorobenzene:chloroform, which is significantly smoother than evaporated films ($R_{rms} \sim$ 1.9 nm). Devices with EMLs prepared from solutions containing $>$25 vol.% chlorobenzene reached efficiencies of 5.0 Cd/A and 3.0 lm/W, compared to 3.9 Cd/A and 1.6 lm/W for evaporated

devices. EML doping with 1.0 wt.% 10-(2-benzothiazolyl)-2,3,6,7-tetrahydro-1,1,7,7-tetramethyl-1H, 5H, 11H-[l]benzopyrano[6,7,8-ij]quinolizin-11-one (Coumarin C545T) yielded 7.6 Cd/A and 5.1 lm/W.

4.2 Introduction

Organic light-emitting diodes (OLEDs) present an impressive opportunity for creation of new lighting technologies with the availability of a broad array of organic materials. Many studies have been devoted to specifically two categories of such materials: small molecules and polymers. While small molecules tend to be easier to synthesize and purify than polymers[1] and often exhibit higher efficiency and lifetime when incorporated into devices,[2,3] their common fabrication technique of thermal evaporation presents complications for doping and difficulties for incorporation into large-scale production.[4] Polymers, on the other hand, lend themselves to solution-based fabrication,[5] rendering tedious co-evaporation processes for doping unnecessary and offering many possibilities for large-scale production.[6]

Recently, attention has shifted to the incorporation of small molecules into solution-processed devices.[1,7–11] With this focus, we gain the high efficiency of small molecules as well as the ease of fabrication by solution processing. He et al.[1] demonstrated the successful spin-coating of small molecule mixed layers. Wang et al.[9] highlighted the value added for a small molecule multi-dopant device and demonstrated the ability to fabricate solution-processed small molecule OLEDs (SMOLEDs) with efficiencies comparable to similar evaporated devices.

In this study, spin-coated small molecule films of mixed N, N′′-bis-(3-Naphthyl)-N, N′′-biphenyl-(1,1′′-biphenyl)-4,4′′-diamine (NPB) and tris-(8-hydroxyquinoline)-aluminum (Alq_3), at a ratio of 85:15, were fabricated using various ratios of chlorobenzene:chloroform (CB:CF) as the solvent and were compared to similar evaporated films, including via atomic force microscopy (AFM) imaging. It was found that the spin-coated films are smoother than the evap-

orated films when the high boiling point solvent, i.e. CB, makes up more than 50 vol.% of the solution. OLEDs were fabricated using these films; their structure was ITO/ 50 nm poly(3,4-ethylenedioxy thiophene):poly(4-styrenesulfonate) (PEDOT:PSS)/ NPB:Alq_3 (85:15)/ 10 nm 2,9-dimethyl-4,7-diphenyl-1,10-phenanthroline (Bathocuproine, BCP)/ 30 nm 4,7-diphenyl-1,10-phenanthroline (BPhen):Alq_3 (1:1)/ 1 nm LiF/ 100 nm Al. PEDOT:PSS (spin-coated hole-injection layer) and BPhen (evaporated electron-transport layer) were added to increase the device efficiency beyond those of the devices reported by He et al.[1] The spin-coated devices have efficiencies equal to or greater than the equivalent thermally-evaporated OLEDs, with power efficiencies of the best spin-coated devices rivaling that of multi-layer OLEDs with a similar EML.[12,13] Luminous efficiency and power efficiency, averaged over multiple pixels, reached 5.0 Cd/A and 3.0 lm/W, respectively in the spin-coated devices, compared to averaged efficiency peaks of 3.9 Cd/A and 1.6 lm/W for the evaporated devices. Doping the EML with various wt.% of C545T (10-(2-benzothiazolyl)-2,3,6,7-tetrahydro-1,1,7,7-tetramethyl- 1H,5H,11H-[l]benzopyrano[6,7,8-ij]quinolizin-11-one) increased the efficiency further, yielding averaged peak efficiencies of 7.6 Cd/A and 5.1 lm/W for a 1 wt.% dopant level.

4.3 Experimental Procedure

The OLEDs were fabricated on 1″x1″ ITO-coated glass substrates; the resistance R of the ITO coating was $R \sim 12\ \Omega$/sq and its thickness $t \sim 120$ nm. Substrates were cleaned, as previously described,[14,15] using surfactant and acetone, and treated in a UV-ozone oven. A hole injection layer of PEDOT:PSS, purchased from Heraeus Materials Technology, was fabricated by spin-coating the solution in air at a speed of 2000 rpm for 60 s, followed by baking at 120°C for 30 min in air and 30 min in argon atmosphere.

The EML consisted of a mix of the hole transport material NPB and the electron transport material Alq_3. He et al. reported that film morphology is improved with increased NPB:Alq_3

ratio, possibly due to the more linear molecular structure of NPB, and is the smoothest at a ratio of 85:15.[1] Therefore an NPB:Alq_3 ratio of 85:15 was used for the EML, which was either spin-coated or thermally evaporated (vacuum pressure $P < 1\text{x}10^{-6}$ mbar) inside an argon-atmosphere glove box ($<$ 20 ppm O_2). Solutions for spin-coating of the NPB:Alq_3 mix were at a total concentration of 5 mg/mL in either CF or a mixture of various ratios of CB to CF. C545T, an efficient green dopant,[16–19] was added to select solutions at 0.5, 0.8, 1.0, 1.5, & 2.8 wt.% in efforts to further increase the efficiency. The ratio of solvents was set at 3:1 CB:CF for the EML consisting of the C545T-doped co-host. Each solution was mixed for at least three hours in an ultrasonic bath, spin-coated at 2000 rpm for 60 s in an argon atmosphere, and baked at 80°C for 30 minutes. The thickness of the thermally evaporated EML was $t = 40$ nm. Film morphology was investigated using AFM.

Subsequent small molecule layers required for the devices were thermally evaporated, including: BCP, hole blocking layer; BPhen:Alq_3 (1:1), mixed electron transport layer; LiF, cathode buffer; and Al, which was deposited through a mask. The resulting devices were 1.5 mm diameter pixels.

Devices were characterized by current-voltage-luminescence measurements, using a Kepco DPS 40-2M programmable power supply, a Keithly multimeter 2000, and a Minolta luminance meter LS-110.

OLEDs used for stability testing were fabricated on patterned ITO-coated substrates, etched using HCl/zinc powder, and encapsulated after the deposition of the Al. The resulting pixels were 2x2 mm^2. Stability measurements were done using Keithley 2400 source meter, Keithly multimeter 2000, and the Minolta luminance meter LS-110.

4.4 Results and Discussion

4.4.1 Atomic Force Microscopy (AFM) Images

AFM images demonstrating the differing morphologies of a thermally-evaporated film and films spin-coated from solutions of various CB:CF ratios are shown in Figure 4.1. It is clear from the images that increasing the fraction of CB in the solution decreases the roughness and improves uniformity. Spin-coated films prepared from mixtures with 50% and 75% CB showed root mean square roughness (R_{rms}) values (measured at an image scale of 10 μm) of 1.4 nm and 1.1 nm, respectively, indicating that the films were significantly smoother than the similar evaporated film, which had an R_{rms} of 1.9 nm. The film prepared from the pure CF solution was significantly rougher with R_{rms} = 4.7 nm. It was also apparent that the PEDOT:PSS layer was smoother than the bare ITO (images not shown). The morphology of the hole-injection layer has been shown to affect the morphology of the spin-coated EML, and consequently the device performance.[9,20,21] Therefore it is likely that the PEDOT:PSS layer improves the device performance beyond the hole-injection enhancement.

CF was originally used for spin-coating as this solvent was previously found to be suitable for dissolving small molecule materials.[7] However, it was apparent that the film spin-coated from CF was much less uniform when compared to the evaporated film, as the device pixels were partially or unevenly lit. CB was added to the small molecule solution as it was previously shown for polymer films that the addition of a higher boiling point solvent improves film uniformity by slowing solvent evaporation.[22,23] Increased drying time improves microstructural ordering, resulting in a smoother film morphology. In addition, it was previously suggested that aromatic solvents lead to alignment of aromatic molecules in films.[23–25] Unlike CF, CBs aromatic structure increases alignment by solvating the aromatic segments (i.e, the rings in NPB and Alq_3) rather than the side chains, thereby improving charge carrier mobility and morphology.[23] Pure CB was not used, as the solubility of Alq_3 in CB is poor.

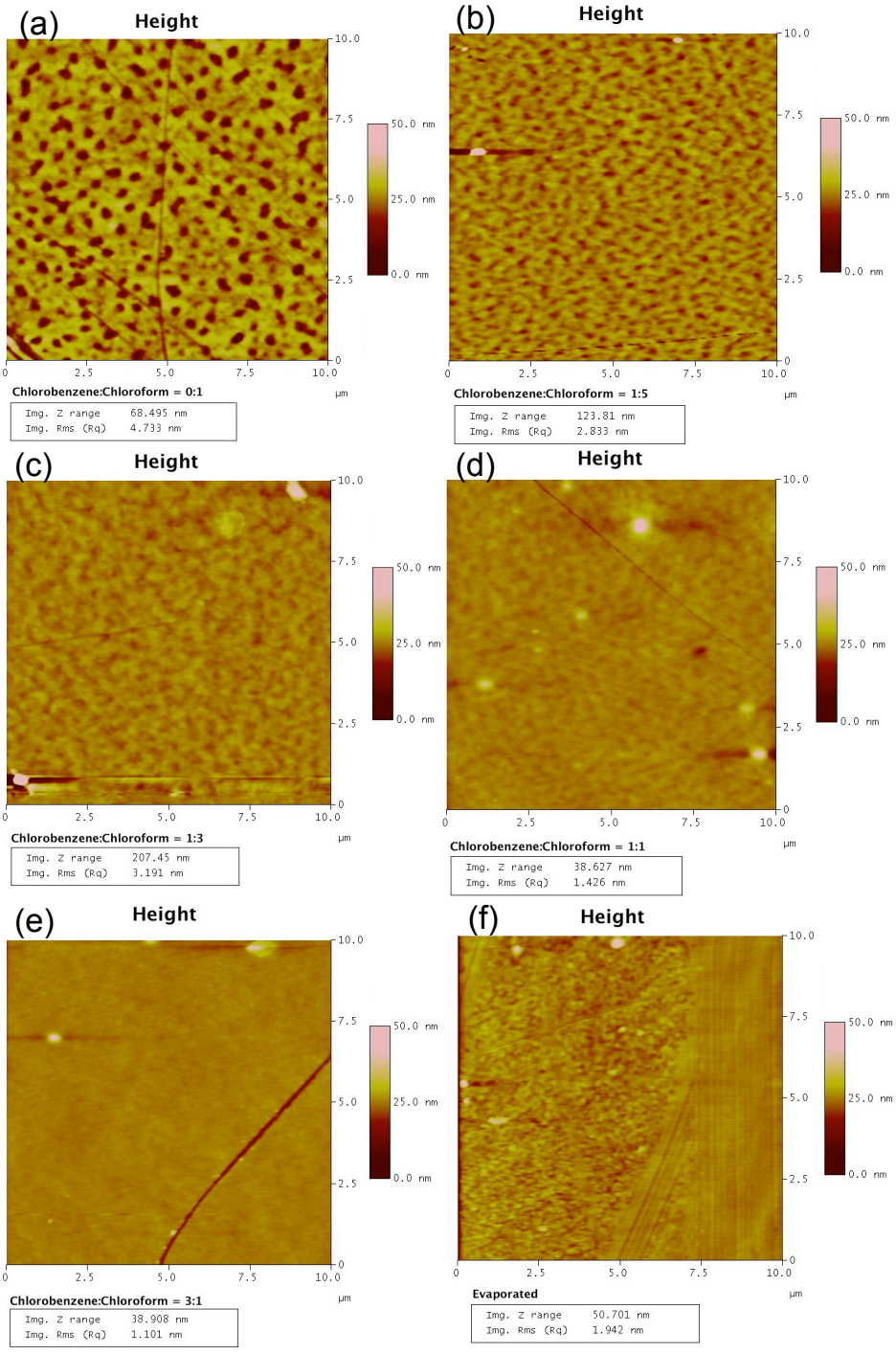

Figure 4.1 AFM images of various NPB:Alq_3 films on ITO/PEDOT:PSS-coated glass substrates: spin-coated from solution with a CB:CF ratio of (a) 0:1 (R_{rms} = 4.7 nm), (b) 1:5 (R_{rms} = 2.8 nm), (c) 1:3 (R_{rms} = 3.2 nm), (d) 1:1 (R_{rms} = 1.4 nm), and (e) 3:1 (R_{rms} = 1.1 nm), and (f) evaporated (R_{rms} = 1.9 nm).

4.4.2 Device Characteristics

Plots of the brightness and current density vs. voltage and luminous efficiency and power efficiency vs. brightness for devices with EMLs that were thermally evaporated or spin-coated from solutions of various CB:CF ratios are shown in Figure 4.2. Typical variation for current and efficiency values are $\pm$ 10 %. The turn-on voltage for the evaporated devices was $\sim$ 4 V; it decreased in the spin-coated devices with high CB fraction to $\sim$ 3 V. The peak brightness reached over 26,000 Cd/m^2 in the device with the EML prepared from a 3:1 CB:CF solution, similar to the evaporated OLED. The averaged luminous efficiency reached $\sim$ 5.0 Cd/A at a brightness of $\sim$ 600 Cd/m^2 ($\sim$ 10 mA/cm^2) in the spin-coated devices having EMLs that were prepared from solutions with CB $\geq$ 25%. In contrast, the device having an evaporated EML reached an averaged luminous efficiency of only $\sim$ 3.9 Cd/A at a brightness of $\sim$ 520 Cd/m^2 ($\sim$ 15 mA/cm^2). Devices with EMLs prepared from solutions with CB $<$ 25% had lower efficiency, peaking at $\sim$ 3.8 Cd/A. Power efficiency of the spin-coated devices made from solutions with CB $\geq$ 25% also exceeded that of the evaporated device. These spin-coated devices exhibited peak power efficiencies of 2.5 - 3.0 lm/W, where the power efficiency of the evaporated device peaked at $\sim$ 1.6 lm/W. The peak power efficiency of the spin-coated devices is comparable to a multilayer device with an equivalent emission layer, highlighting the importance of spin-coated EMLs to the reduction of power usage and operating voltage in OLEDs.[12,13]

It is apparent that the efficiency is increased above that of the evaporated structure with CB $\geq$ 25%. This aligns with the effect of CB on the morphology of the film, as shown by the AFM images (Fig. 4.1). In past studies, smoother EML morphology has been associated with higher efficiency devices.[9,23,25] The morphology change seen here is likely a cause for the improved efficiency with the addition of CB to the small molecule solution.

Luminous efficiency and power efficiency of devices doped with various wt.% C545T are shown in Figure 4.3. The addition of C545T raised the luminous efficiency to a peak of 7.6 Cd/A and the power efficiency to 5.1 lm/W at a concentration of 1.0 wt.%.

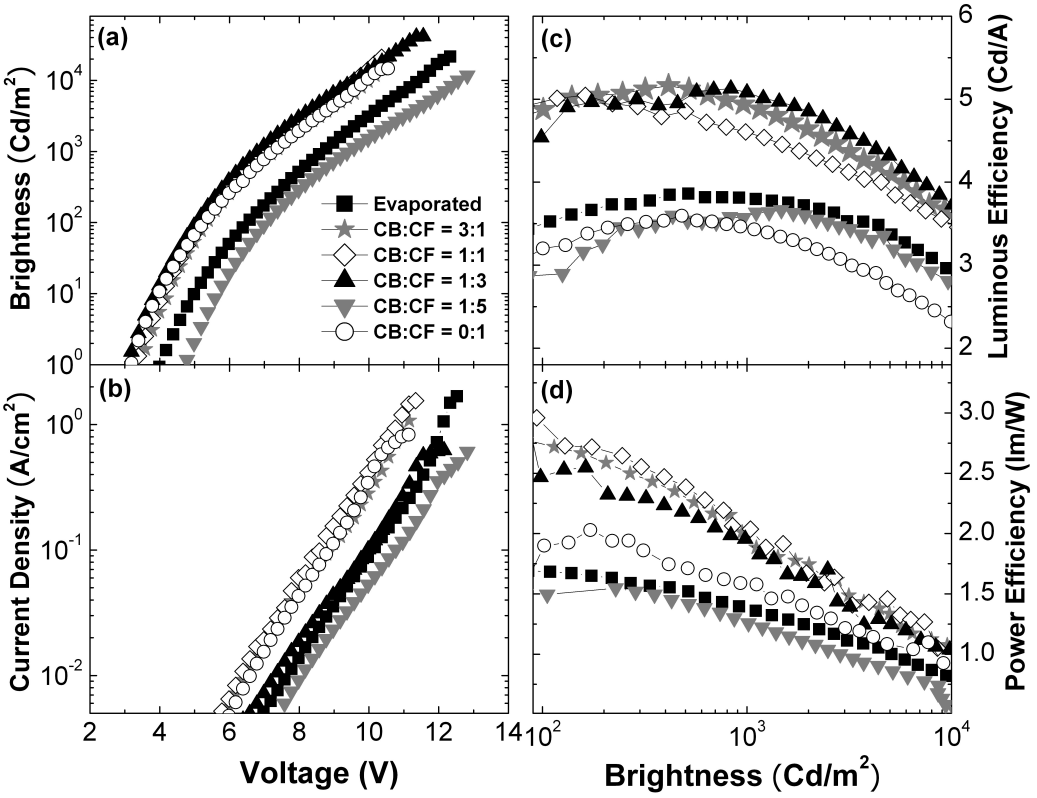

Figure 4.2 (a) Brightness vs. voltage, (b) current density vs. voltage, (c) luminous efficiency vs. brightness, and (d) power efficiency vs. brightness for the evaporated device and spin-coated devices with various CB:CF ratios.

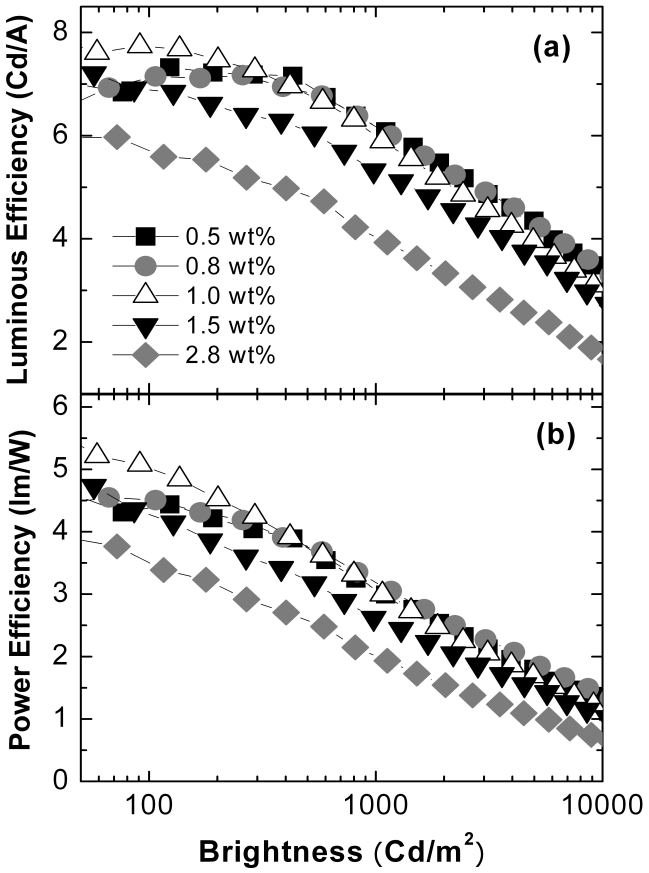

Figure 4.3 (a) Luminous efficiency vs. brightness and (b) power efficiency vs. brightness for various concentrations of C454T doped into 85:15 NPB:Alq_3.

The extrapolated lifetime of the spin-coated devices with initial brightness of 100 Cd/m^2 was about 30% of the evaporated device. It has been suggested that the reduced stability of the spin-coated devices is due to decreased packing density and the increased likelihood of crystallization.[20] The solvent effect demonstrated in this study provides a potential route to better control the film morphology, and therefore improve the packing density and the device stability.

4.5 Summary

In summary, films and devices based on spin-coated small molecule EMLs were fabricated and compared to similar devices with a thermally-evaporated EML. AFM images showed that the R_{rms} in films prepared from solutions with a high fraction of CB in a mixture with CF is significantly lower than the R_{rms} of a similar thermally-evaporated film. The effect of improved film morphology with the addition of CB highlights a possible avenue for improvement of film packing density, and ultimately device lifetime. It is evident that the spin-coated devices prepared from solutions with high CB percentage have a considerably higher efficiency than the evaporated devices. The luminous and power efficiencies of devices with spin-coated EMLs reached 5.0 Cd/A and 3.0 lm/W, respectively, whereas the corresponding values for evaporated devices were only 3.9 Cd/A and 1.6 lm/W. These efficiencies increased with the addition of the green dopant C545T to over 7.6 Cd/A and 5.1 lm/W. The recent attention to spin-coated SMOLEDs has demonstrated the benefits of such devices, including ease of fabrication, scalability, and the non-complex production of multi-dopant OLEDs. This study demonstrates the usability of small molecules in spin-coated OLEDs and indicates that their characteristics are comparable to or better than similar evaporated devices.

4.6 Acknowledgements

Research supported by the U.S. Department of Energy, Basic Energy Sciences, Materials Sciences and Engineering Division, under Contract No. DE-AC 02-07CH11358.

References

[1] L. He, J. Liu, Z. Wu, D. Wang, S. Liang, X. Zhang, B. Jiao, D. Wang, X. Hou, *Thin Solid Films* **518**, 3886 (2010).

[2] C. Adachi, M. A. Baldo, S. R. Forrest, M. E. Thompson, *Appl. Phys. Lett.* **77**, 904 (2000).

[3] J. S. Huang, M. Pfeiffer, A. Werner, J. Blochwitz, K. Leo, S. Y. Liu, *Appl. Phys. Lett.* **80**, 139 (2002).

[4] B.W. Drsquoandrade, M.E. Thompson, S.R. Forrest, *Adv. Mater.* **14**, 147 (2002).

[5] M. Granstrom, O. Inganas, *Appl. Phys. Lett.* **68**, 147 (1996).

[6] D.A. Pardo, G.E. Jabbour, N. Peyghambarian, *Adv. Mater.* **12**, 1249 (2000).

[7] K.-H. Kim, S.-Y. Huh, S.-m. Seo, H. H. Lee, *Appl. Phys. Lett.* **92**, 093307 (2008).

[8] D. Wang, Z. Wu, X. Zhang, D. Wang, X. Hou, *J. Lumin.* **130**, 321 (2010).

[9] D. Wang, Z. Wu, X. Zhang, B. Jiao, S. Liang, D. Wang, R. He, X. Hou, *Org. Electron.* **11**, 641 (2010).

[10] L. Hou, L. Duan, J. Qiao, W. Li, D. Zhang, Y. Qiu, Appl. *Phys. Lett.* **92**, 263301 (2008).

[11] M. Cai, T. Xiao, E. Hellerich, Y. Chen, R. Shinar, J. Shinar, *Adv. Mater.* **25**, 3590 (2011).

[12] D. Liu, C.-G. Zhen, X.-S. Wang, D.-C. Zou, B.-W. Zhang, Y. Cao, *Synth. Met.* **146**, 85 (2004).

[13] S. W. Shi, D. G. Ma, J. B. Peng, *Eur. Phys. J. Appl. Phys.* **40**, 141 (2007).

[14] F. Li, H. Tang, J. Anderegg, J. Shinar, *Appl. Phys. Lett.* **70**, 1233 (1997).

[15] F. Li, H. Tang, J. Shinar, O. Resto, S. Z. Weisz, *Appl. Phys. Lett.* **70**, 2741 (1997).

[16] K. Okumoto, H. Kanno, Y. Hamaa, H. Takahashi, K. Shibata, *Appl. Phys. Lett.* **89**, 063504 (2006).

[17] C. Shufen, L. Xue, X. Wenfa, Z. Yi, L. Chuannan, L. Shiyong, *Thin Sol. Films* **516**, 3364 (2008).

[18] H. Tang, X. R. Wang, Y. Li, W. G. Wang, R. G. Sun, *Displays* **29**, 502 (2008).

[19] J. Zhong, J. B. Cheng, W.B. Chen, G. Yang, Q. Jiang, *Proc. SPIE.* **6117**, 61171c (2006).

[20] L. Duan, L. Hou, T.-W. Lee, J. Qiao, D. Zhang, G. Dong, L. Wang, Y. Qiu, *J. Mater. Chem.* **20**, 6392 (2010).

[21] F. Wang, X. Qiao, T. Xiong, D. Ma, *Org. Electron.* **9**, 985 (2008).

[22] J.-F. Chang, B. Sun, D. W. Breiby, M. M. Nielsen, T. I. Solling, M. Giles, I. McCulloch, H. Sirringhaus, *Chem. Mater.***16**, 4772 (2004).

[23] Y.-H. Kim, Y. U. Lee, J.-I. Han, S.-M. Han, M.-K. Han, *J. Electrochem. Soc.* **12**, 154 (2007).

[24] Y. Shi, J. Liu, Y. Yang, *J. Appl. Phys.* **87**, 4254 (2000).

[25] J. Liu, Y. Shi, Y. Yang, *Adv. Funct. Mater.* **11**, 420 (2001).

CHAPTER 5.

Deep blue/ultraviolet microcavity OLEDs based on solution-processed PVK:CBP

Emily S. Hellerich,[a,b] *Robert Heise,*[a,c] *Eeshita Manna,*[a,d] *Rana Biswas,*[a,b,d,e]

Ruth Shinar,[d,e] *and Joseph Shinar*[a,b]

[a]Ames Laboratory-USDOE, Ames, IA 50011, USA.

[b]Department of Physics and Astronomy, Iowa State University, Ames, IA 50011, USA.

[c]Simpson College, Indianola, IA 50125, USA

[d]Department of Electrical and Computer Engineering, Iowa State University, Ames, IA 50011, USA.

[e]Microelectronics Research Center, Ames, IA 50011, USA.

5.1 Abstract

An array of deep blue to near ultraviolet microcavity OLEDs ($\lambda \sim$ 373–469 nm) are made using a mixed emitting layer (EML) of poly(*N*-vinyl carbazole) (PVK) and 4,4′-bis(9-carbazolyl)-biphenyl (CBP), with the structure: Ag 40 nm/ MoO_x X nm/ PVK:CBP (3:1) ∼30 nm/ BPhen Y nm/ LiF 1 nm/Al 100 nm, where X = 5, 10, 15, 20 nm and Y = 10, 15, 20, 30 nm. In the short wavelength microcavity devices, only CBP emission was observed, while in the long wavelength microcavity devices the emission from both PVK and CBP was evident. To better understand this behavior structural analysis of the EML and the preceding MoO_x layer as well as simulations based on the scattering matrix method were performed. The source profile of the EML is extracted from the measured electroluminescence (EL) of ITO-based

devices. The calculated microcavity spectra indicate that in the thinner devices the emission is primarily from CBP; in the thicker devices both CBP and PVK contribute to the EL. The optical cavity length affects the relative contributions of PVK and CBP EL.

5.2 Introduction

OLEDs are becoming more applicable for solid state lighting and display technologies. They are also attractive for analytical applications, advancing development of compact sensors and on-chip spectrometers.[1–15] However, there still exists a need for improvement in deep blue OLEDs for lighting and displays and ultraviolet OLEDs as excitation sources in sensing applications. Particularly of interest for analytical applications are narrow-band multi-color microcavity OLED arrays, which can be used in on-chip spectrometers or in multianalyte chemical or biological sensing.[1,2,16,17]

Microcavity OLED arrays with narrow band emission have been previously studied using various techniques, including doped-layer thickness variation and grayscale lithography.[2,18] Recently, Liu et al. incorporated a simple method of hole injection layer thickness variation using various thicknesses of molybdenum oxide (MoO_x).[16] Multi-color microcavity OLED arrays require broad-band base emission. That is, the emission of the analogous ITO-based devices should be broad enough to cover wavelengths desired for the microcavity OLEDs. In this way, high quality, narrow peaks can be obtained across a range of wavelengths.

Herein we present a unique approach for multi-colored OLED arrays in the deep blue and UV wavelengths. Mixing the polymer poly(*N*-vinyl carbazole) (PVK) with the small molecule 4,4′-bis(9-carbazolyl)-biphenyl (CBP) results in a combined emission that is broad across the near UV and blue regions. A blend of PVK and CBP was used previously, at various ratios, as a host for Ir-complex emitters requiring a large gap host.[19–21] In these previous studies, PVK was the matrix, while CBP was the charge carrier transport material. This work uses the blend of PVK and CBP to expand the work of Liu et al.[16] and add microcavity peaks in the

UV and deep-blue for future use in an on-chip spectrometer. Using the combined emission of PVK and CBP as a base for microcavity OLEDs, we are able to produce multiple emission peaks by varying the thickness of the hole injection layer (MoO_x) and electron transport layer (4,7-diphenyl-1,10-phenanthroline, BPhen). In efforts to understand and improve the emission properties of such microcavity devices, the origins of the source emission are investigated using scattering matrix-based simulations. The simulations suggest that the spontaneous emission rates strongly depend on the local electric fields at the emitting sites.

5.3 Results and Discussion

5.3.1 ITO-based Devices and Source Profile

A mixed emitting layer (EML) composed of PVK and CBP results in a broad electroluminescence (EL) band that can be used for generating UV-to-blue microcavity pixel arrays. Different weight ratios, including 1:1, 2:1, and 3:1 PVK:CBP, were tested first in ITO-based devices to optimize a wide emission spectrum, as shown in Fig. 5.1(a). The device structures were: ITO/ MoO_x 5 nm/ EML/ BPhen 20 nm/ LiF 1 nm/ Al 100 nm. As expected, with increased PVK weight fraction, the longer wavelength emission, seen only in the PVK EL spectrum, is more prominent. A PVK:CBP ratio that results in a broader EL spectrum in ITO-based OLEDs yields narrower full widths at half maximum (FWHMs) microcavity emission bands for devices optimized for longer wavelength peaks, such as for the device with the $\sim$440 nm peak shown in Fig. 5.1(b). As can be seen, the micro-cavity devices made from 3:1 PVK:CBP ratio have a narrower FWHM and a weaker shoulder at shorter wavelengths. The FWHM and spectral shape of the peaks at shorter wavelength, however, is not altered with increasing PVK fraction.

To better understand the emission profiles of microcavity structures with the PVK:CBP 3:1 EML, analogous ITO-based devices (differing by only the anode) with different MoO_x thicknesses were tested. The structures were: ITO/ MoO_x [5, 10, 15 or 20 nm]/ PVK:CBP 3:1

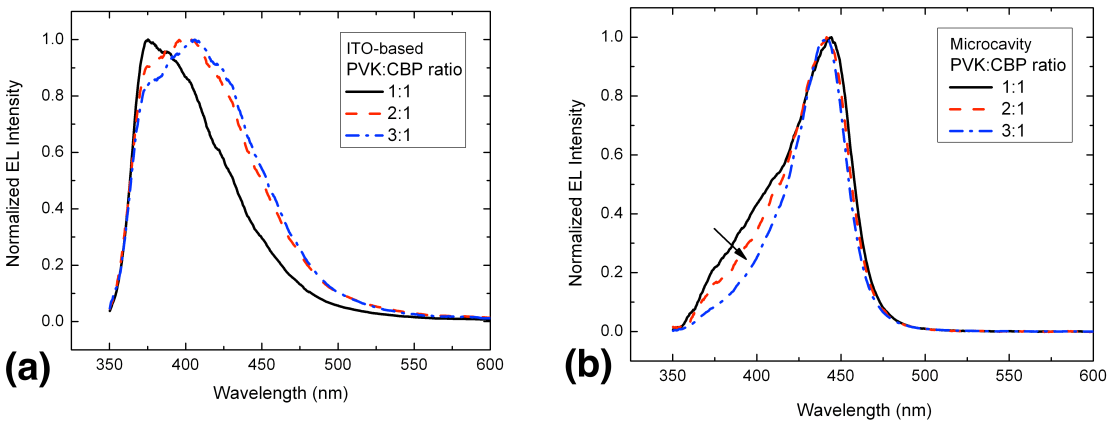

Figure 5.1 EL spectra of (a) ITO-based devices with EMLs of various PVK:CBP ratios and (b) microcavity devices with emission peak at ∼440 nm using different EMLs.

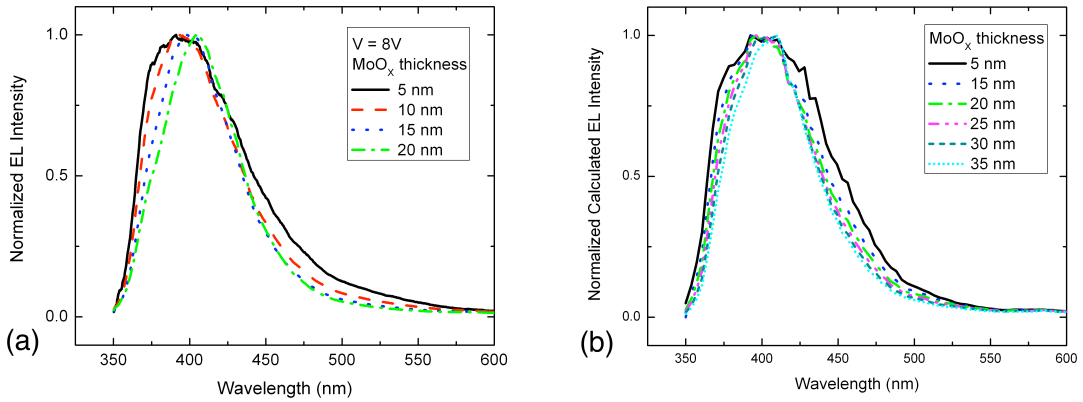

Figure 5.2 Spectra of ITO-based devices with various MoO_x thicknesses, (a) measured and (b) calculated.

$\sim$30 nm/ BPhen 20 nm/ LiF 1 nm/ Al 100 nm. Figure 5.2(a) shows the emission spectra of these devices. Although, for a given devices structure, there is slight spectral shift with change in applied voltage (not shown), the variations between pixels is minimal. It is clear that with increasing MoO_X thickness, the emission is narrowed (FWHM decreases from 77 nm to 61 nm) and red-shifted (peaks shift from $\sim$391 nm to $\sim$406 nm). It is known that there is a weak microcavity effect present, even in devices with a non-metallic anode,[23] and that this effect is dependent on the optical cavity length, which changes with changing MoO_X thickness. Figure 5.2(b) shows the calculated curves, discussed below, which match well to the red-shift and narrowing of the measured spectra.

Figure 5.3(a) shows the current vs. voltage curves for ITO-based devices with MoO_X thickness of 5, 10, 15, or 20 nm and BPhen thickness of 20 nm. The typical variation of these I-V curves is approximately $\pm$ 10%. It is clear that at a given voltage, increasing the MoO_X thickness increases the current, with the largest difference being between 5 nm and 10 nm thick MoO_X devices. In previous studies, the current decreases with increasing MoO_X thickness, presumably due to the increase in resistance from the thicker MoO_X.[16] Atomic force microscopy (AFM) images of the MoO_X films were done to determine the cause of the contrasting characteristic seen here. Figure 5.4 shows the AFM images of ITO/MoO_X films with MoO_X thicknesses of 5 & 20 nm; the root-mean-square roughness (R_{RMS}) values are shown in Table 5.1 for MoO_X thicknesses of 5, 10, 15, & 20 nm. Clearly, the roughness of MoO_X does not change significantly with changing thickness and mirrors the underlying ITO layer roughness, known to be $\sim$ 4.4 nm.[22] It is therefore likely that the 5 nm MoO_X on ITO is significantly discontinuous, having a roughness similar to its thickness. The thin, discontinuous layer would have poorer injection and, consequently, lower current compared to the thicker, more continuous MoO_X layers.

Current vs. voltage for ITO-based devices with changing BPhen thickness (10, 15, 20, & 30 nm), but constant MoO_X thickness (15 nm), are shown in Fig. 5.3(b). The current decreases slightly at a given voltage with increasing BPhen thickness, likely due to increased resistance

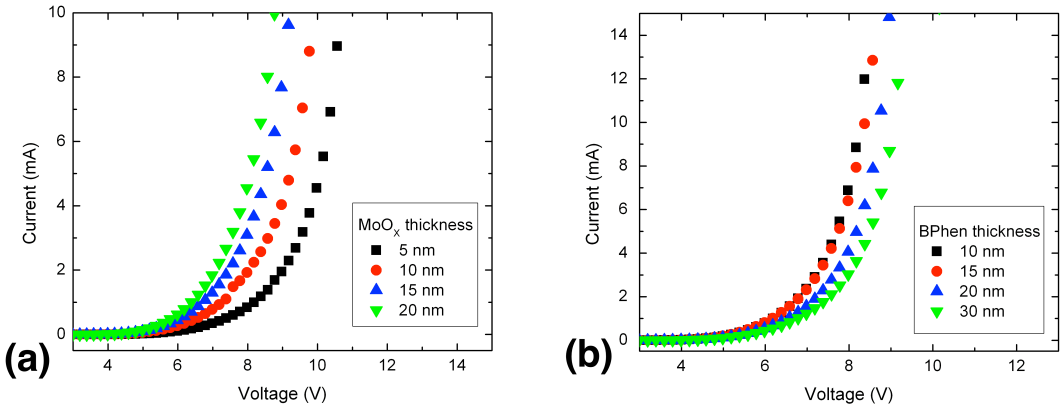

Figure 5.3 Current vs. voltage of ITO-based devices with (a) various MoO_X thicknesses and (b) various BPhen thicknesses.

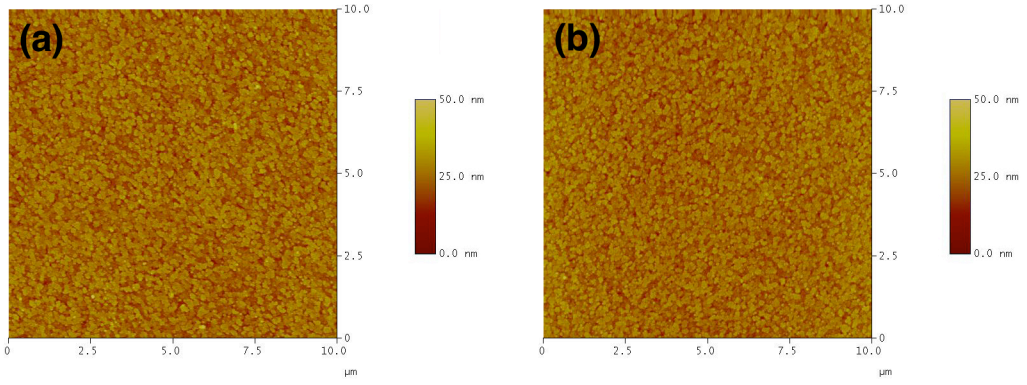

Figure 5.4 AFM images of MoO_X films on ITO, with thickness of (a) 5 nm ($R_{RMS} \sim 4.2 \pm 0.2$) and (b) 20 nm ($R_{RMS} \sim 4.0 \pm 0.2$).

Table 5.1 Values of R_{RMS} from AFM scans.

Film	R_{RMS} (nm)	Spread in R_{RMS} (nm)
MoO_x on ITO		
ITO/ MoO_x 5nm	4.2	0.2
ITO/ MoO_x 10nm	4.1	0.2
ITO/ MoO_x 15nm	4.1	0.1
ITO/ MoO_x 20nm	4.0	0.2
MoO_x on Ag		
Ag 40nm/ MoO_x 5nm	0.9	0.1
Ag 40nm/ MoO_x 15nm	1.0	0.1
Ag 40nm/ MoO_x 20nm	1.0	0.1
PVK:CBP EML		
ITO/ MoO_x 5nm/ PVK:CBP (3:1)	0.8	0.05
ITO/ MoO_x 20nm/ PVK:CBP (3:1)	1.1	0.1
Ag 40nm/ MoO_x 5nm/ PVK:CBP (3:1)	0.4	0.05
Ag 40nm/ MoO_x 20nm/ PVK:CBP (3:1)	0.4	0.05

from the thicker BPhen.

In order to predict the microcavity emission with the PVK:CBP EML, the source profile is determined by comparing simulations with measurements for the ITO-based device with 5 nm thick MoO_x and 20 nm thick BPhen (variations of the source profile with thicker MoO_x were small). The emitting species is represented by infinitesimal dipoles residing within the PVK:CBP blend layer. The transmission intensity $T_{cal}(\lambda)$ from the ITO-based device in all directions is simulated using these emissive sources (via the scattering matrix method). The source profile $I_{source}(\lambda)$ of the emitting source is then fitted to the measured data through the relation:

$$E_{meas}(\lambda) = T_{cal}(\lambda) \cdot I_{source}(\lambda) \tag{5.1}$$

where $E_{meas}(\lambda)$ is the experimentally measured emission (at normal incidence). The extracted source profile is shown in Fig. 5.5(a), after smoothing of the simulated data. To reduce multiple interference effects, the simulations are averaged over a 0-10° angle of emission. The source profile has i) a sharp peak near 370 nm and ii) a broad tail at longer wavelengths extend-

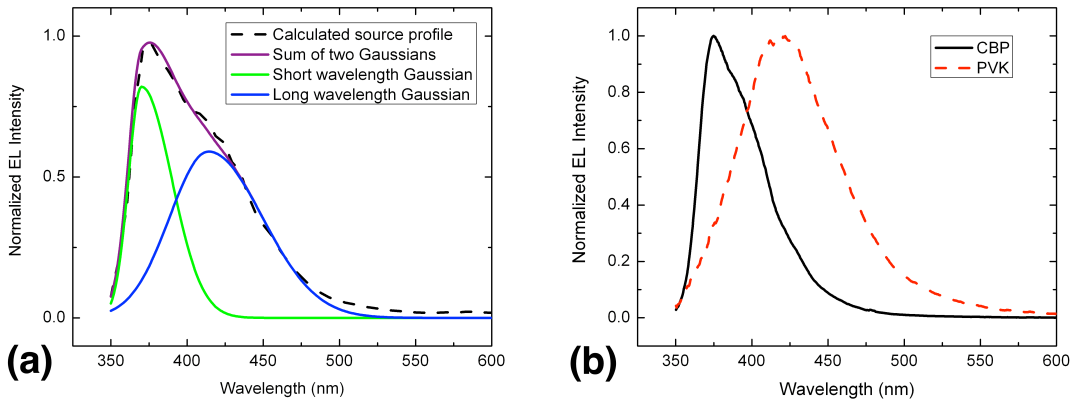

Figure 5.5 Spectra of (a) the source profile calculated from the experimental data and extracted Gaussian fits and (b) neat CBP and PVK.

ing beyond 550 nm, which may then be conveniently decomposed into two Gaussians. The Gaussian centered at ∼370 nm represents emission from CBP, with the peak at ∼420 nm representing emission from the PVK (Fig. 5.5(a)). Because the sum of the two Gaussians matches closely to the experimentally derived source profile, there is little evidence for secondary emission such as that from excimers. The two Gaussians are similar to the experimental EL spectra for neat CBP and neat PVK (shown in Fig. 5.5(b)), strengthening the model analysis.

The source profile is used to simulate the emission from ITO-based devices as a function of the MoO_X thickness (Fig. 5.2(b)). The red shift and narrowing of the emission spectrum predicted by simulation agrees well with that measured.

5.3.2 Microcavity Devices

Figure 5.6(a) shows the EL spectra of microcavity devices of the structure: Ag 40 nm/ MoO_X X nm/ PVK:CBP (3:1) ∼30 nm/ BPhen Y nm/ LiF 1 nm/ Al 100 nm, where X = 5, 10, 15, 20 nm and Y = 10, 15, 20, 30 nm. To optimize the microcavity EL peaks, the thickness of MoO_X and BPhen were changed. It was shown previously that thicker Ag gives narrower peaks, at the expense of transparency and so 40 nm silver is used here instead of the

more efficient 25 nm thickness.[16] The peaks shown range from 373 to 469 nm, with FWHM ranging from 21 to 41 nm. At longer wavelengths, the FWHM is wider, likely due to the lower intensity of the source profile at these wavelengths.

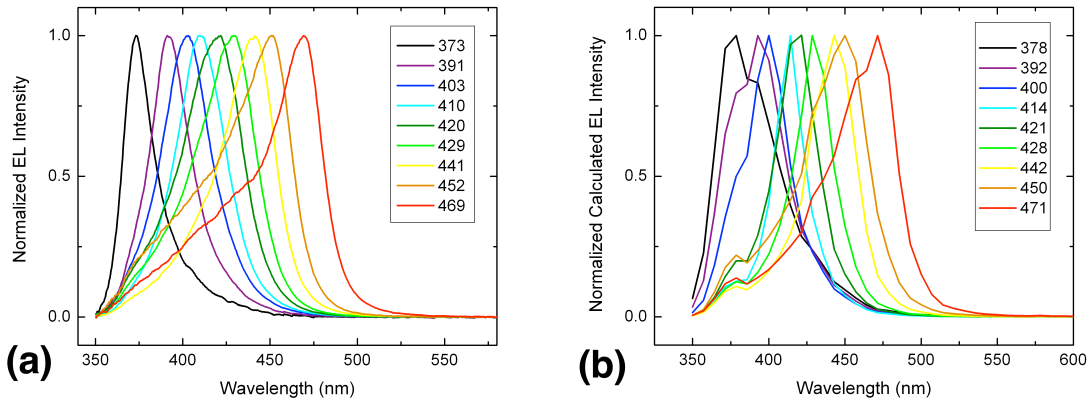

Figure 5.6 EL spectra of microcavity OLEDs, (a) measured and (b) calculated.

Figure 5.7 shows the I-V curves of microcavity devices of the structure: Ag 40 nm/ MoO_x [5,10,15 nm]/ PVK:CBP (3:1)/ BPhen 20 nm/ LiF 1 nm/ Al 100 nm. The microcavity devices show the same trend as the ITO-based devices, though not as pronounced, in that the current increases at a given voltage with increasing MoO_x thickness.

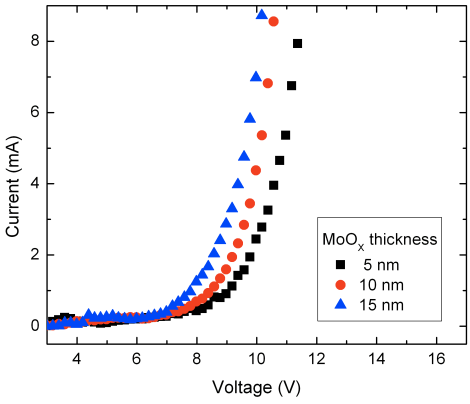

Figure 5.7 Current vs. voltage of microcavity devices with various MoO_x thicknesses.

Initial simulations, performed to fit the experimental microcavity peaks (see Fig. 5.6(b)), used the source profile calculated from the ITO-based device with 5nm MoO_X and 20nm BPhen, shown above. It can be seen that the initial fit is poor at the shortest wavelengths, best in the mid range, and fairly good at the long wavelengths. The thicknesses used in the simulations differ slightly from the experimental values in order to match the peak wavelength, as listed in Table 5.2. It is possible that the experimental thicknesses are not precise, as the spin-coated layer thickness was estimated from AFM measurements and the thickness monitor, which measures the evaporated layers, is subject to systematic errors resulting from inaccurate parameters, such as the acoustic impedance and material density, as well as the relative sample position in the evaporation chamber.

Table 5.2 Layer thicknesses and spectral characteristics for measured and best-fit calculated devices.

Measured Spectra				**Best-Fit Calculated Spectra**			
MoO_X (nm)	BPhen (nm)	Peak λ (nm)	FWHM (nm)	MoO_X (nm)	BPhen (nm)	Peak λ (nm)	FWHM (ave. 0-10°) (nm)
5	10	373	21	2	7	378	46
5	20	391	28	4	15	392	46
10	15	403	34	10	15	400	37
5	30	410	34	5	30	414	23
15	10	420	41	23	15	421	33
15	15	429	41	22	22	428	29
15	20	441	47	20	30	442	36
20	10	452	50	32	20	450	47
15	30	469	41	20	40	471	49

Since the short wavelength fits were unsatisfactory, we next used a different approach to simulate the spectra. In this approach, each Gaussian source profile is multiplied by the calculated transmission profile ($T_{cal}(\lambda)$) of the shortest optical length device ($t_{MoO_x} = 2$ nm, $t_{BPhen} = 7$ nm). Similarly, the two Gaussian profiles were also multiplied by the calculated transmission profiles for the longest optical length device ($t_{MoO_x} = 20$ nm, $t_{BPhen} = 40$ nm), see Fig. 5.5. The results are shown in Fig. 5.8. The best fit suggests that at shorter wavelengths, the emission is almost entirely from CBP, while at longer wavelengths the emission

from PVK is more prevalent, with a weak shoulder at short wavelengths due to CBP. The best-fit simulation for the microcavity device emission therefore suggests differing source profiles for devices with different optical lengths.

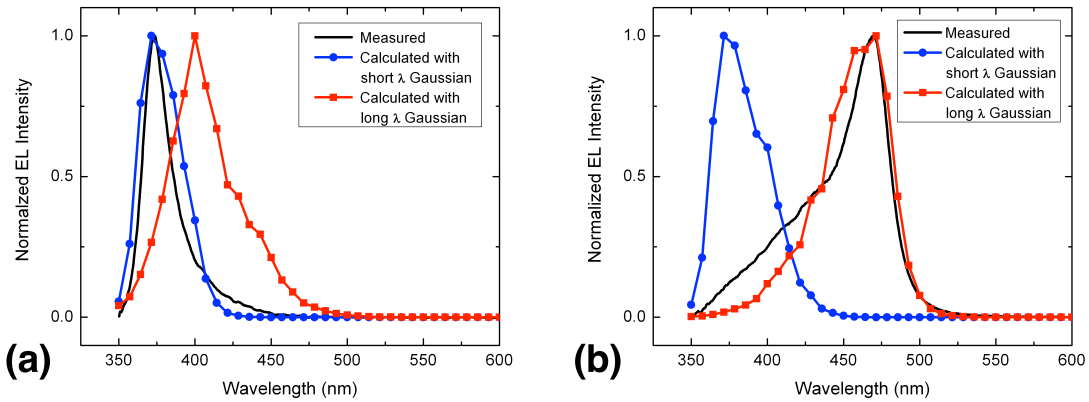

Figure 5.8 Measured EL spectra and spectra calculated individually from the two Gaussian source profiles for (a) 373 nm and (b) 469 nm experimental peaks.

The deviations of the simulated spectra from the observed profiles may be due to (i) the inaccurate values of the refractive index ($n(\lambda)$) for MoO_x, which likely depend on x, and (ii) the unknown $n(\lambda)$ for CBP and PVK, which may differ significantly from $n(\lambda)$ of N,N′-bis-(3-Naphthyl)-N,N′-biphenyl-(1,1′-biphenyl)-4,4′-diamine (NPB) that was used for all of the organic layers.

To determine the cause of the optical length-dependence of the source profiles, we also investigated the effects of MoO_x thickness on the morphology of the organic layers. AFM images were taken of the Ag/MoO_x films, with MoO_x thicknesses of 5, 10, 15, & 20 nm, and of the spin-coated EML on [ITO or Ag]/ MoO_x. R_{RMS} values are listed in Table 5.1 and selected images are shown in Figs. 5.9 & 5.10. It can be seen that the MoO_x on silver is much smoother than on ITO and does not vary significantly with MoO_x thickness. The smooth MoO_x layers indicate that there is likely no dependence of the spin-coated layer morphology on device structure. AFM scans of the EML on [ITO or Ag 40nm]/ MoO_x [5 or

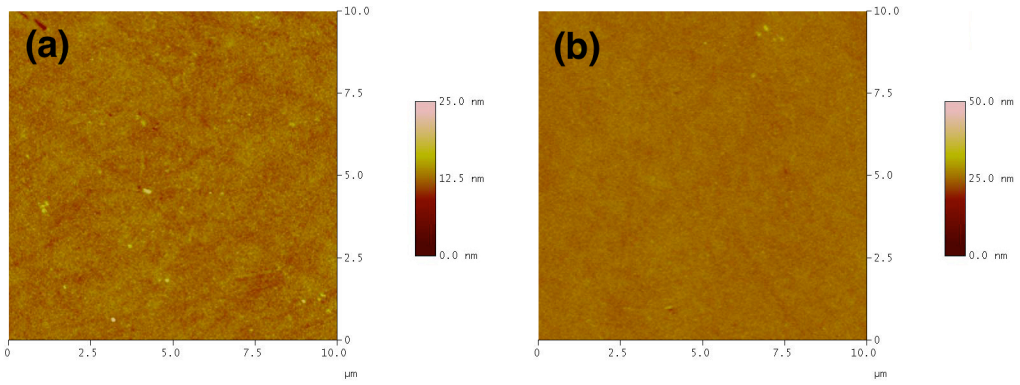

Figure 5.9 AFM images of MoO_x films on silver (40 nm), with thickness of (a) 5 nm ($R_{RMS} \sim 0.9 \pm 0.1$) and (b) 15 nm ($R_{RMS} \sim 1.0 \pm 0.1$).

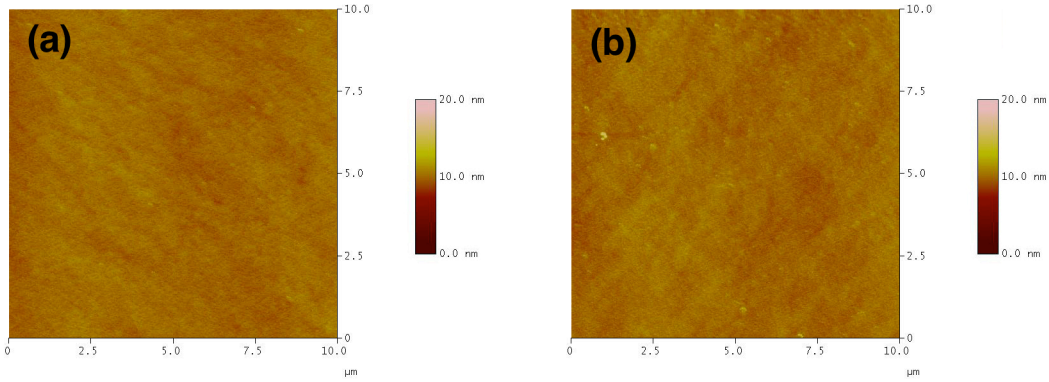

Figure 5.10 AFM images of PVK:CBP films on (a) Ag 40nm/ MoO_x 5 nm ($R_{RMS} \sim 0.4 \pm 0.05$) and (b) Ag 40nm/ MoO_x 15 nm ($R_{RMS} \sim 0.4 \pm 0.05$).

20 nm] show that the PVK:CBP layer is smooth ($R_{RMS} \leq 1$ nm), slightly more so with Ag than with ITO. Previous studies have shown that smooth AFM images correspond to films that are homogeneous.[24–26] We therefore conclude that the PVK:CBP is likely not phase separated or aggregated.

To roughly visualize the homogeneous mixture of PVK and CBP, the two can be approximated as spheres, as PVK's unconjugated backbone likely coils upon itself (see Fig. 5.11).[26] PVK has a molecular weight between 25,000 and 50,000, compared to the small molecule CBP

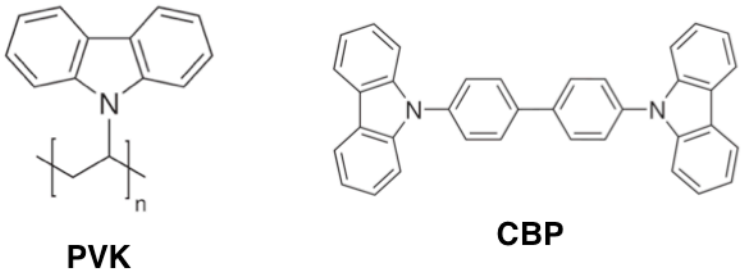

Figure 5.11 Molecular structure of PVK and CBP.

whose molecular weight is ∼485. Therefore PVK's spherical radius would be ∼4–5 times that of CBP. The random binary mixture of spheres (with a volume ratio of the two components similar to the present work) simulated in a previous study[27] suggests a percolating network of the smaller CBP molecules surrounding the larger PVK molecules (see Fig. 5.12), despite the 3:1 PVK to CBP weight ratio. This structure has implications for charge transport, as described in the next section.

5.3.3 Role of the Photon Density of States (DOS)

The simulation presented above takes into account the optical properties of the materials, which include their refractive indices and thicknesses. However, the simulations did not consider the effects of changes in the photon DOS, which result in changes in the emission rates depending on the cavity resonant frequency. The spontaneous emission rate (R) is dependent

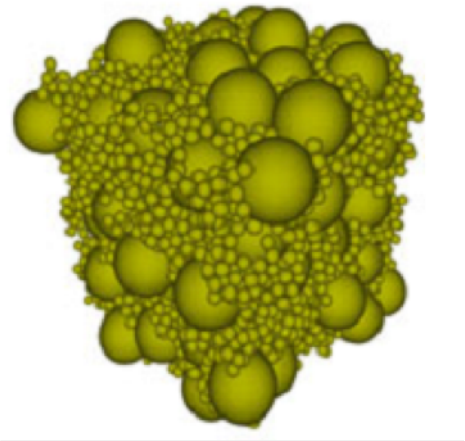

Figure 5.12 A random binary mixture of spheres with a radius ratio of 5.[27] Figure reproduced with permission. Copyright 2010, Springer.

on the dipole transition matrix element and the DOS, as expressed by:

$$R = \frac{2\pi}{\hbar} |M_{ij}|^2 \rho(\omega) \tag{5.2}$$

where $|M_{ij}|$ is the dipole transition matrix element, $\rho(\omega)$ is the DOS, and ω is the frequency. Therefore, if the DOS increases at the resonant frequency, R increases at that frequency. The current computational program does not incorporate this field enhancement factor into the intensity and requires the addition of a third term in Eq. 5.1.

Based on the foregoing structure (Fig. 5.12) and the much higher electron and hole mobilities in CBP in comparison to PVK, almost all charge transport occurs in the percolating CBP matrix.[28] Moreover, within the PVK:CBP layer, the electron density in the PVK component is likely much lower than that in CBP as the PVK LUMO level is 0.5 eV above that of CBP, see Fig. 5.13. Therefore, it is likely that most excitons form on CBP. However, as there is still obvious PVK emission in the long optical length devices, some excitons transfer to PVK molecules. We also suspect that as the HOMO level of PVK is higher than that of CBP, it likely traps holes into coiled sites.[26]

In the thin cavity devices, the short wavelength R is increased, meaning that CBP will likely emit faster, lowering the chance for charge or energy transfer to PVK. In thick cavity de-

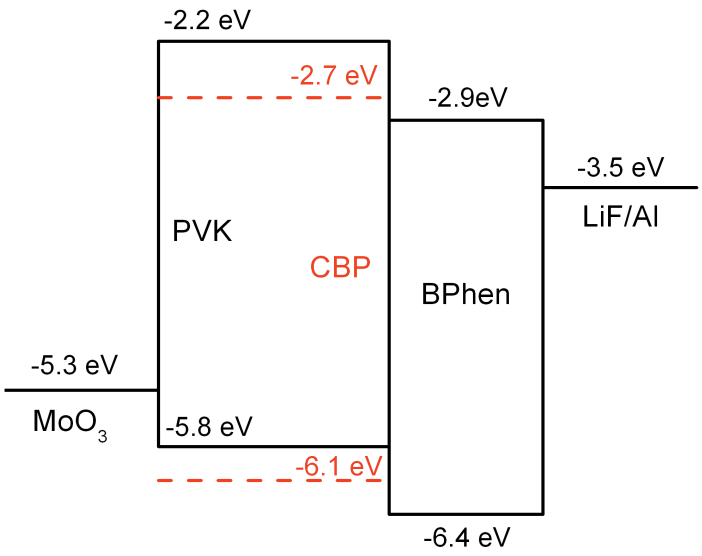

Figure 5.13 Energy diagram of materials used in OLEDs.

vices, the long wavelength R is increased, possibly increasing the likelihood of PVK emission occurring before the exciton can dissociate and transfer an electron into the CBP LUMO.

Current efforts are underway to improve the simulations to include these rate effects.

5.4 Conclusions

A mixture of PVK and CBP at a ratio of 3:1 was used to create a broad band source profile, optimized for use as the EML in microcavity OLEDs. Narrow spectra (FWHM $\sim$ 20 – 40 nm) in the range of $\lambda \sim 373$ – 469 nm were obtained for such devices. The source profile was extracted from an ITO-based device emission spectrum and used to calculate the microcavity EL spectra. It was found that the calculated spectra did not match well at short wavelengths, likely because the simulation did not take into account the effects of the optical cavity length and the resulting change in the photon DOS on the wavelength-dependent emission rate. This work highlights interesting characteristics of the emission of a near UV-to-blue OLED array and the

effects of the component attributes. Potential refinement of the simulations is being explored. The narrow band multicolor OLED pixels should be usable for an expanded wavelength range of on-chip spectrometers as well as for other analytical applications.

5.5 Experimental

5.5.1 Device fabrication and testing

OLEDs were fabricated on nominally 12 Ohm/sq, 140 nm-thick ITO-coated glass substrates purchased from Colorado Concept Coatings or the same glass substrates with ITO removed. The substrates were cleaned using surfactant, acetone, and isopropanol and treated with UV-ozone to increase the work function of ITO and further clean the glass. On the plain glass substrates, 40 nm silver was deposited by thermal evaporation under a vacuum pressure of $\sim$ 4x10^{-7} mbar. MoO_X was then deposited on all substrates in the thermal evaporation system using a sliding shutter to control thicknesses. The EML solution, a mixture of PVK and CBP with total concentration of 9 mg/mL in chlorobenzene, was spin-coated in a nitrogen-filled glovebox ($<$ 20 ppm O_2) atop the MoO_X, then baked at 60°C for 30 min. The samples were then transferred into a thermal evaporation system and pumped to a vacuum pressure of $\sim$ 4x10^{-7} mbar overnight to remove residual solvent. The films used for roughness analysis were removed and then measured by two or more atomic force microscopy (AFM) scans (model TESPA, working at tapping mode) to obtain an average value of the root-mean-square roughness (R_{RMS}) and the related spread for that film. Those used to fabricate devices were kept under vacuum to thermally evaporate the subsequent layers, including 4,7-diphenyl-1,10-phenanthroline (BPhen) (an electron transport/ hole blocking layer), LiF cathode buffer, and Al, which was deposited through a mask. The structure was: [ITO or Ag 40 nm]/ MoO_X [5,10,15,20 nm]/ PVK:CBP $\sim$ 30nm/ BPhen [10,15,20,30 nm]/ LiF 1 nm/ Al 100 nm. The resulting devices were 1.5 mm diameter pixels.

Devices were characterized by current-voltage measurements, using a Kepco DPS 40-2M

programmable power supply and a Keithly multimeter 2000, and by EL spectra obtained using an Ocean Optics CHEM2000 spectrometer.

5.5.2 Simulation method

The emission from OLEDs was simulated with the scattering matrix method that has been recently developed.[29] It is based on the scattering matrix method that has been very successful in simulation of optical properties of photonic crystals[31,32] and can be applied to OLEDs.[30] In this technique Maxwell's equations are solved in Fourier space, i.e. in a plane wave basis, for emitting species within an OLED architecture.

In each layer of the OLED stack, the materials are represented by realistic frequency dependent absorptive dielectric functions obtained from experimental measurements of N,N′-bis-(3-Naphthyl)-N,N′-biphenyl-(1,1′-biphenyl)-4,4′-diamine (NPB) and measurements for Ag,[33] MoO_x,[34] and ITO.[33] Individual scattering matrices are computed with each layer. A standard convolution algorithm[35] links the scattering matrix of the emissive layer to that of the air region above the OLED, from which the emission is obtained. The parallel components of the electric and magnetic fields are discontinuous in the emissive layer, but continuous at other layers. The simulation of the emitted fields is obtained for each three-dimensional orientation of the dipole, which is summed to obtain the total emitted field in the air region. More details on the simulation method will be given in an upcoming publication.

References

[1] J. Shinar, R. Shinar, *J. Phys. D: Appl. Phys.* **41**,133001 (2008).

[2] M. C. Gather , N. M. Kronenberg , K. Meerholz, *Adv. Mat.* **22**, 4634 (2010)

[3] B. Choudhury, R. Shinar, J. Shinar, *J. Appl. Phys.* **96**, 2949 (2004).

[4] R. Shinar, D. Ghosh, B. Choudhury, M. Noack, V. L. Dalal, J. Shinar, *J. Non Cryst. Solids* **352**, 1995 (2006).

[5] R. Shinar, Z. Zhou, B. Choudhury, J. Shinar, *Anal. Chim. Acta* **568**, 190 (2006).

[6] S. Vengasandra, Y. Cai, R. Shinar, J. Shinar, D. Grewell, *Annual Technical Conference-Society of Plastics Engineers* **66**, 508 (2008).

[7] Y. Cai, R. Shinar, Z. Zhou, J. Shinar, *Sensors and Actuators B* **134**, 727 (2008).

[8] K. S. Nalwa, Y. Cai, A. L. Thoeming, J. Shinar, R. Shinar, S. Chaudhary, *Adv. Mater.* **22**, 4157-4161 (2010).

[9] R. Liu, Y. Cai, J.-M. Park, K.-M. Ho, J. Shinar, R. Shinar, *Adv. Funct. Mater.* **21**, 4744-4753 (2011).

[10] R. Liu, T. Xiao, W. Cui, J. Shinar, R. Shinar, *Anal. Chim. Acta* **778**, 70-78 (2013).

[11] M. Ramuz, D. Leuenberger, R. Pfeiffer, L. Brgi, C. Winnewisser, *Eur. Phys. J. Appl. Phys.* **46** (2009) 12510.

[12] E. L. Ratcliff, P. A. Veneman, A. Simmonds, B. Zacher, D. Huebner, S. S. Saavedra, N. R. Armstrong, *Anal. Chem.* **82**, 2734 (2010).

[13] E. Kraker, A. Haase, B. Lamprecht, G. Jakopic, C. Konrad, S. Kstler, *Appl. Phys. Lett.* **92**, 033302 (2008).

[14] T. Mayr, T. Abel, B. Enko, S. Borisov, C. Konrad, S. Kstler, B. Lamprecht, S. Sax, E. J. W. List, I. Klimant, *Analyst* **134**, 1544 (2009).

[15] F. Lefèvre, A. Chalifour, L. Yu, V. Chodavarapu, P. Juneau, R. Izquierdo, *Lab Chip* **12**, 787 (2012) .

[16] R. Liu, C. Xu, R. Biswas, J. Shinar, R. Shinar, *Appl. Phys. Lett.* **99**, 093305 (2011).

[17] U. Giovanella, C. Botta, F. Galeotti, B. Vercelli, S. Battiatoc, M. Pasinia, *J. Mater. Chem. C* **1**, 5322 (2013).

[18] K. O. Cheon, J. Shinar, *Appl. Phys. Lett.* **83**, 2073 (2003).

[19] B. Tong, Q. Mei, S. Wang, Y. Fang, Y. Menga, B. Wang *J. Mater. Chem.* **18**, 1636 (2008).

[20] P. Ivanov, R. Tomova1, P. Petrova1, S. Stanimirov, I. Petkov, *J. Phys. Conf. Ser.* **398**, 012052 (2012).

[21] J. J. Park, T. J. Park, W. S. Jeon, R. Pode, J. Jang, J. H. Kwon, E.-S. Yu, M.-Y. Chae, *Organic Electronics* **10**, 189 (2009).

[22] M. Cai, T. Xiao, R. Liu, Y. Chen, R. Shinar, J. Shinar, *Appl. Phys. Lett.* **99**, 153303 (2011).

[23] M. Cai, Z. Ye, T. Xiao, R. Liu, Y. Chen, R. W. Mayer, R. Biswas, K.-M. Ho, R. Shinar, J. Shinar, *Adv. Mater.* **24**, 4337 (2012).

[24] Y.-Y. Noh, C.-L. Lee, J.-J. Kim, K. Yase, *J. Chem. Phys.* **118** , 2853, (2003).

[25] M. Cai, T. Xiao, E. Hellerich, Y. Chen, R. Shinar, J. Shinar, *Adv. Mater.* **23**, 3590 (2011).

[26] E. S. Hellerich, J. J. Intemann, M. Cai, R. Liu, M. D. Ewan, B. C. Tlach, M. Jeffries-EL, R. Shinar, J. Shinar, *J. Mater. Chem. C* **1** 5191, (2013).

[27] A. V. Kyrylyuk, A. Wouterse, A. P. Philipse, *Progr. Colloid Polym. Sci.* **137**, 29 (2010).

[28] P. W. M. Blom, M. J. M. de Jong, M. G. van Munster, *Phys. Rev. B: Condens. Matter Mater. Phys.* **55**, R656 (1997).

[29] R. Biswas, C. Xu, W. Zhao, R. Liu, R. Shinar, J. Shinar, *J. Phot. Ener.* **1**, 011016 (2011).

[30] R. Liu, C. Xu, R. Biswas, J. Shinar, R. Shinar, *App. Phys. Lett.* **99**, 093305 (2011).

[31] D. Whittaker, I. Culshaw, *Phys. Rev. B* **60**, 2610 (1999).

[32] H. Rigenault, F. Lemarchand, A. Sentenac, *J. Opt. Soc. Am. A* **17**, 1048 (2000).

[33] *Handbook of the Optical Constants of Solids II*, ed. E. Palik, Academic Press, Boston, 1991.

[34] F. Hamelmann, A. Brechling, A. Aschentrup, U. Heinzmann, P. Jutzi, J. Sandrock, U. Siemeling, T. Ivanova, A. Szekeres, K. Gesheva, *Thin Solid Films* **446**, 167 (2004).

[35] Z.Y. Li, L. L. Lin, *Phys. Rev. E.* **67**, 046607 (2003).

CHAPTER 6.

Summary and future work

The excitement over organic electronics is still growing and we continue to see new products with OLED screens and OLED lighting panels. We are on the cutting edge of new technology, while still investigating the basic workings of these materials and devices.

The new EML mixture, presented in chapter 2, of a polymer guest with a small molecule host is both simple in name, yet complex in nature. Using a small molecule as a host for polymer dopants opens the door to new possibilities for polymer emissive materials. Also, the suspicion that PVK likely coils upon itself in the film introduces a possible cause for low efficiency in PVK-based devices. Future work could include investigating phosphorescent polymers in small molecule hosts. Blue phosphors are particularly difficult because of the need to pair with high triplet energy hosts and transport materials. Being able to use small molecules that are compatible with polymer guests can make these phosphorescent devices more efficient and more easily fabricated.

Chapter 3 focused on newly fabricated materials and investigated which chemical structure change gives the best efficiency. We expect the efficiency difference between the two BBO-based structures is caused by the change in the conjugation pathway in the BBO copolymers and is related to the interaction of the host and guest exciton dipoles. It would be interesting to model dipole effects in these BBO materials to better understand the nature of the enhanced efficiency. Is the dipole orientation changed, as expected? Where is the greatest charge density on the molecule?

Much new work has been done in the last few years on spin-coating small molecules and

the importance of spin-coating conditions on the resultant film quality. As presented in chapter 4, efficient devices can be achieved by solution-processed small molecules that do not require a polymer matrix to create a quality film. Besides choice of solvent, which effects the drying time and film roughness (as discussed in chapter 4), there are many other conditions that could affect the film. For example, temperature of the solution and the substrate or pressure and air movement in the area can affect drying time. The use of different spin chucks (e.g. metal vs. glass) can affect the resultant thickness because of drying effects. All of these conditions can be optimized with each particular device structure, but further study could be conducted to better understand how these conditions affect micro-morphology and how that is related to mobility and/or emission efficiency.

Chapter 5 presents a novel approach to create microcavity OLEDs in the deep blue and UV by using a mixed EML of two different short wavelength emitters. The understanding gained from the previous studies of spin-coating and polymer:small molecule mixtures helped to design these devices with a broad band emission. It would be beneficial to continue studying these devices, including measurements on efficiencies with the new power meter setup optimized to measure optical power at short, near-UV wavelengths. This work is being expanded, by Eeshita Manna, to combine these microcavity devices with CBP-only UV microcavity devices and those previously published by Liu et al. ranging from λ = 493–639 into an on-chip spectrometer. It would be interesting to investigate the affect of changing device component thicknesses on the FWHMs. As shown in the appendix, there is potentially a FWHM dependance on the MoO_X vs. BPhen thickness. Also, the oxygen content of MoO_X is unknown and would affect the layer's refractive index. Such unknown change in $n(\lambda)$ would have significant affects on the emission characteristics.

APPENDIX A.

Supplemental Material

A.1 Fluorescent polymer guest:small molecule host solution-processed OLEDs: Further study

A.1.1 F8BT

Poly[(9,9-dioctylfluorenyl-2,7-diyl)-alt-co-(1,4-benzo-2,1,3-thiadiazole)] (F8BT) is a yellow-emitting co-polymer, known to be an efficient fluorescent emitter.[1] F8BT has been tested in a similar fashion to the materials discussed in chapter 2, using F8BT as a guest with both CBP and PVK as hosts. The results are shown below. Figure A.1 shows the molecular structure of F8BT.

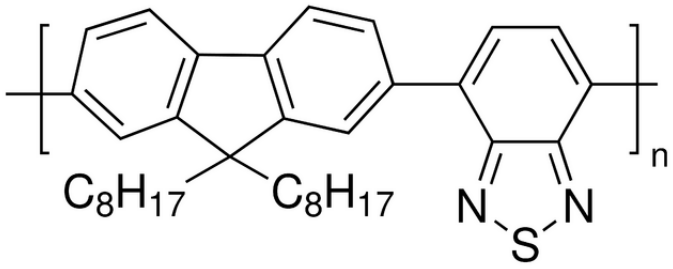

Figure A.1 Molecular structure of F8BT.

Figure A.2 shows the spectra of F8BT in CBP and PVK at dopant levels (i.e. low wt%). Some host emission exists at the lower concentrations of the guest in both hosts. Efficiency plots are shown in Figs. A.3, A.4, & A.5. Luminous Efficiency is similar in both hosts for low

concentrations of the guest, but the CBP-based devices persist to much higher brightness. At higher F8BT concentrations (20 & 50 wt%), the CBP-based devices are much more efficient.

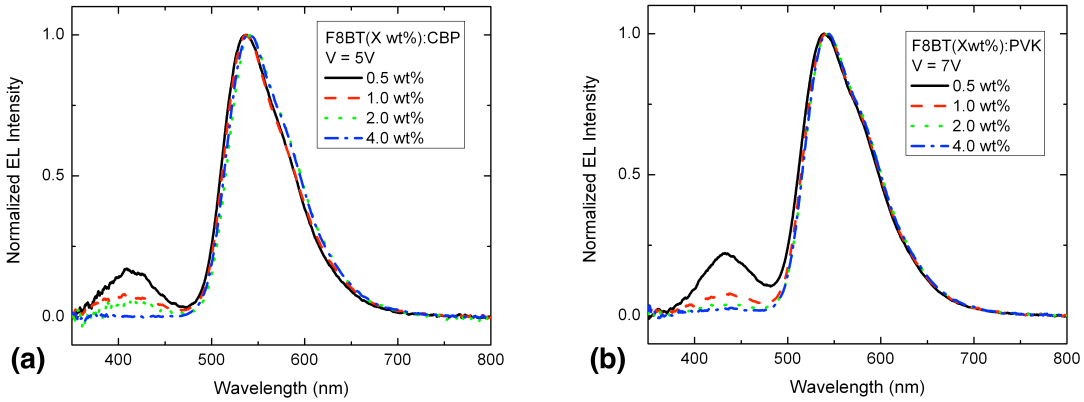

Figure A.2 Spectra of F8BT [0.5, 1.0, 2.0, $ 5.0 wt%] in (a) CBP and (b) PVK.

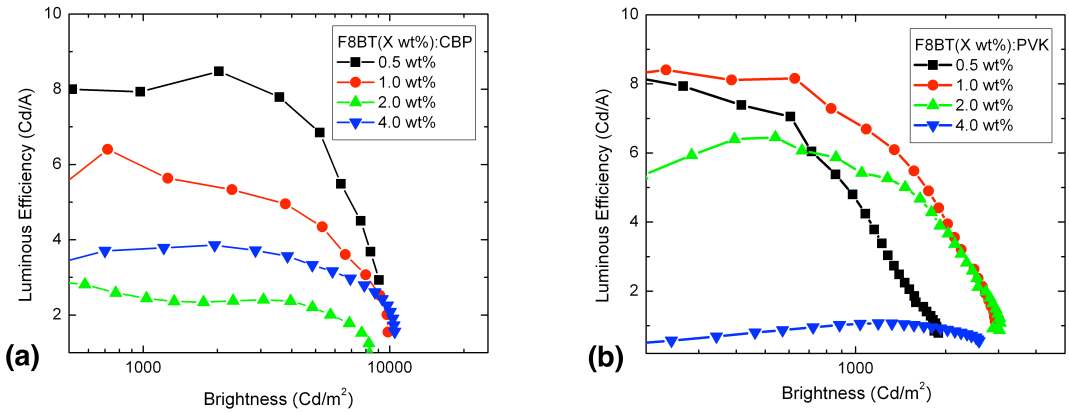

Figure A.3 Luminous efficiency vs. EL brightness for F8BT in (a) CBP and (b) PVK.

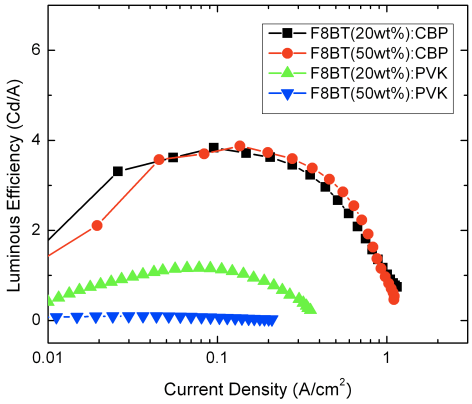

Figure A.4 Luminous efficiency vs. current density for F8BT at high concentrations in CBP and PVK.

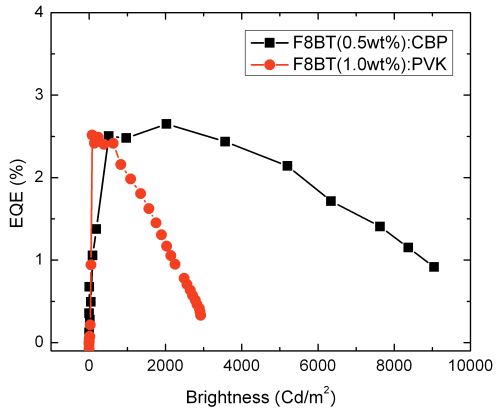

Figure A.5 EQE vs. EL brightness for most efficient concentration of F8BT in CBP and PVK.

A.1.2 4,8-PBOTF

Another BBO-based polymer with an altered conjugation pathway, 4,8-PBOTF, was fabricated and compared to the analogue material previously reported,[2] (see below). It was also tested as a guest in CBP and PVK, in the manner described in chapter 2. Figure A.6 shows the molecular structure of 4,8-PBOTF. There is slight host emission in both hosts.

Efficiency plots show that the CBP-based devices are more efficient than the PVK-based devices with various concentrations of 4,8-PBOTF.

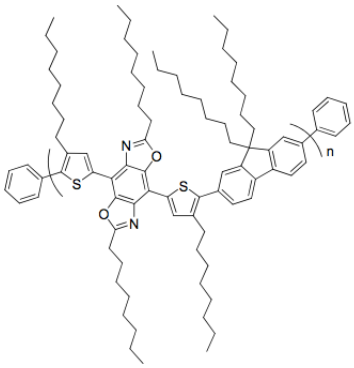

Figure A.6 Molecular structure of 4,8-PBOTF.

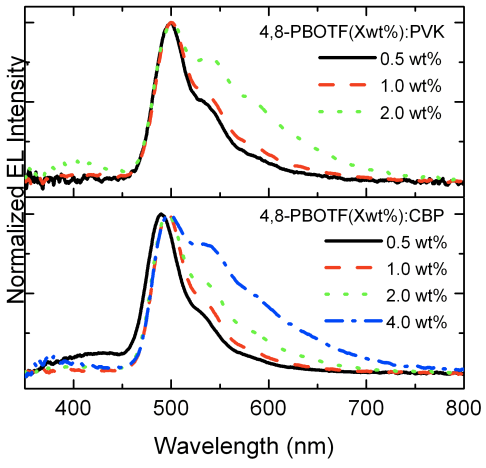

Figure A.7 Spectra of 4,8-PBOTF [0.5, 1.0, 2.0, & 4.0 wt%] in (a) CBP and (b) PVK.

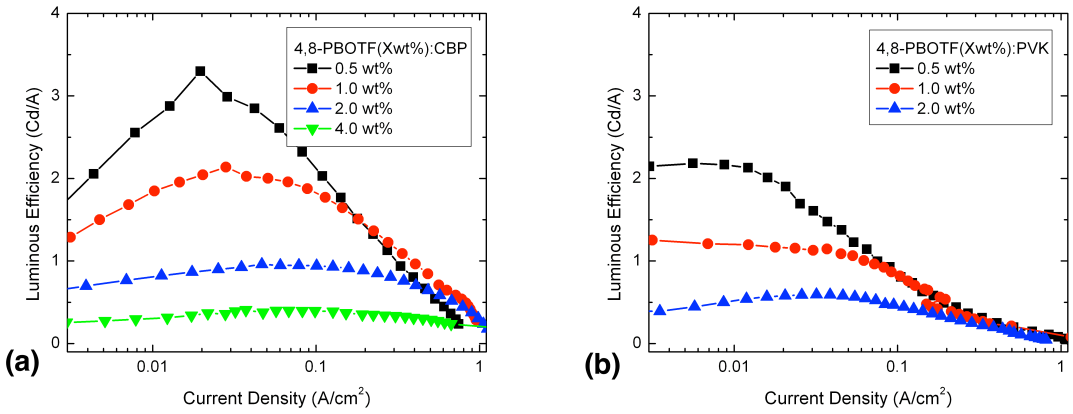

Figure A.8 Luminous efficiency vs. current density for 4,8-PBOTF in CBP and PVK.

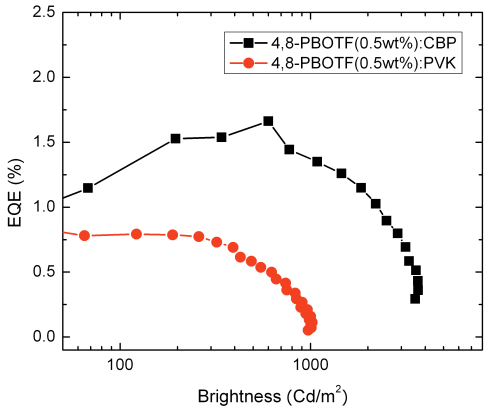

Figure A.9 EQE vs. EL brightness for most efficient concentration of 4,8-PBOTF in CBP and PVK.

A.2 Fluorescent OLEDs based on new benzobisoxazole-based emitters with altered conjugation pathways: 2,6-PBOTF vs. 4,8-PBOTF

The new BBO-based co-polymer mentioned above was designed in comparison to 2,6-PBOTF, by altering the conjugation pathway to be through the central benzene ring instead of through the oxazole rings. This is the same alteration that is described in chapter 3. The structure of the two co-polymers are shown for comparison in Fig. A.10. The spectra show

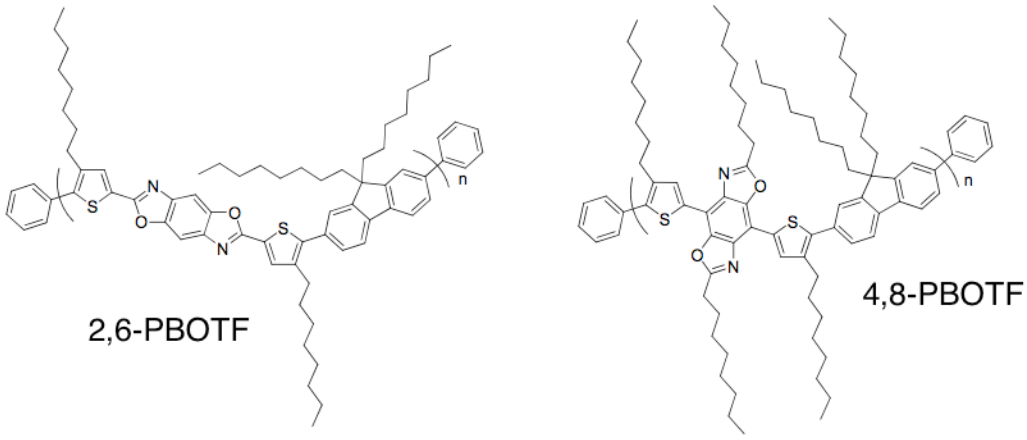

Figure A.10 Molecular structure of 2,6-PBOTF and 4,8-PBOTF.

that 4,8-PBOTF has much more efficient energy transfer than 2,6-PBOFT, as there is almost no host emission in the 4,8-PBOTF devices and a combined emission of host and guest in the 2,6-PBOFT devices. The efficiencies are shown below. It is obvious that, similar to the materials described in chapter 3, 4,8-PBOTF is more efficient than 2,6-PBOTF.

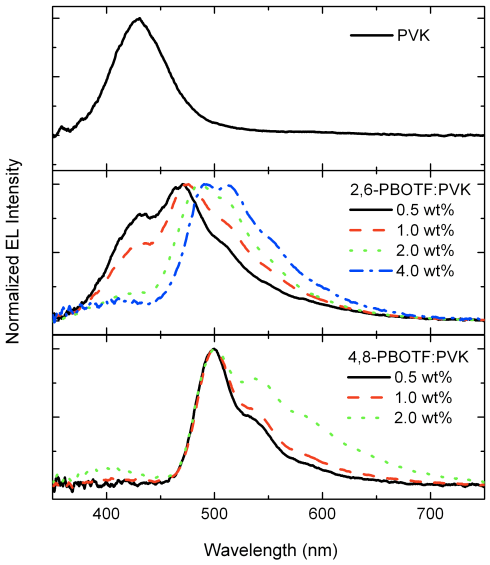

Figure A.11 Spectra of PVK, 2,6-PBOTF:PVK and 4,8-PBOTF:PVK.

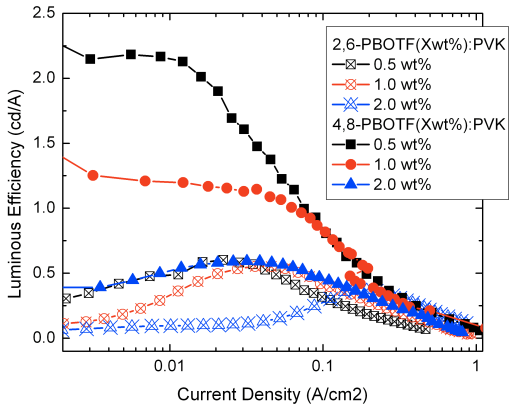

Figure A.12 Luminous efficiency vs. current density for 2,6-PBOTF and 4,8-PBOTF in PVK.

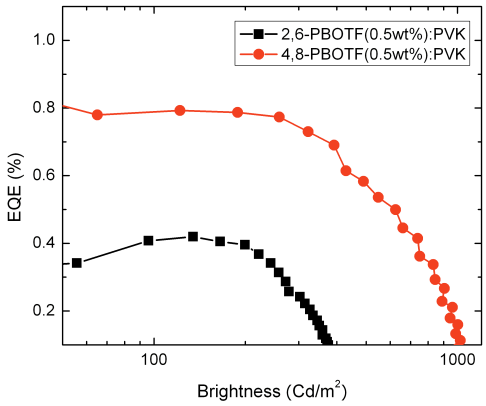

Figure A.13 EQE vs. EL brightness for most efficient concentration of 2,6-PBOTF and 4,8-PBOTF in PVK.

A.3 Deep blue/ultraviolet microcavity OLEDs based on solution-processed PVK:CBP: Further study

It was observed that the full width at half maximum (FWHM) of microcavity spectra differed in devices with the same EL peak but different structures. Below, shown in Figs. A.14 & A.15, are four devices from two different batches that show this trend. It is suspected that the devices with thicker MoO_x have wider FWHMs. Devices with the same peak but thicker BPhen have narrower peaks. The origin of this difference is potentially the different refractive indices of these materials and their resulting affect of the emission characteristics. More investigation is needed. With the expansion of the simulation, we may be able to better understand this effect.

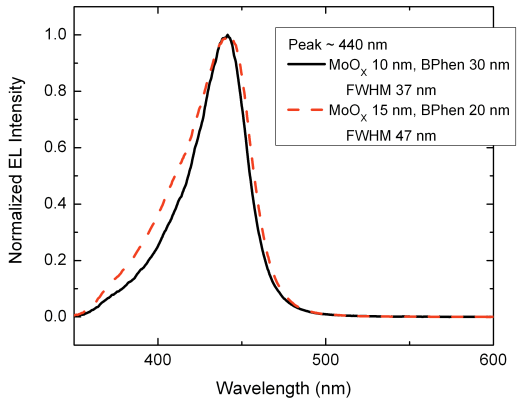

Figure A.14 EL spectra from microcavity OLEDs with PVK:CBP (3:1) EML and different MoO_x and BPhen thicknesses, at a peak wavelength of ∼440 nm.

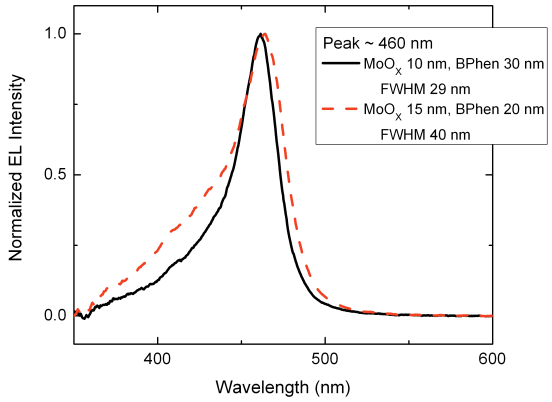

Figure A.15 EL spectra from microcavity OLEDs with PVK:CBP (3:1) EML and different MoO_x and BPhen thicknesses, at a peak wavelength of ∼460 nm.

A.4 Chemistry structure terms

arene: aromatic hydrocarbon, alternating double and single bonds between carbon atoms.

alkyl: hydrocarbon, single bonds of carbon and hydrogen.

alkynyl: hydrocarbon, characterized by its triple bond.

oxazole: five member ring, oxygen and nitrogen separated by one carbon.

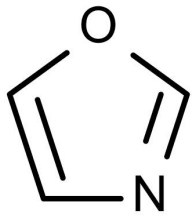

Figure A.16 Oxazole.

fluorene

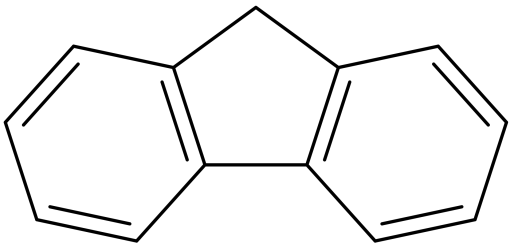

Figure A.17 Fluorene.

phenylene

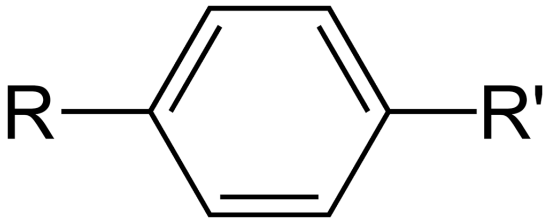

Figure A.18 Para-phenylene.

carbazole

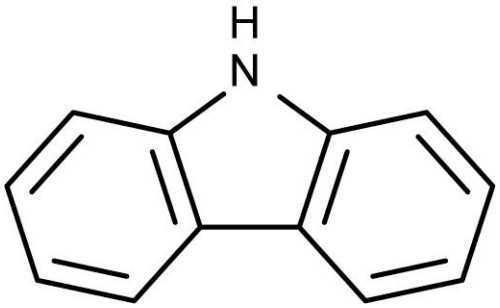

Figure A.19 Carbazole.

benzobisoxazole

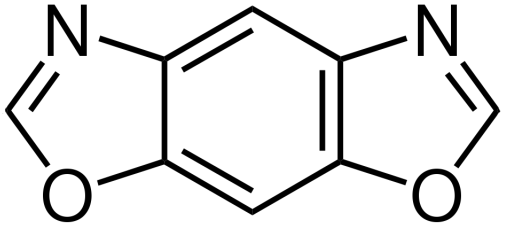

Figure A.20 Benzobisoxazole.

References

[1] D. Kabra, L. P. Lu, M. H. Song, H. J. Snaith, R. H. Friend, *Adv. Mater.* **22**, 3194 (2010).

[2] J. F. Mike, J. J. Intemann, M. Cai, T. Xiao, R. Shinar, J. Shinar, M. Jeffries-EL, *Polym. Chem.* **2**, 2299 (2011).

[3] **Structures**:*http://chemistry.about.com/od/chemicalstructures/a/structures.htm*

Acknowledgements

I would like to express my deepest gratitude to my advisers Prof. Joe Shinar and Prof. Ruth Shinar, without whom I would not be where I am today. I have learned countless things and have grown as a scientist thanks to their guidance, discussion, and the opportunities provided by them.

I also extend very special thanks to my past and present group members for great discussions, trouble-shooting, friendship, and support. Thanks to Ying Chen, Min Cai, Rui Liu, Yuankun Cai, Teng Xiao, Zhengqing Gan, Weipan Cai, Eeshita Manna, Dusan Danilovic, and Fadzai Fungura. I'm grateful to Ying Chen and Min Cai, who were great teachers for me as an incoming student.

I would like to express my very great appreciation to a number of collaborators who offered support throughout my graduate education. It was a pleasure to work with Prof. Malika Jeffries-EL and her group, particularly Jeremy Intemann and Monique Ewan. I am appreciative of the many discussions, from which I learned a great deal and which sparked interest in many aspects of materials chemistry. Also, thanks to Jeremy's friend Michael Zenner, who took beautiful pictures of our blue OLEDs. I am grateful to Prof. Rana Biswas for his interesting and helpful discussions and for all the work he and Rob Heise have done to examine and explore OLEDs through simulation and calculation. His thoughtful analysis has taught me a lot. Thanks also to Prof. Kai-Ming Ho's group, especially Joong-Mok Park and Geyuan Liu, with whom I have worked on many interesting projects. Special thanks to Wai Leung, who is always quick with helpful ideas. I am grateful to Professors Adam Kaminski, Bruce Harmon, Craig Ogilvie, and Jay Kim for serving on my Program of Study Committee. An acknowledgment is duly deserved for the administrative staff who helped in countless ways throughout the

years, especially Lori Hockett, Larry Stoltenberg, and Gloria Oberender. Having a helpful and kind person available is truly indispensable. Thanks also to Rebecca Shivvers, who taught me much about lab safety. I am grateful to my professors at Augsburg College, especially Prof. Mark Engebretson and Prof. Ken Erickson, and to my professors here in the Department of Physics and Astronomy at Iowa State University for inspiring me to learn, to understand, and to explore.

Special thanks to my best ladies Stella Kim and Xiao Lin for being supportive and fun throughout the years. I am lucky to have had such good girlfriends in physics. I'm also thankful to Valentin Taufour for teaching me LabVIEW. Thanks to many of my classmates for working with me through the homework and for all the fun times.

I would also like to thank my dance troupe, Lisa, Tara, Stephanie, and Jessi, and all those I've danced with over the years, who have shimmied with me through it all and have balanced my equations with music and dance.

Lastly, I would like to especially thank my husband Dan, my parents, my sisters Trisha and Andrea, and my cat Chloe, for making me smile and for their patience and support. Special thanks to my entire family, my grandparents, aunts, uncles, and in-laws, for listening to my stories, however long, and for always expressing pride and enthusiasm for my accomplishments.

I'm grateful for the funding that supported this research. This work was performed at the Ames Laboratory under contract number DE-AC02-07CH11358 with the U.S. Department of Energy.